SALT FILM DEVELOPMENT DURING PITTING OF

NICKEL

BY

JINGLI LUO, B.ENG.

A Thesis

Submitted to the school of Graduate Studies

in Partial Fulfilment of the Requirement

for the Degree

Doctor of Philosophy

McMaster University

SALT FILM DEVELOPMENT DURING PITTING OF NICKEL

DOCTOR OF PHILOSOPHY (1992) McMASTER UNIVERSITY

(Material Engineering) Hamilton, Ontario

TITLE: SALT FILM DEVELOPMENT DURING PITTING OF NICKEL

AUTHOR: Jingli Luo, B.Eng. (Beijing University of Iron and Steel

Technology)

SUPERVISOR: Professor M.B. Ives

NUMBER OF PAGES: xxiii, 118

ABSTRACT

Pitting corrosion is one of the major causes of industrial failure of metallic parts. Unfortunately, such attack cannot always be detected before perforation occurs. Understanding the mechanism of pit development will provide us with a clue of how to prevent pitting corrosion in advance. From an engineering point of view, it is important to keep the pit, once it forms, repassivated rather than allow continuous growth, leading to the perforation. The key factors controlling pit development must therefore be determined.

A comprehensive model of pitting processes is proposed which considers interfacial dissolution, salt film formation, multiple species in solution, reaction equilibria, migration and diffusion. The model is capable of determining local chemistry within pits and characterizing the conditions necessary for stabilization of pitting corrosion.

The model is experimentally verified using microelectrodes developed to measure the local properties of pitting sites. The electrodes were characterized through studies on their potential stability, spatial resolution, and the interference of other ions involved in the corrosion of nickel. The study was performed on a nickel model pit in a saline environment.

The in situ measurements obtained by microelectrodes provide the direct evidence of existence of a salt layer, comprised of corrosion products, at the bottom

of a developing pit. The condition for formation of the salt film in active pits appears to require that the pit depth be sufficient to ensure the maintenance of a critical local solution chemistry. The experimental results are consistent with the theoretically predicted critical depth at which a metal chloride salt layer starts to form at the pit bottom.

The measurements of the potential distribution within the salt film have provided data for the potential drop across the salt film, its thickness and therefore its conductivity. These help us to achieve a better understanding of the nature of the salt film.

The anodic behaviour of nickel was studied in solutions which simulate the pit electrolyte, based on the in situ measurements of the local pH and chloride ion concentration within a pit at different stages of development. The factors controlling the pit growth were deduced.

ACKNOWLEDGEMENTS

TABLE OF CONTENTS

LIST OF TABLES

LIST OF FIGURES

LIST OF SYMBOLS

a_j activity of species j

B_{ij} parameter in Pitzer's activity coefficients equation

c_j concentration of species j

$c_j(y,t)$ concentration of species j at y position and t time in the diffusion field of species j

$c_{H^+,1}$ bulk concentration of the hydrogen ions in the agar gel layer 1

$c_{H^+,2}$ bulk concentration of the hydrogen ions in the agar gel layer 2

$c_{Cl^-,s}$ saturated concentration of the chloride ions in NaCl solution

C constant in Equations [3.8], [3.10], and [a.1]

$C^{\ast}_{ij}$ Pitzer parameter

d diameter of a pit

D_{ji} inter-diffusion coefficient which describes the effect of the concentration gradient of species i on the diffusion flux of species j

D_j chemical diffusion coefficient of species j

E potential at the point considered

E° standard potential

E_0 equilibrium potential of an electrode

E_{Appl} applied potential

E_{ocp} open circuit potential

E_{Ni}	measured potential of the Ni sample vs. reference electrode
E_{pot}	measured potential of the potential probe vs. reference electrode
E_{pp}	passive potential at which the active-to-passive transition occurs
$E(SCE)$	potential with respect to a saturated calomel electrode
F	Faraday constant
h	pit depth
h_t	transition depth
h_f	thickness of the salt film
h_i	the initial pit depth
i^o	exchange current density
i	current density
i_{app}	applied current density
I	current or ionic strength in Pitzer's activity coefficients equation(Appendix B)
IR_{in}	ohmic drep inside a pit
IR_{out}	ohmic drop outside a pit
IR_{tot}	total solution ohmic drop from the reference electrode and the pit bottom
J_j	the flux of species j
k_{ij}	selectivity coefficient for species i in the presence of species j (a measure of the interference of ion j in the potentiometric determination of species i)
K_f	conductivity of the salt film

K_1	equilibrium constant
K_{sp}	solubility product
M	molarity
m	molality
M_f	atomic weight of the salt film
n	number of electrons involved in the reaction
n_j	charges carried by ion j
N	normal concentration
N_i	total number of i
R	gas constant
S	area
t	time
t_f	time at which probe reaches nickel/film interface
t_j	transport number of ion species j
T	temperature on Kelvin scale
u_j	mobility of species j
V_j	molar volume of metal j
v_d	velocity of the solution drift towards the pit
v_{ME}	moving speed of micro-electrode
v_{pit}	rate of pit deepening

y	position of micro-probe in the diffusion field: distance between the chloride probe and the NaCl crystal/solution interface or the distance between the pH probe and the interface of two agar gel layers
Z	the distance between a specific point and the pit mouth
Z_f	position of the probe inside the salt film with $z_f = 0$ at the nickel/film interface
α	charge transfer coefficient for the reduction reaction
$\beta^{(j)}$	Pitzer interaction coefficient
γ	molal activity coefficient
η_{cr}	charge transfer overvoltage
η_f	potential drop across the salt film
θ_{η}	Pitzer's coefficient for like charged ion interactions
ρ_f	the density of the salt layer
ϕ_s	the potential difference between metal and the film/solution interface. When there is a surface film, ϕ_s is the sum of η_{CT} and η_f.
Φ	potential in solution
$\Psi_{\eta k}$	Pitzer triple ion interaction parameter

Subscripts

a	anion
b	bulk solution
c	cation

CT	charge transfer
f	salt film
in	inside the pit
j	species number
M	cation
ME	microelectrode
N	neutral
out	outside the pit
pot	potential probe
s	surface
S	saturated
tot	total
x	anion
0	equilibrium
1	agar gel layer 1
2	agar gel layer 2

CHAPTER 1. INTRODUCTION

Pitting corrosion is a type of localized attack which is responsible for a significant fraction of the failures of metallic structures. The danger of this type of attack is that its progress may be impossible to monitor by visual inspection until the metallic part has been completely perforated. The ability to predict failure in service is constrained in many cases by a lack of detailed knowledge of the processes occurring within active pits. Thus, the growth of the pits and its kinetics is not only of scientific interest but also of major importance concerning the practical performance of corrosion-resistant materials since local breakdown is difficult to avoid under practical conditions. Sufficient knowledge of the mechanisms of growth and stability is therefore a necessary requirement for the correct prediction of the corrosion behaviour of metals and for the development of new, highly corrosion-resistant alloys.

One of the most critical, and technologically important, aspects of pitting corrosion is the criterion which determines whether a pit, once nucleated, grows or repassivates. The growth of pits is considered to be dependent upon the local conditions within them. After pit initiation, the composition of the pit electrolyte, especially as it changes during the growth of the pit, is extremely important for the clarification of the mechanism of pitting corrosion. However, a major impediment to any understanding of the nature of the local attack is the small

dimensions of the occluded cells. Numerous pieces of information on pit development are scattered in the literature.

1.1. Literature review

1.1.1. Theories of pit growth

Several theories have been suggested that attempt to rationalize the phenomena observed during pit growth. Each is focused on the major factor expected to control the pit development. They may be grouped into the three categories listed below as:

1.1.1.1. The active dissolution theory;

1.1.1.2. Salt film theory;

1.1.1.3. Mass transport control theory.

An overview of each group of theories is presented in the following sections. None can be used to explain all of the phenomena accompanying pit growth. As it is still a "frontier topic", more fundamental studies are required to acquire a better understanding of the mechanisms of these processes.

1.1.1.1. The active dissolution theory

The active dissolution theory is based on the presumption that pit development is charge transfer controlled or mixed charge transfer-ohmic controlled[1,2]. The theory is developed from the following facts:

(1). The electrolyte within the pits is of a relatively high acidity due to the hydrolysis reaction of metal ions and the high chloride ion concentration. It is a condition at which metals are likely dissolved actively.

(2). The resistance of the electrolyte path increases with the depth of a pit.

To explain the fast dissolution within a pit while the rest of the surface is still in the passive state, Pickering[3,4] suggested that there is a critical ohmic drop, IR* as noted in Figure 1.1[5], for a stable local cell. Figure 1.1. shows a typical anodic polarization curve obtained by the potentiodynamic technique for a passivating metal electrode. It has an active nose and a passive range. The IR* causes the potential at the pit bottom to drop into the active regime. Large potential variations within pits were reported several years ago[6,7]. Pickering and Frankenthal[8,9,10] concluded that the resistance of the electrolyte path increases with depth of a pit and the observed large potential drops may be explained only by a high-resistance path resulting from constrictions caused by bubbles. They proposed that the bubbles consist of hydrogen
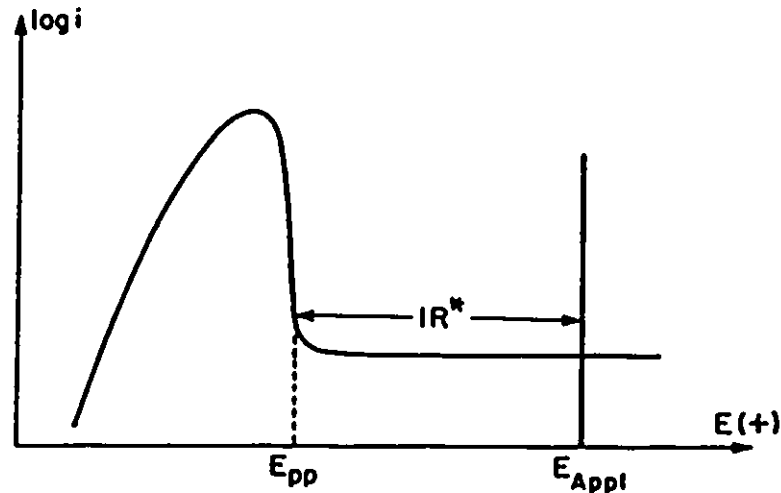
Figure 1.1 Schematic illustrating anodic dissolution behaviour of an active passive metal and the critical ohmic drop (IR*). (Adapted from Pickering[5]).

and result from the high ohmic drop in pits. The evolution of the hydrogen is also evidence for the active dissolution model[11]. Similar arguments in favour of large potential drops may be applied in the case of covered pits, as is observed on stainless steels[12,13].

(3). The metal dissolution rates in a pit follow the Tafel law.

Kaesche[14] and Schwenk[15] determined that the metal dissolution rates in pits follow the Tafel law which describes a typical potential and current relation in the active dissolution region. The metal dissolution rate in a pit is comparable to the value of the active dissolution current density[16].

Contradictory observations were also reported. Strehblow and Ives[17], and Beck and Alkire[18] have suggested that since current density values typically found in the active range were several orders of magnitude below that measured in pits, the metal may not be at an active dissolution potential.

Although this theory explains some of the pitting corrosion phenomena, several difficulties emerge during a more detailed investigation. It is difficult to explain the potential drop within pits which, in some cases, should be more than 1 V. Such a high overvoltage can scarcely be expected in the pit electrolyte which, with its high salt concentration and high acidity, must have a relatively high conductivity.

1.1.1.2. Salt film theory

A salt film theory was proposed[4,11,19,20,21,22,23] to explain the large potential drop within the pits to support the active dissolution theory. According to this theory, the pit surface is covered with a thin salt layer formed by the metal cations and the aggressive anions, because sufficient changes in concentration can

occur adjacent to an active metal surface to cause precipitation. The assumption of a precipitated salt film at the pit surface is supported by the observation of the polished pit surface[24]. This film is supposed to have a property quite different from that of the passive layer, and prevents the formation of the passive oxide on the pit surface by its presence. Strehblow, et al.,[25,26] suggested that the stability of a corrosion pit is due to a salt layer at the pit surface. The detail of the salt films is summarized in Section 1.1.2.

1.1.1.3. Mass transport control theory

Evidence that mass transfer controls stable pitting has been widely discussed[23,27,28,29,30,31]. Pitting corrosion occurs only when the electric potential exceeds a minimum, called the critical pitting potential. Tester and Isaacs[32], Gaudet et al.[33] and Beck[11] suggested that the corrosion rate in this range of potential is possibly controlled by the diffusion rate of metal ions out of the pit. Various authors[34,35,36,37,38,39,40] have suggested that critical concentrations of ionic species must be exceeded for stable pit growth to occur. Boehni[27,41] observed that the real pits formed in stainless steels grow at a potential-independent rate at high potentials, suggesting a diffusion controlled mechanism.

Concerning the practical significance of a diffusion-controlled pit growth rate, it must be pointed out that this type of pit growth is not often observed since it requires high potentials.

1.1.2. Salt film formation and its properties

1.1.2.1. The condition for the salt film formation

The formation of a salt film is the result of metal dissolution with a high

rate at the metal surface within the pits[28,42,43]. Rosenfeld, et al.,[44] and Alkire and Beck[18,45] contributed arguments in favour of salt film formation even at very early stages of pit growth. On the other hand, Vetter and Strehblow[20,21], concluded from theoretical considerations that during the early stage of growth of a hemispherical pit, the metal chloride concentration within the pit indeed does increase but not sufficiently for precipitation to occur. Instead, they proposed an ion-conducting salt layer present on the metal surface resulting from adsorption of aggressive anions. In later stages of pit growth, the existence of a salt layer on anodic surfaces during steady state diffusion controlled dissolution of metal is now generally accepted[46,47,48,49,50].

The metal chloride at the sample surface has often been studied in galvanostatic experiments[51,52,53,54,55,56]. Strehblow and Wenners[56] studied the chloride layer formation by galvanostatic transient measurements on exposed cylindrical samples in solutions of high chloride concentrations with current densities in the range 1-100 A/cm^2. Under this experimental condition, the metal specimen surfaces were in a completely dissolving state without any passive part on the surface. A steep increase of the potential to some volts is observed after a transition time. The transition time does not depend appreciably either on the chloride concentration or the pH value with only the concentration of the cation and the applied current density having a pronounced influence on it. The transition time was interpreted as the total time required for the precipitation of a metal chloride at the electrode surface.

Boehni and Hunkeler[27,57] suggested that there is a critical potential for

the salt film formation, below which no salt can exist. The salt film formation potential changes with the composition of the alloy and does not depend significantly on the bulk concentration. It is suggested that a salt film is more stable than the passive film at potentials above this critical value[58].

1.1.2.2. The properties of the salt layer

Although salt films are of great importance and are necessary to explain the stability of steadily growing pits[18,26,42,59,60,61,62], only a few investigators[29,63] have studied the electrical properties of the solid salt films. Hunkeler, Krolikowski and Bohni[29] studied the salt film on nickel by impedance and transient measurements. They found that significant ohmic potential drops are presented within the salt film. It increases with time, pit depth and potential, and ranges between 100 and 700 mV. The electrical conductivity of the salt film is approximately $0.44 \times 10^{-4} \ \Omega^{-1} \cdot cm^{-1}$ The thickness of the salt film linearly increases with potential and varies between 3 and 8 μm. Vetter and Strehblow[21] suggested that the values of the layer thickness are 50 to 100 Å and consequently, not optically visible. Beck and Alkire suggested that typical values of the layer thickness are 40 to 190 Å [18]. Beck[11] reported a value of 110 μm for thickness of a metal chloride layer. Strehblow and Wenners[26,53] estimated the thickness of the salt layer by Faraday law and concluded that it could be 3.6 μm or less. They also reported that microscopic in situ observation of the metal surface does not give evidence of its presence. Grimm[63] investigated the salt film by impedance measurements and found that when the applied potential changes from 1 V to 3 V, the potential drop across the salt film increases from 0.702 V to 2.450 V, the thickness of the salt film increases from 30

to 90 Å, and therefore, the electric field strength ranges between 2.1×10^6 to 2.7×10^6 V/cm.

1.1.2.3. The structure of the salt film

Based on the observed large ohmic potential increase during galvanostatic transient measurements, Strehblow and Wenners[56] proposed that in the presence of chlorides, an adsorption layer or a thin pore-free salt film is formed at the beginning to prevent repassivation. This layer grows in thickness and finally a porous layer appears by precipitation from a saturated solution as shown in Figure 1.2. The
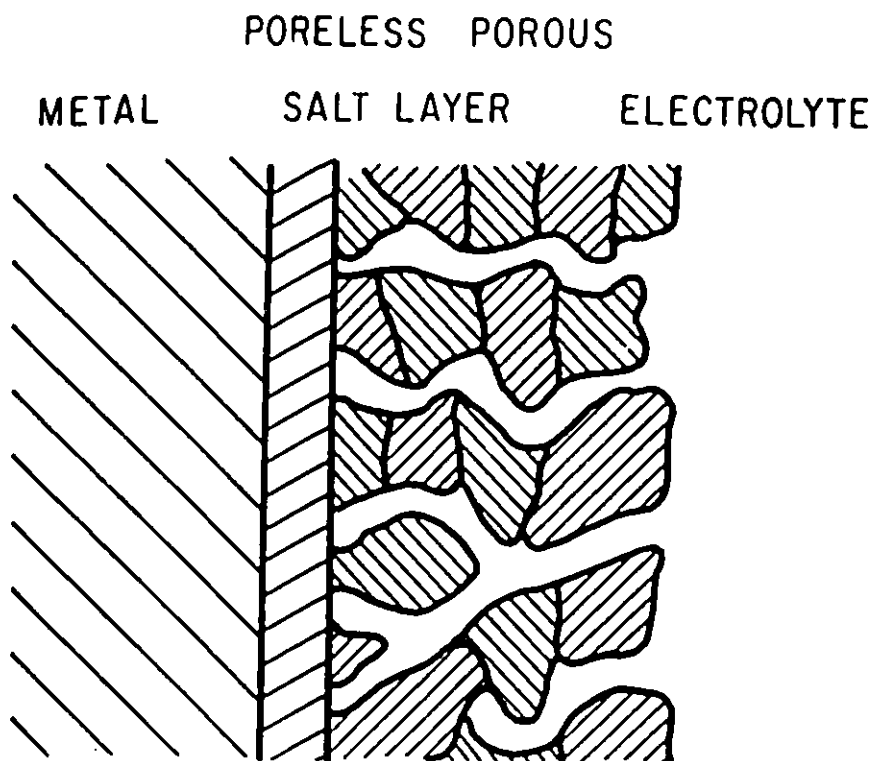
Figure 1.2 Schematic representation of the salt layers formed during dissolution at hight current densities[56].

thickness of the porous layer increases linearly with time. West et. al.[63,64], employed an impedance technique to study iron dissolution in concentrated $FeCl_3$. They assumed that ferrous ions transport through the film by migration. The transport mechanism cannot be completely characterized by either high-field or low field conduction. Consequently, a duplex film structure, consisting of a compact inner layer and porous outer layer, is assumed to exist. Beck[11,65] found that by stirring the precipitate formed at the bottom of a pit on titanium, a layered structure could be observed. Typically there was a compact layer about 10 μm thick that was next to the metal surface with a layer about 100 μm thick above it. Most of the precipitate was easily removed with a jet of water after experiments except for the inner layer that adhered to the surface.

1.1.2.4. Some concluding remarks

In summary, the contributions of the previous reported work have provided evidence of the existence of the salt film, examined the conditions of its formation, studied its properties and proposed its structure. However, there are certain weaknesses.

The transition times measured at the exposed cylindrical electrode cannot be regarded the same as in case of a corrosion pit because the geometry is quite different. In the case of a pit, transport is dependent on the shape and size of a pit, which also changes with time during the corrosion process.

Because the thickness of a salt film varies with time, the electrode potential or current density and mass transport rate of metal cations and anions, it is not surprising that the reported values are so scattered. Evidence from the direct

measurements of the properties of the salt film is still needed.

The duplex structure of the salt film proposed is also lacking direct experimental evidence. Furthermore, the previous researchers studied the salt film formed under high current densities, up to 100 A/cm² which only correspond to the early stage of pit growth. As a matter of fact, during pitting development, the current densities encountered are mostly lower than those values. It is known that the structure of the salt film may vary depending on the experimental conditions. Obviously, the low current density condition may be more close to a real pitting situation and should also be studied.

1.1.3. Local chemistry measurements

It has been observed that the environment inside an occluded cell differs greatly from the bulk solution[66,67,68,69] and the growth of pits is considered to be dependent upon the local conditions within the pits[70,71,72,73,74]. The restricted geometry of a cavity makes measurements difficult. This has led to the development of a variety of experimental techniques for determining the solution composition and potential within the localized sites. It is possible to classify these techniques into two groups: Ex situ measurements and in situ measurements.

1.1.3.1. Ex situ measurements

(1). Solution extraction and analysis

The solution extraction technique involves draining off solution from the cavity and analyzing for the various species of interest. This analysis may be immediate at the site of extraction, for example, by the method of Smith et al.[75], in which miniature pH electrodes were used to measure the pH of the solution

extracted at the tip of a stress corrosion crack. Indicator paper has also been used to measure the pH[76,77]. More commonly, microvolumes of solution are removed from the cavity and analyzed at a later stage[78,79,80,81], for example, Suzuki et al[82]. measured the concentration of metallic ions inside a pit by performing atomic absorption spectroscopy on solution aliquots removed from the pits.

(2). Freezing technique followed by solution analysis

The freezing technique involves freezing of the solution in a pit, extracting the frozen contents from the pit[83] or crevice[84] and analyzing for ionic species as the solution melts, using indicator papers. The freezing technique does not inspire confidence for most applications and its use has declined.

1.1.3.2. In situ measurements

(1). Isotope

The application of the isotope technique to the study of the localized corrosion has been reported recently. Mizuno[85] did in situ analysis of chloride ions adsorbed on an iron surface during pitting corrosion using a radioactive ^{36}Cl. It was found that after pits initiate, the concentration of the chloride ions on a pit surface increases linearly with time until it reaches a maximum value, then it becomes constant.

(2). Microelectrodes

The essential criterion for in situ measurement by electrodes is that probes should be sufficiently small with minimum perturbation of the system under study and hence this restricts the technique to the use of microelectrodes. A wide range of ion selective microelectrodes has been developed particularly in the field

of biological studies[66]. The application of these electrodes to the study of localized corrosion processes is increasing[62,87,88,89,90,91,92].

Microelectrode measurements have been employed to map the local conditions across pits or over a corroding sample surface. A scanning reference electrode was used by Isaacs, et al.[93,94,95], to measure the number of active pits in stainless steel and to make an in situ current map over a passive surface during pitting by using a vibrating microelectrode technique[92]. Tuck[96] used three types of microelectrodes: silver/silver chloride, tin/tin oxide and calomel, for potential scanning over a corroding metal surface. Butler, et al.[97], studied the variation in both pH and potential across a growing pit by using microelectrodes of antimony/antimony oxide for pH and silver/silver chloride for potential, respectively. It was found that the pH falls from about 8.0 at some distance from the pit to about 2.0 at the centre of the pit mouth.

The measurements of the local conditions inside a pit have also been developed. Micro-reference electrodes with a glass capillary of tip diameter ranging from 5 to 50 µm were used by different workers to measure the potential inside pits[8,10,11,98]. A bare Ag/AgCl microelectrode was employed to monitor the time dependence of chloride ion concentration within a hole, 15 mm in diameter and 30 mm deep[80]. A 5.5 mm diameter glass pH meter electrode was used to measure the pH inside a 5 to 7 mm diameter artificial pit[82]. In Tsuru and his co-workers' study[99], a small glass pH electrode, 2 mm in diameter, and a bare Ag/AgCl microelectrode were used to measure the local chemistry within an artificial pit.

The tungsten microelectrode for the measurement of pH was first

reported in a biological application. In 1954, Caldwell[100] used micro tungsten electrodes to investigate the intracellular pH of crab muscle. It was suggested[101] that tungsten electrodes could be used to record current flow in the extracellular clefts between glial cells. They were used to obtain isolated extracellular recordings from single nerve cells and their axons. They have been successfully used to record the action potentials of retinal ganglion cells and their unmyelinated intraocular axons in a rabbit, cat and monkey[102]. Practical methods were described in detail by Levick[103] and Merrill[104] for the construction of glass-coated tungsten microelectrodes. Nie, et al.[105], tried to use a tungsten probe with a tip 0.1 mm in diameter and 2 mm long protruding from a glass tube in a corrosion study. Working curves were given, but the selectivity coefficients for pH in the presence of cations were not measured.

From the brief review of the history for measuring the local conditions, it is seen that the local potential measurement is quite successful, however, the technique to measure the ionic species in a localized corrosion site still needed improvement. For ex situ measurements, there are two factors which must be taken into consideration: (1) interaction of the extracted solution with the atmosphere, and (2) the volume of solution extracted in relation to the volume of the pit. A deficiency in the in situ investigations is that the exposed area of the microelectrodes is too large to be used in pitting studies. As a consequence, this only provided the average change in the concentration of the ionic species in the localized region. Furthermore, there always exists the possibility of perturbing the environment in the pit with the

probe. Careful checks must be made to ensure that the overall pattern of growth is not affected.

1.2. Shortcomings of the current state of knowledge

(1).   Although the measurement of the local condition in a pit is very important for studying pitting processes, because of the localized nature of pitting and the difficulties associated with the small dimensions of active occluded cells, in situ measurements of pitting environments have not been very successful to date.

(2).   There has been no reported work about the direct in situ study of the salt film formation, its characteristics and its role on pit development by microelectrodes. Although the importance of salt layers during pitting is now generally accepted, the details are still far from clear and lacking of direct evidence.

(3).   There is no complete model which includes all the factors involved in pit growth to indicate which factor has the most important effect on the dissolution of the metal within the pits.

1.3. Objectives

Determination of the local environmental conditions within pits and the electrochemical response of the metal in the local environment is the most important feature in advancing understanding of localized corrosion processes. Thus, the present study was undertaken with the following objectives:

(1). building a comprehensive model

    a. to determine the local environmental conditions within pits;

    b. to evaluate the conditions for the formation of the salt layer; and

    c. to characterize the conditions necessary for the stabilization of pitting corrosion;

(2). testing the model by

    a. developing the microelectrodes which are suitable for the research of pitting corrosion and to study their characteristics;

    b. probing the local conditions within pits by in situ measurements by the microelectrodes;

    c. exploring the metal/solution interface during pitting corrosion and therefore to find whether there is a salt film formed at the pit bottom, and if yes;

    d. defining the conditions for salt film formation, the characteristics of the film and its role in pit development;

    e. studying the anodic electrode kinetics of nickel under the conditions corresponding to the various stages of pitting processes;

    f. and thus determine the controlling factor of the pit development.

Each of these components of the research is presented in detail in the following chapters of this thesis.

CHAPTER 2. MODEL DEVELOPMENT

In this work, a model of pitting development is proposed which considers the interfacial salt film, multiple species in solution, reaction equilibria, migration and diffusion. Nickel in 0.05 N sodium chloride solution was chosen as the system to model the pit development.

In order to apply fundamental knowledge about dissolution kinetics to pitting corrosion, it is necessary to characterize the local chemical environment within pits. The local chemical environment within corrosion pits is invariably different from the external bulk solution owing to transport and reactions which lead to the accumulation or depletion of ions inside the pit. Several authors have developed models to simulate conditions inside a corrosion pit[8,35,36,37,106,107,108]. Although these models may be used to describe the distribution of the ionic species within pits from the theoretical point of view, the common drawback is the lack of the experimental evidence. Based on the present understanding, it is possible to discard some of the simplifying hypotheses present in the previous models and to amplify these models by introducing additional features in an effort to more accurately simulate the phenomena involved in pit development. The major improvements of the proposed model over the previous ones in the literature are:

(1). Formation of a salt film at the pit bottom has been accounted for;

(2). The diffusivities are no longer arbitrarily taken as constants. Instead, they are

considered as functions of the concentrations of the species, based upon the information available in the literature;

(3). The moving boundary condition is included;

(4). Because the concentrations of the ionic species within a pit are very high, the activity coefficients of the species must be considered. A model, due to Pitzer[109], is used to calculate the activity coefficient of each species.

Figure 2.1 shows the schematic of the pit model. During growth of a pit, rapid anodic dissolution occurs within the pit while a cathodic reduction reaction takes place on adjacent surfaces. The dissolution of metal tends to produce an excess of positive ions within the pit, with the chloride ions inward migration to maintain
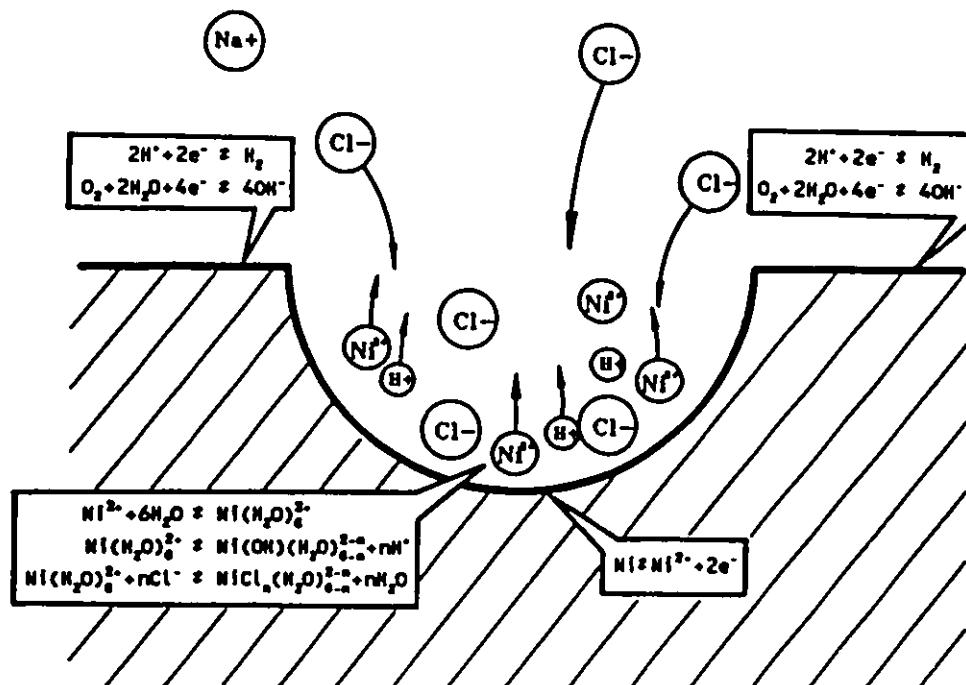
Figure 2.1 Schematic of the pitting corrosion processes.

electro-neutrality. The hydration and the hydrolysis processes for metal ions and the chloro-complex formation take place after the anodic reaction. The hydrolysis of metal ions produces protons in the pitting site. Thus, there are high concentrations of chloride and hydrogen ions inside the pit.

2.1. Speciation, equilibria, reaction and activity coefficients

For a pitting system represented in Figure 2.1, the species, j, included in the model are listed and numbered for convenience as shown below:

$0 : Ni^{2+}$	$1 : Ni(H_2O)_6^{2+}$	$2 : H_2O$
$3 : Ni(OH)(H_2O)_5^+$	$4 : H^+$	$5 : Ni(OH)_2(H_2O)_4$
$6 : Cl^-$	$7 : NiCl(H_2O)_5^+$	$8 : NiCl_2(H_2O)_4$
$9 : Na^+$		
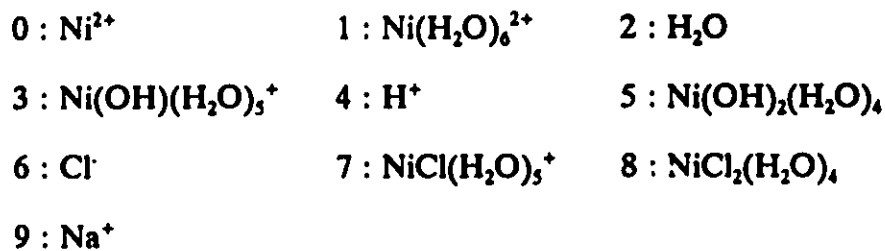
The dissolution of nickel into an aqueous solution takes place within a pit

$$Ni \rightleftharpoons Ni^{2+} + 2e^- \qquad [2.1]$$

The reaction is assumed to be followed by hydration and the hydrolysis processes for nickel ions which may be represented by:

$$Ni^{2+} + 6H_2O \overset{K_1}{\rightleftharpoons} Ni(H_2O)_6^{2+}, \qquad K_1 = \frac{a_1}{a_0 a_2^6} \qquad [2.2]$$

$$Ni(H_2O)_6^{2+} \overset{K_2}{\rightleftharpoons} Ni(OH)(H_2O)_5^+ + H^+, \qquad K_2 = \frac{a_3 a_4}{a_1} \qquad [2.3]$$

$$Ni(OH)(H_2O)_5^+ \overset{K_3}{\rightleftharpoons} Ni(OH)_2(H_2O)_4 + H^+, \qquad K_3 = \frac{a_4 a_5}{a_3} \qquad [2.4]$$
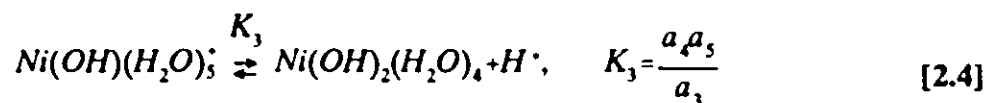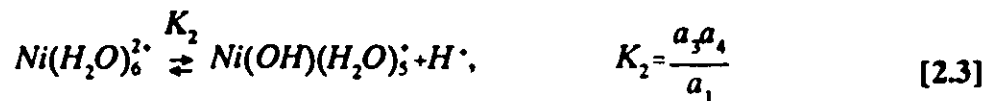
In chloride containing solutions, Ni^{2+} is expected to form chloro-complexes as described by several authors[110,111,112,113,114,115,116,117]. The following equilibrium reactions are written to describe the chloro-complex formation:

$$Ni(H_2O)_6^{2+} + Cl^- \overset{K_4}{\rightleftharpoons} NiCl(H_2O)_5^+ + H_2O, \qquad K_4 = \frac{a_4 \beta_2}{a_1 a_6} \qquad [2.5]$$

$$NiCl(H_2O)_5^+ + Cl^- \overset{K_5}{\rightleftharpoons} NiCl_2(H_2O)_4 + H_2O, \qquad K_5 = \frac{a_5 \beta_2}{a_6 a_7} \qquad [2.6]$$
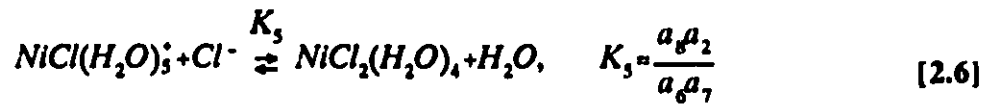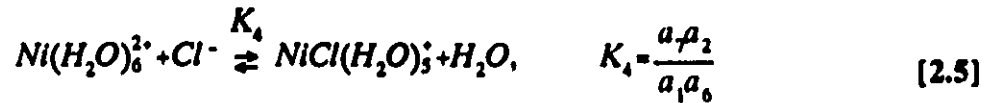
Although still an area of active research[110,115,116], there is clear evidence for formation of the 1:1 complex, $NiCl(H_2O)^+$, [111,112,113,114]. Formation of the 1:2 complex, $NiCl_2(H_2O)_4$ has also been reported[110,114]. Anion complexes such as $NiCl_4(H_2O)^{-2}_2$ do not form in aqueous solution, even in the presence of very high chloride concentrations[112,113,114,118].

2.2. Mass balance and transport equations

An equation describing a material balance on each species, specifying how the concentration changes with time in response to transport and chemical reaction is[119]:

$$\frac{\partial c_j}{\partial t} = -\nabla J_j + R_j \qquad [2.7]$$

In a multicomponent solution, the flux of the species j can be expressed by Equation [2.8][120,121], describing how the species moves under the influence of a concentration gradient, an electric field, and fluid motion.

$$J_j = -\sum_i D_{ji} \nabla c_i - u_j c_j \nabla \phi + v_j c_j \qquad [2.8]$$

The first two terms in the flux equation represent transport by diffusion and migration, respectively. v_d is equal to the rate of pit growth in depth.

The mass conservation of the species containing nickel is given by:

$$J_0 + J_1 + J_3 + J_5 + J_7 + J_8 + \frac{h_f \rho_f}{t M_f} = \frac{i}{n_0 F}$$ [2.9]

The last term in Equation [2.9] corresponds to the nickel consumed by the formation of the salt film. The mass conservation of the species containing H^+ is expressed by:

$$12 J_1 + 2 J_2 + 11 J_3 + J_4 + 10 J_5 + 10 J_7 + 8 J_8 + 12 \frac{h_f \rho_f}{t M_f} = 0$$ [2.10]

The mass conservation of the species containing O^{2-} is represented by:

$$6 J_1 + J_2 + 6 J_3 + 6 J_5 + 5 J_7 + 4 J_8 + 6 \frac{h_f \rho_f}{t M_f} = 0$$ [2.11]

The mass conservation of the species containing Cl^- is represented by:

$$J_6 + J_7 + 2 J_8 + 2 \frac{h_f \rho_f}{t M_f} = 0$$ [2.12]

The mass conservation of the species containing Na^+ is represented by:

$$J_9 = 0$$ [2.13]

The set of equations is completed with a charge neutrality condition:

$$\sum n_j c_j = 0$$ [2.14]

Table 2.1 Input Parameters for the Transport Model

Symbol	Value	Description
i F R T	0.0637 (A/cm^2) 96486 (C/eq) 8.314(J/mol/K) 295(K)	current density Faraday constant gas constant temperature

Transport	Parameters		
Species	$Dx10^5$ (cm^2/s)	n_j	Ref.
Ni^{2+}	Table 2.2	2	118
$Ni(H_2O)_6^{2+}$	Table 2.2	2	118
H_2O	Table 2.2	0	118
$Ni(OH)(H_2O)_5^+$	0.73	1	69
H^+	9.31	1	69
$Ni(OH)_2(H_2O)_4$	0.78	0	69
Cl^-	Table 2.2	-1	118
$NiCl(H_2O)_5^+$	0.47	1	106
$NiCl_2(H_2O)_4$	Table 2.2	0	118
Na^+	1.33	1	69

Equilibrium	Constants	
Symbol	Value	Ref.
K_1	6.3×10^4	124
K_2	1.0×10^{-9}	123
K_3	7.94×10^{-10}	69
K_4	0.3	111
K_5	0.233	106

The input parameters for the modelling calculation available from literature are given in Table 2.1. The hydration constant[122,123] in medium C_4H_9OH is $10^{5.8}$. In aqueous solution, nickel ions and water have weaker attraction than that in C_4H_9OH, and hence as a rule of thumb, the equilibrium constant will be smaller

by about 1 or 2 orders of magnitude[124]. In this model, a value of $10^{4.8}$ was used. For the first complexation constant, K_3, in pitting solution under stagnant conditions the value of 0.3 reported by Netzel and Droll[111] was used. It is reported that the pH of the solution has no effect on the saturation concentration for nickel chloride[32,57,125], which is 4.55 mol/l at room temperature[57]. This value was used for setting a boundary condition for the salt layer.

Table 2.2 Diffusion coefficients[118]

C	$D(Ni^{2+})$	$D(Cl^-)$	$D(H_2O)$	$D(NiCl_2)$
(Moles/l)	$X\ 10^5$	(cm^2/s)		
0.0	0.705	2.030	2.235	1.250
0.1	0.688	1.850	2.278	1.050
0.2	0.671	1.775	2.134	1.042
0.5	0.623	1.580	1.975	1.052
1.0	0.542	1.317	1.736	1.091
1.5	0.460	1.101	1.045	1.114
2.0	0.391	0.914	1.102	1.096
2.5	0.322	0.748	0.979	0.963
3.0	0.261	0.598	0.801	0.844
3.5	0.207	0.436	0.630	0.717
4.0	0.157	0.337	0.433	0.588

2.3. Assumptions used in building a model

Because of the lack of information from the literature and complications in mathematical treatment, such as irregular shape of the natural pits, a number of simplifications must be made to obtain a tractable physical model.

In the usual approximation, the cross effects of the concentration gradients of all species in the solution on the diffusion flux of species j, the first term in Equation [2.8], can be expressed by $D_j \nabla c_j$. Where D_j is the measured phenomenological diffusion coefficient of species j and includes all cross effects of species on the diffusion flux of species j. Then u_j in Equation [2.8] is determined by the Nernst-Einstein relation[126]:

$$u_j = \frac{n_j F D_j}{RT}$$

[2.14]

The second assumption is a one dimensional pit model. It is reported that the rate law for pit growth can be very similar for the model pits and natural growing
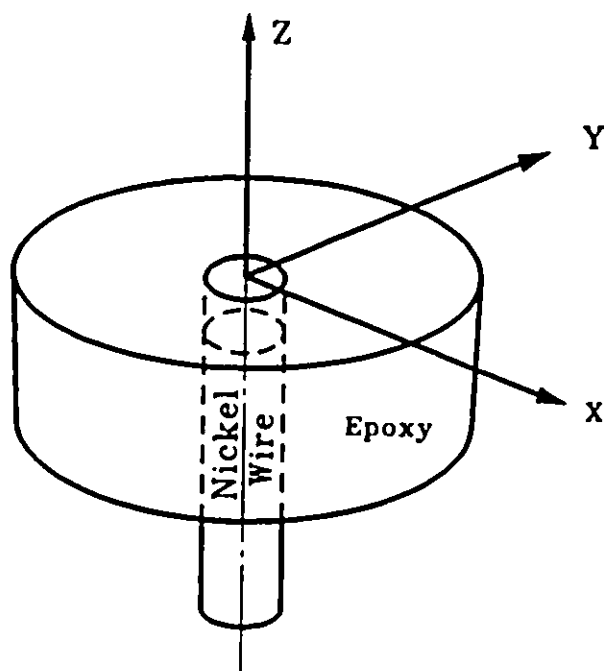
Figure 2.2 Structure of the "lead-in-pencil" pit, with co-ordinates defined.

pits[127]. Therefore, nickel model pits were used. Figure 2.2 shows the structure and co-ordinate system for a "lead-in-pencil" pit. It comprises passive wall and surface, and an active bottom represented by the cross-section of the nickel wire. Z is the position along the pit axis direction with zero point at the pit mouth and the negative direction being toward the bottom of the pit. During the growth of a pit, dissolution of the nickel occurs only at the bottom of the pit. In this way a unidirectional pit model is obtained, with a considerable simplification in mathematical treatment. The flux of the species j, J_j, can take the simple form:

$$J_j = -D_j\frac{\partial c_j}{\partial Z} - u_j c_j\frac{\partial \phi}{\partial Z} + v_j c_j \qquad [2.16]$$

This assumption is not valid for pits with growth rate larger in radius direction than in depth direction. From this study, it can be deduced that this type of pits will not keep growing. Therefore, it is reasonable to exclude this type of pits in the model of pit development.

The third assumption is that the ions in the present model are considered to be in local equilibrium. This assumption is made based on the fact that the hydration and the hydrolysis processes are rapid[128], with equilibrium being reached after only a few microseconds[129] and the rate of complexation is fast with the equilibrium state with respect to the other processes under consideration[106].

Fourth, as a boundary condition, the activities of the ions at the opening of the pit, Z=0, are assumed to be equal to those in the bulk solution. The potential at the pit mouth is assumed to be equal to the open circuit potential.

Next, the activity of the water is assumed to be one in all positions even

though the concentration of the ionic species is the very high. Because of the lack of the parameters needed in the Pitzer model for complexes, the activity coefficient for all complexes was assumed to be unity.

The final assumption in this model is that the system is taken to be at quasi-steady state. A mathematical treatment for a unidirectional pit was made to verify this assumption(see Section 2.5). The results show that the quasi-steady state is reached once the salt film is formed. Since the model is used to study the stage when a salt film is formed, the quasi-steady state approximation is appropriate in the time range of interest.

2.4. Results of the modeliing calculation

Equations [2.2]-[2.6] and [2.9]-[2.14] represent a system of nonlinear equations. To solve these equations simultaneously, the following numerical procedure is implemented. It is noted that only Equations [2.9]-[2.13] of the system contain the derivatives of the variables. The system is then linearized with respect to these derivatives by eliminating Equations [2.2]-[2.6] through substitution. The resulting system of differential equations is then numerically solved by the Runge-Kutta method[130]. The model due to Pitzer[109](see appendix B) is used to calculate the activity coefficient of each species.

The calculated results are shown in Figure 2.3 where it is found that the activity of the nickel-containing species increases with the distance from the pit mouth. Due to the migration, there exists an accumulation of chloride ions and a depletion of sodium ions inside the pits, relative to the bulk solution. The activity

variation of the sodium ions, Ni(OH)$^+$, Ni(OH)$_2$ and protons is very small relative

to the scale used in Figure 2.3 and close to the abscissa, therefore, the curves are

difficult to see. The activity of uncomplexed chloride ions at the bottom of the pit

is about 92 times the bulk activity. The chloride ion is known to be aggressive and

may be important in maintaining pit stability. The results of Figure 2.3 illustrate

clearly the significant difference between the electrolyte inside the pit and the bulk

solution.

In the calculation, the depth at which c(tot Ni)•c(tot Cl)^2 reached the
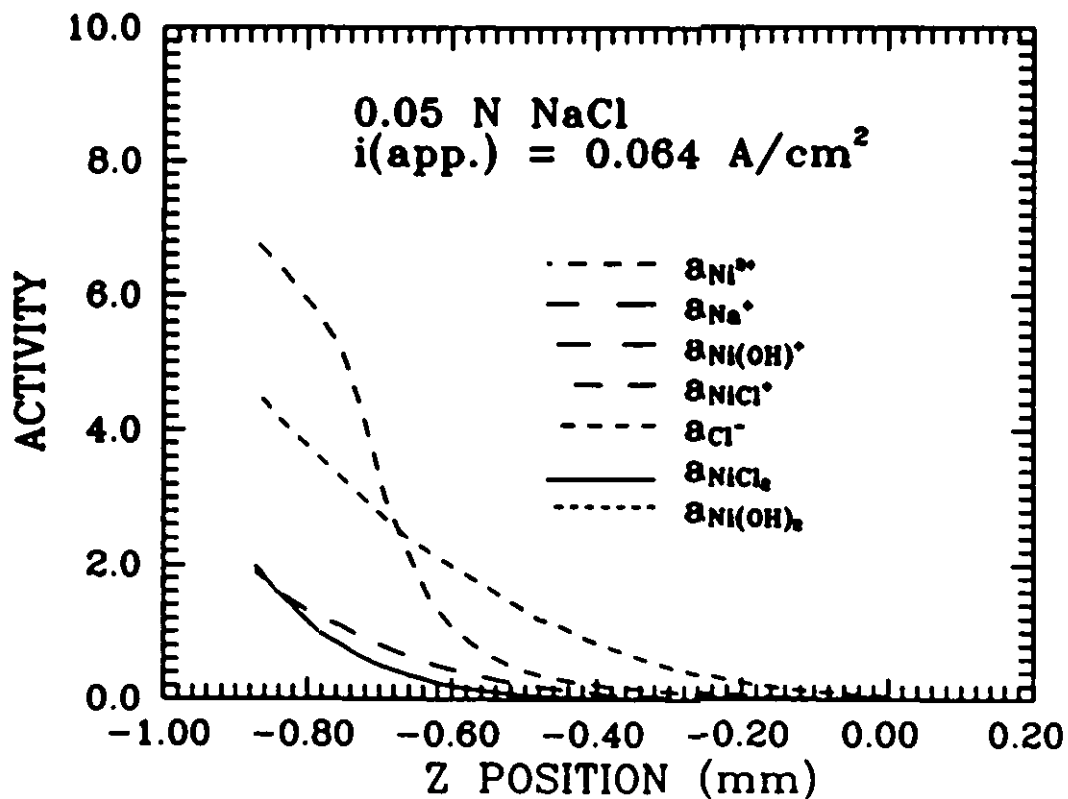
Figure 2.3 Theoretical determined distribution of the activity of the species as a function of the distance from the pit mouth
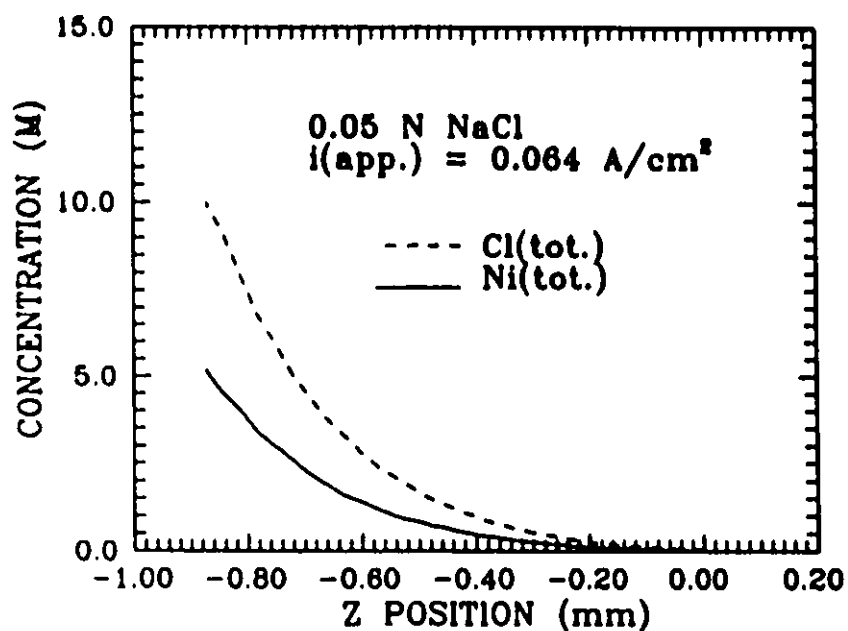
Figure 2.4 Theoretical determined distribution of total concentration of the nickel-
containing species and chloride-containing species as a function of the
distance from the pit mouth.

solubility product(K_{sp}), is designated as the critical depth for the salt layer formation.

Figure 2.4 shows the theoretically determined distribution of total concentration of

the nickel-containing species and chloride-containing species as a function of the

distance from the pit mouth. According to the calculations, when the pit depth is

larger than 0.88 mm, conditions at the bottom of the pit approach a situation in

which the precipitation of a salt film may occur.

2.5. Verification of the assumption of the quasi-steady state

In order to verify the assumption of the quasi-steady state, Equation [2.7]

can be used. To simplify the estimation, the possibility of secondary reactions in

which the products of the electrolysis take part are excluded. For a unidirectional pit model, Equation [2.7] can be simplified as:

$$\frac{\partial c_j}{\partial t} = -\frac{\partial J_j}{\partial Z} = \frac{\partial}{\partial Z}(D_j \frac{\partial c_j}{\partial Z}) + \frac{\partial}{\partial Z}\left[(u_j \frac{\partial \phi}{\partial Z} - v_d)c_j\right]$$ [2.17]

The current density in the solution results from the movement of the charged species and can be expressed as

$$i = F\sum_j n_j J_j$$ [2.18]

From Equations [2.16] and [2.18], the following expressions can be deduced:

$$\frac{\partial \phi}{\partial Z} = \frac{\left[(-i) - F\sum_j n_j D_j \frac{\partial c_j}{\partial Z} + Fv_d \sum_j n_j c_j\right]}{F\sum_j n_j \mu_j c_j}$$ [2.19]

The boundary conditions at the pit mouth are

$$c_j = c_{bulk};$$ [2.20]

The boundary conditions at the pit bottom are

$$J_{cl} = 0$$

$$J_{Na} = 0$$

$$J_{Ni} = \frac{i}{n_{Ni}F}$$ [2.21]

$$h = h_i + v_{pit} t$$

In Equations [2.21], h is substituted by $h_i + v_{pit} t$ to account for the pit

deepening. The parameters used in the calculation are listed in Table 2.1. It is assumed that v_{pit} = 2.178x10^{-6} cm/s before surface layer formation and v_{pit} = 2.807x10^{-8} cm/s after the surface layer formed.

The initial condition is

$$at\ t=0,\ c_j=c_{bulk} \tag{2.22}$$

The calculation was performed on the McMaster University VAX mainframe computer by PDECOL (General Collocation Software for Partial differential Equations)[31] in TOMS (Transactions on Mathematical Software) Library.

The solutions which satisfy the differential equation [2.17] and the conditions in Equations [2.20]- [2.22] are shown in Figures 2.5, 2.6 and 2.7. It is found that the enrichment rate of the ionic species at any specific position inside a pit increases with time until the salt film forms in the pit bottom. Take a point $Z=0.7$ mm from Figure 2.5 as example, one can see that when time changes from 560 minutes to 620 minutes, chloride concentration changes from 0.43 M to 0.87 M within 60 minutes, at later stage, when time changes from 680 minutes to 685 minutes, the chloride concentration changes from 4.69 M to 8.96 M within 5 minutes. At time 685 minutes and later, the concentration of the nickel and chloride ions at the bottom of the pit reaches the saturated value, and a surface layer will be formed. Due to the salt film growth, the receding rate of the solution/salt film interface is smaller than the pit deepening rate before the formation of the film. At this stage, the change in the concentration of the chloride ions with time is very small. The
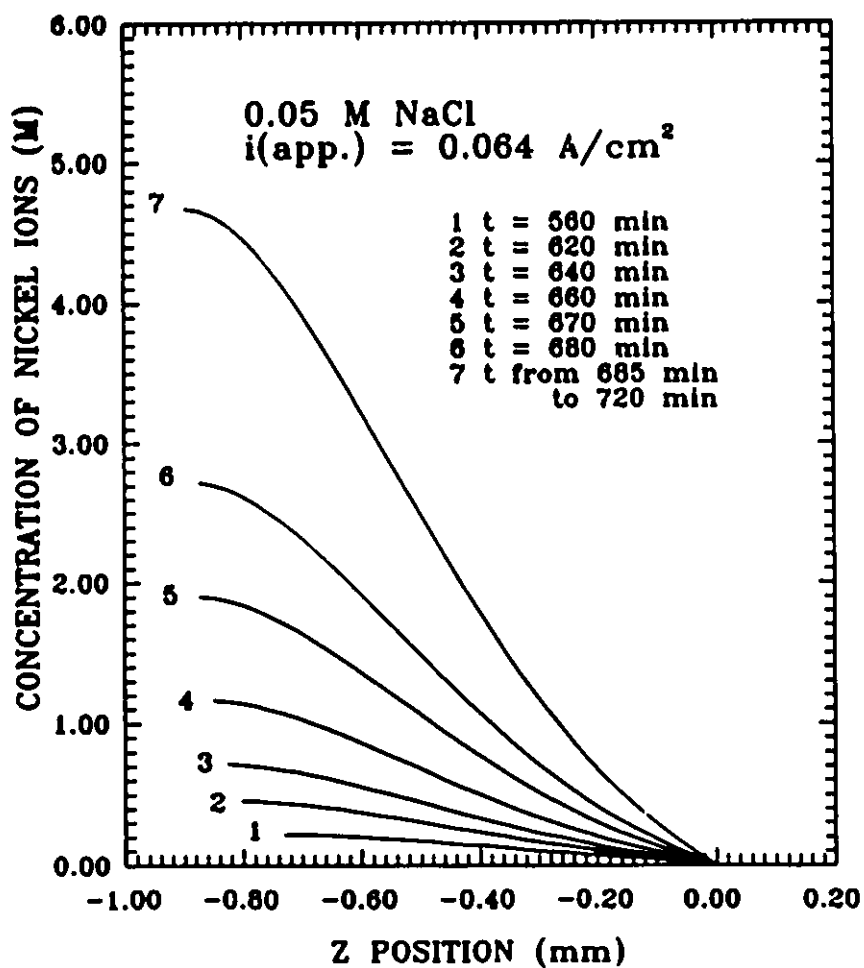
Figure 2.5 Variation of concentration of nickel ions as a function of distance from the pit mouth at different times.
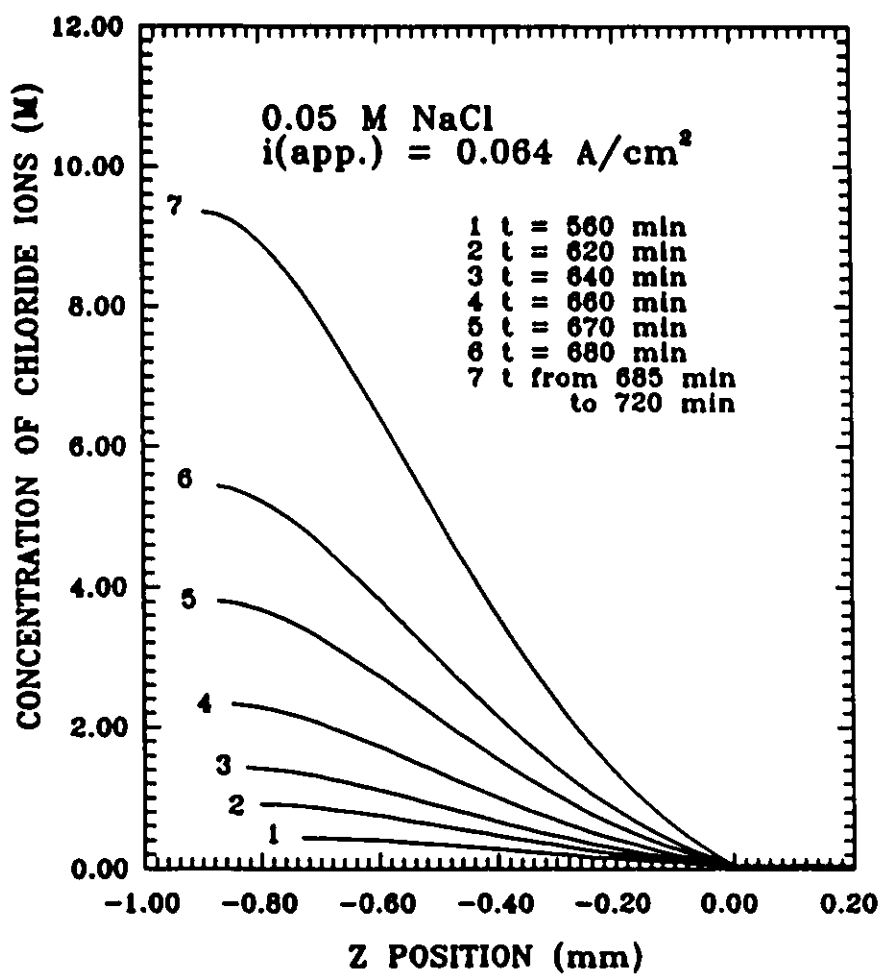
Figure 2.6 Variation of concentration of chloride ions as a function of distance from the pit mouth at different times.
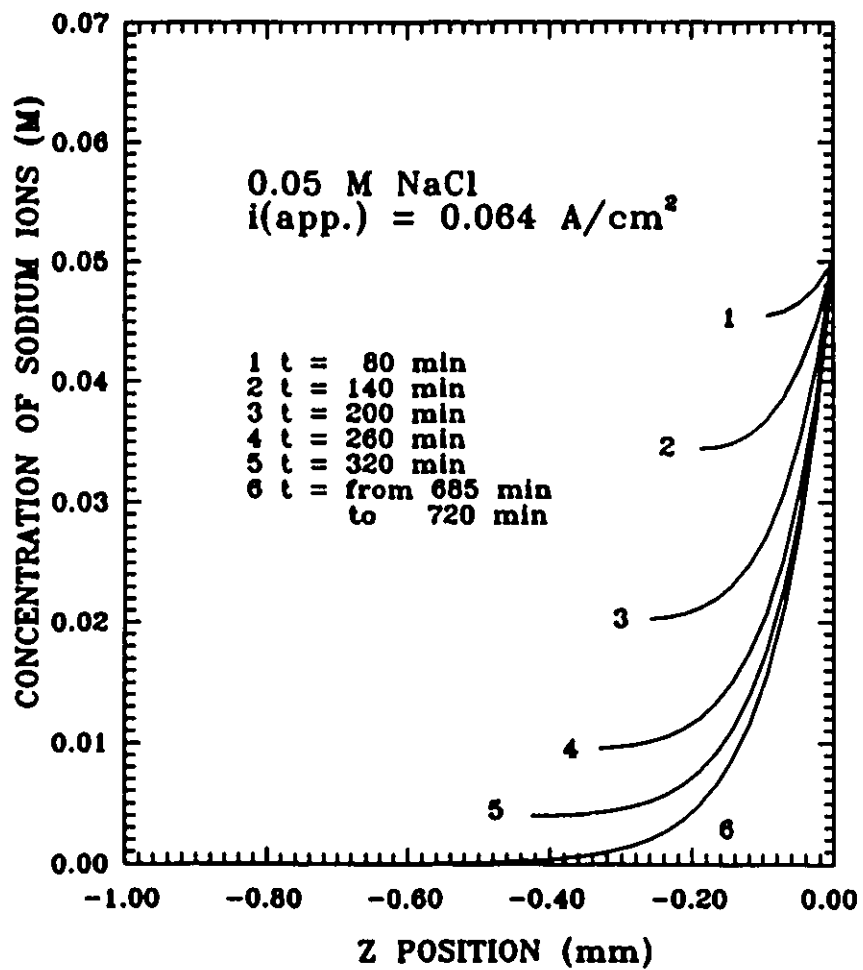
Figure 2.7 Variation of concentration of sodium ions as a function of distance from the pit mouth at different times.

concentration variation of the nickel ions follows the same treno. Only then, is the assumption of the quasi-steady state appropriate. At localized corrosion sites, one should be careful about the assumption of quasi-steady state, even though most authors[9,34,35,37,106] invoke it.

Figures 2.8 and 2.9 show that the concentration of the chloride and nickel ions at the pit bottom increases with the pit depth, and the deeper the pit, the faster the increase. This is because the transport processes are slow with respect to the movement of the boundary, resulting in accumulation of the nickel and chloride ions
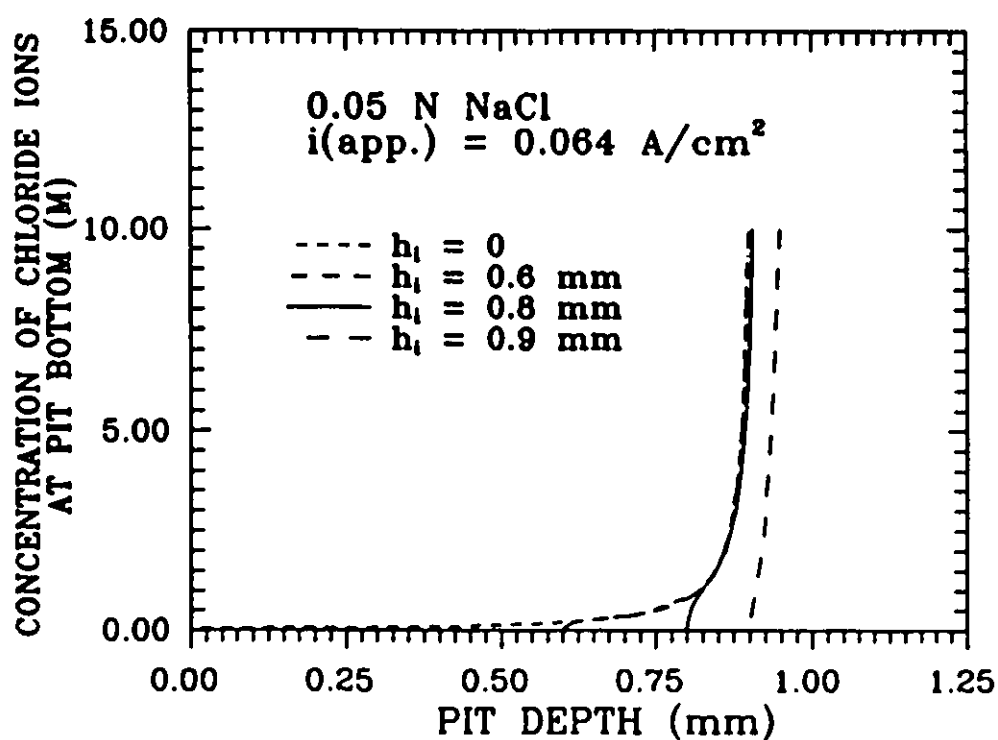
Figure 2.8 Concentration of chloride ions at the pit bottom as a function of pit depth.

at the pit bottom. For the conditions chosen for this model, when the pit depth
reaches 0.90 mm, the enrichment of the chloride and nickel ions is so large that the
ionic product ($c_{Ni^{2+}} \cdot c_{Cl^-}{}^2$) is equal to the solubility product(K_{sp}). As previously
mentioned, this depth is defined as the critical depth at which the salt layer will be
formed. This critical depth is independent of the initial pit depth as shown in Figures
2.8 and 2.9. When the initial depth is 0.90 mm, the chloride and nickel ions increase
immediately to the saturated value. The critical depth for the salt film formation
obtained here is not equal to 0.88 mm, the value calculated by the steady state
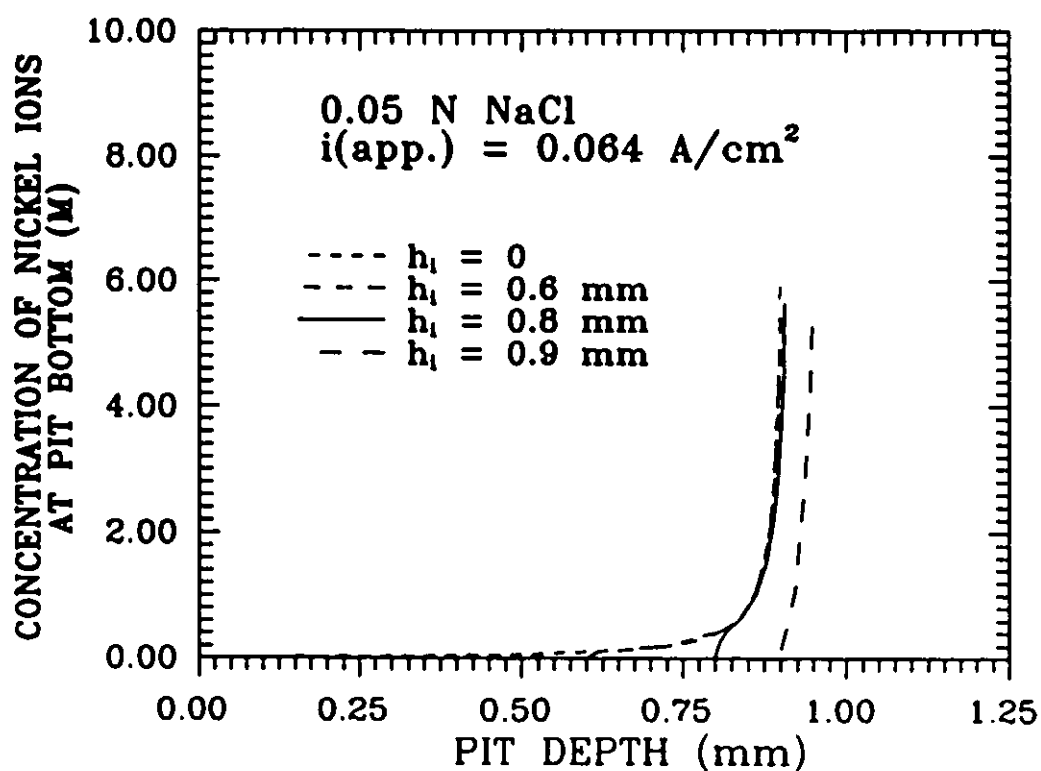
Figure 2.9 Concentration of nickel ions at the pit bottom as a function of pit depth.

model. This discrepancy may be due to excluding the possibility of secondary reactions of nickel ions.

2.6. Summary of the results

The results of the modelling calculation can be summarized as follows:

(1). The distributions of the species within a nickel pit in 0.05 N NaCl solution are obtained. There exist accumulations of the nickel-containing species, chloride ions and a depletion of sodium ions inside the pits, relative to the bulk solution. The activity of uncomplexed chloride ions at the bottom of the pit is about 92 times the bulk activity. The results illustrate clearly the significant difference between the electrolyte inside the pit and the bulk solution.

(2). As a pit grows, the diffusion length becomes longer, the transport processes are slow with respect to the movement of the boundary. As a result, the accumulation rate of nickel and chloride ions within a pit increases with the pit depth until a salt film is formed at the bottom of the pit. Only then, is the assumption of the quasi-steady state appropriate.

(3). It is predicted that critical condition for the salt film formation is the pit depth, at which the concentration of the nickel and chloride ions at the bottom of the pit reaches the saturated value. This pit depth is defined as the critical depth or transition depth for the salt film formation.

(4) The calculated results also show that the critical pit depth is independent on the initial pit depth.

Results from (2) to (4) are the consequence of the improvement of the proposed model for pit development over the previous models in the literature.

2.7. Direction of experiments for model testing

The mathematical models developed have enabled a more complete understanding of the interaction of mass transport and electrochemical processes in pits and predictive nature has provided a coherent basis for experimentation. However, mathematical models, despite their apparent complexity, necessarily represent a simplified picture of reality. Experimental measurements are therefore imperative in providing a test of model predictions and a more representative database. In the following chapters, emphasis will be given to experimental technique development and experimental results and where appropriate, modelling will be used to provide the framework for interpreting and explaining these results.

CHAPTER 3. DESIGN, CONSTRUCTION AND CHARACTERIZATION OF MICROELECTRODES

The experimental method is based on the use of microelectrodes developed to measure the local properties of pitting sites. The electrodes are characterized through studies of their potential stability, spatial resolution, and the interference of ions, other than the detected one, involved in the corrosion of nickel.

3.1. Development of microelectrodes

The probes necessary for localized corrosion analysis are a. a chloride ion probe, b. a probe to determine the local electric potential, and c. a pH probe. The probes developed in this study are shown schematically in Figure 3.1. The optical micrographs of a chloride probe and a pH probe (Figure 3.2) show the details of the probe tips.

3.1.1. Chloride ion probe

The structure of a chloride ion probe is shown in Figure 3.1. a. and Figure 3.2. a. The freshly-cut end of a 0.13 mm diameter silver wire coated with teflon was treated in concentrated nitric acid for 1 minute, and then chloridized by anodically polarizing at 0.16×10^{-3} A/cm^2 for 5 hours in 0.1 N hydrochloric acid. This treatment produces a layer of silver chloride at the tip. Prior to use, electrodes were aged in 0.1 N hydrochloric acid for 24 hours to stabilize their potential[112].

37
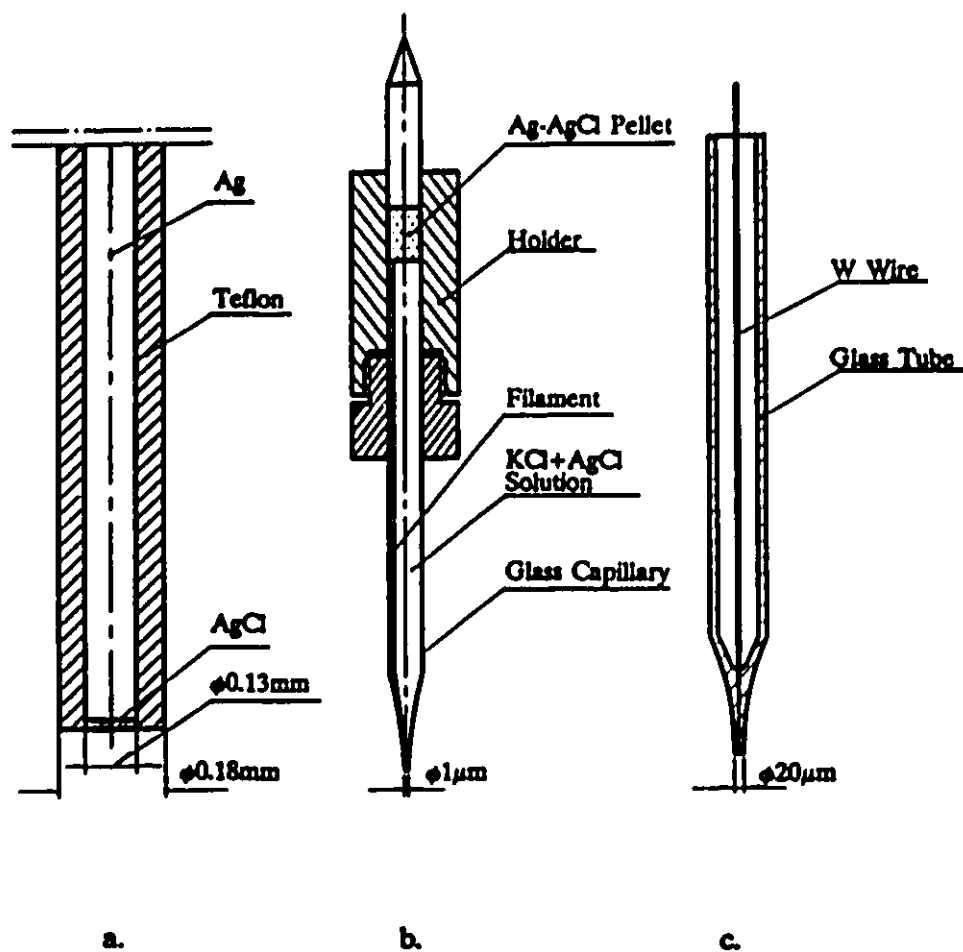
Figure 3.1 Schematic diagram of the micro-electrodes: (a). the chloride ion probe, (b). the potential probe, and (c). the pH probe.

During operation, the electrode reaction at the surface of the silver wire is expressed as:

$$AgCl + e^- \rightleftharpoons Ag + Cl^- \qquad [3.1]$$

This electrode reaction is reversible with respect to the chloride ion activity. The rate of precipitate exchange reaction for silver halide precipitates has been found to be
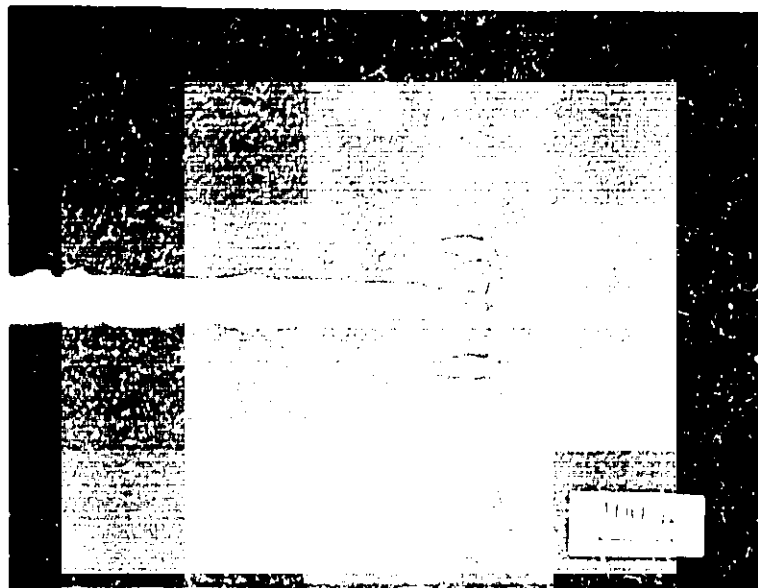
a
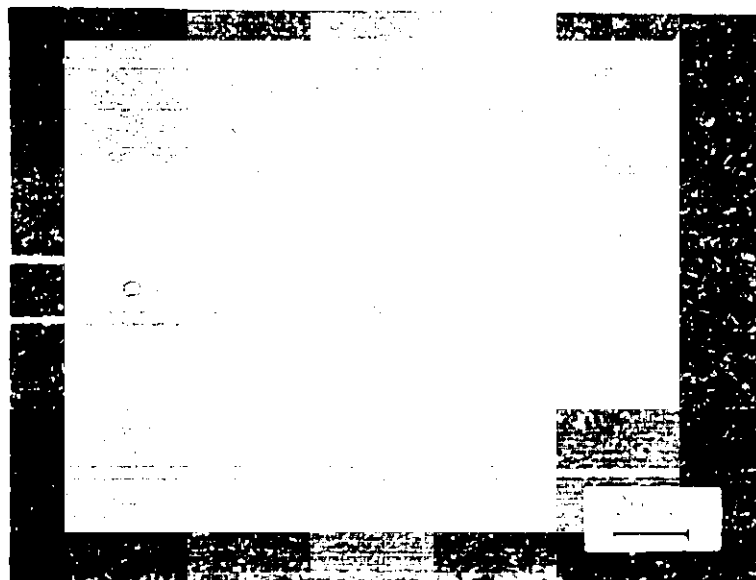
b

Figure 3.2 Optical micrographs of (a). a chloride probe and (b). a pH probe.

fast[131], which is important because of the response time of the electrode. Its equilibrium potential follows the Nernst equation given by:

$$E_0 = E^o - \frac{RT}{F} \ln a_{Cl^-}.$$

[3.2]

3.1.2. Ag/AgCl reference probe

Figure 3.1. b. shows the structure of the potential probe. A glass capillary is filled with 0.5 N KCl+AgCl solution, connecting with a Ag-AgCl pellet. An inner filament within the barrel facilitates rapid filling. A commercial holder* containing the Ag-AgCl pellet and capillary was used.

Because the activity of chloride ions in the filling solution is fixed, Equation [3.2] suggests that the potential of the probe is constant. This microelectrode can then be employed as a potential reference probe.

3.1.3. pH Probe

The structure of the pH probe used in this work is shown in Figure 3.1. c. It is composed of a tungsten wire placed within a glass tube, following which both wire and tube are hot drawn to a fine tip, thereby firmly encasing the wire in the glass with the exception of the tip. The manufacturing procedures[103,104] include straightening and etching the tungsten wire and glass insulation by pulling very gently through an induction heating coil. Practical methods for the construction of glass coated tungsten microelectrodes were described in detail by Levick[103] and Merrill[104]. Only approximately 1 μm of the tip of the tungsten wire, with a diameter of 10 μm,

---

*   Available from World Precision Instruments, Connecticut, USA.

is subsequently exposed to the solution as shown in Figure 3.2. b. The total probe tip diameter is 20 μm.

The possible reactions involved are complex. According to Pourbaix[134], tungsten and its oxides may exhibit the following equilibrium reactions, at the potentials noted (pH = -log a_{H^+}):

$$W + 2H_2O \ = \ WO_2 + 4H^+ + 4e^-$$

$$E_{0,WO_2/W} \ = \ -0.119 - 0.0591 pH$$

$$2WO_2 + H_2O = W_2O_5 + 2H^+ + 2e^-$$

$$E_{0,W_2O_5/WO_2} \ = \ -0.031 - 0.0591 pH$$

$$W_2O_5 + H_2O = 2WO_3 + 2H^+ + 2e^-$$

$$E_{0,WO_3/W_2O_5} \ = \ -0.029 - 0.0591 pH$$

[3.3]
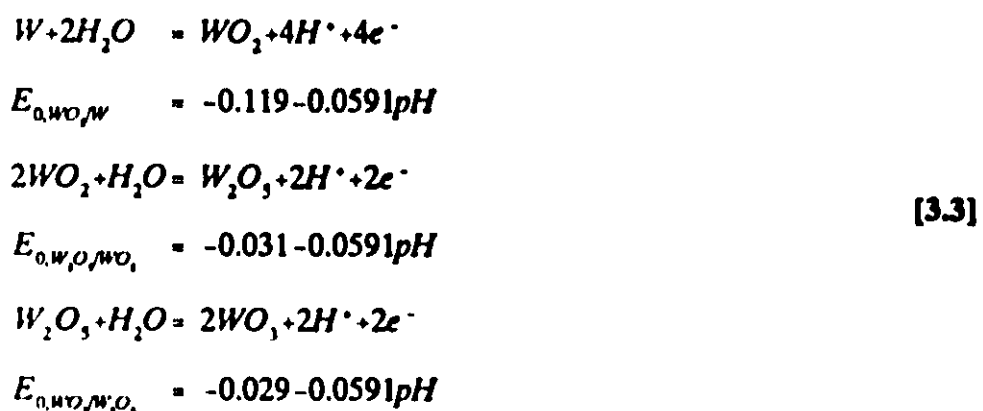
Regardless of the precise reaction operating, because of the involvement of H^+ ions in each case, the equilibrium potential between tungsten and its oxides will be a linear function of pH. In spite of the very high chloride ion concentration in the solutions of interest, tungsten is thermodynamically unlikely to form complexes with chloride ions[135]. The pH probes were conditioned for at least five hours in the solution being investigated before the measurements were taken, in order to dissolve any air-formed oxide and to establish a stable new oxide film in the solution.

3.2. Characterization of microelectrodes

Before being used in specific localized corrosion measurements, the electrodes were calibrated, and their stabilities and spatial resolution were

determined. Interference effects on the chloride and pH probes by other ions were also measured. A saturated calomel electrode was employed as the reference electrode in all electrochemical measurements. All the experiments were performed at 20 ± 1 °C.

3.2.1. Calibration

Figure 3.3 is the calibration curve of the chloride ion probe, obtained by measuring the electrode potential in a series of sodium chloride solutions with
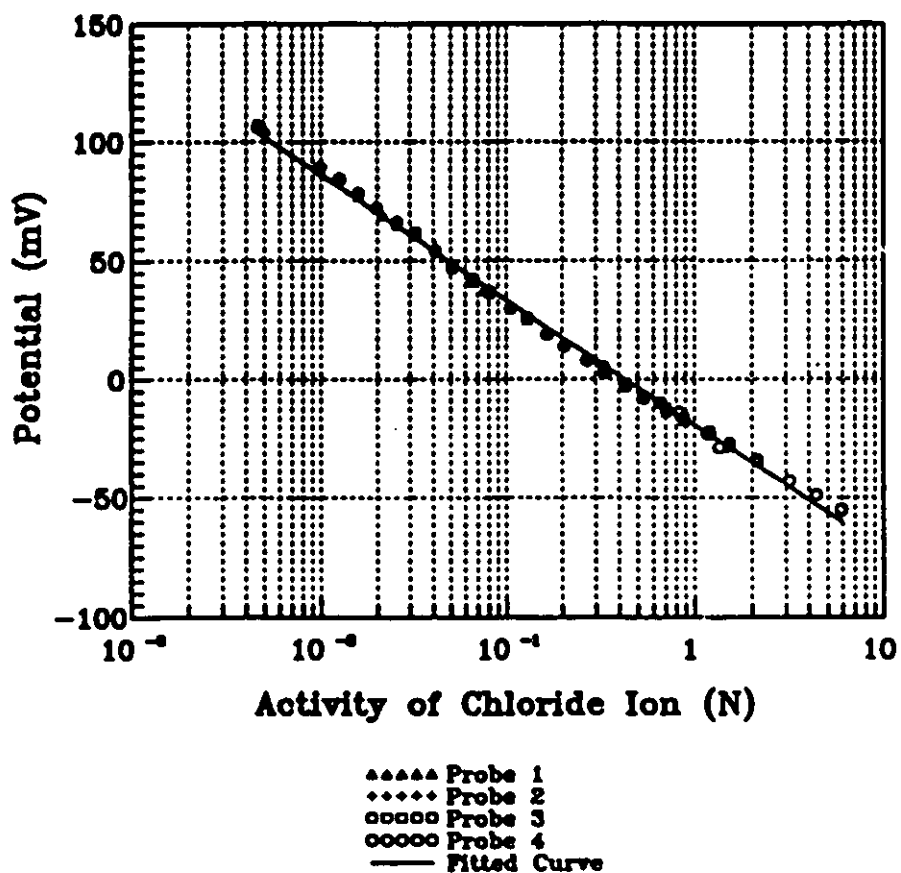
Figure 3.3 Working curves of the chloride ion probes.

chloride ion activity in the range anticipated at typical localized corrosion sites. Activity of the chloride ions was calculated from concentration using a model developed by Pitzer[109,136,137] and used by Harvie et al.[138], Paige[139] and Filippov et al.[140,141,142]. The data may be fitted empirically to the equation:

$$E_0(mV,SCE) = -19.31 - 52.66\log a_{Cl}.$$ [3.4]

The potential of the chloride ion probe has a linear relation with the activity of the chloride ions. The correlation coefficient is equal to 0.999. The calibration indicated that the potentials of the chloride ion probe were reproducible to within 1 mV, thus being capable of quantifying chloride ion activity from 4.6×10^{-3} to 5.92. The potential of the microelectrode vs. concentration of chloride ions is similar to the results obtained by Gilbert[143] on macro electrodes.

The tungsten electrode was calibrated in solutions of H_2SO_4 and NaCl using pH values in the range from -0.38 to 9.28. The behaviour of an individual probe varies slightly. A specific working curve must be determined for each pH electrode. A typical working relationship is shown in Figure 3.4. The potential of the pH probe has a linear relation with pH, but the slope varies in different pH ranges. The experimental data may be fitted to Equation [3.5]:

$$
\begin{aligned}
E(mV,SCE) &= -106.56 - 31.81pH & -0.4 &< pH < 1.4 \\
E(mV,SCE) &= -98.81 - 37.27pH & 1.4 &< pH < 4.7 \\
E(mV,SCE) &= -262.62 - 2.07pH & 4.7 &< pH < 7.9 \\
E(mV,SCE) &= -140.53 - 17.50pH & 7.9 &< pH < 9.3
\end{aligned}
$$
[3.5]
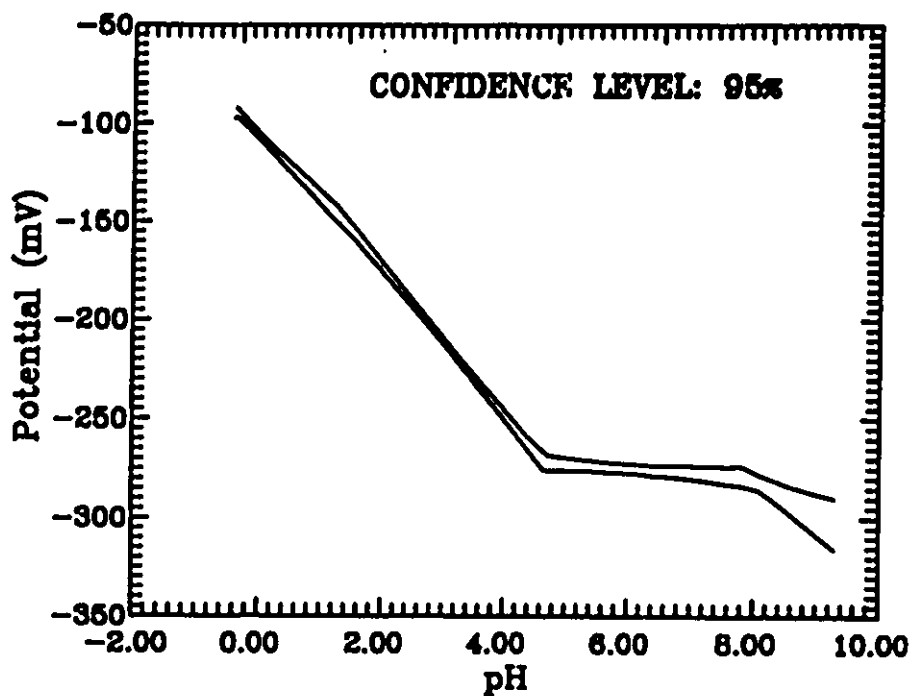
Figure 3.4 Working curve of the pH probes.

3.2.2. Stabilities of the electrode potential

Each microelectrode was tested under specified solution conditions to detect any potential drift with time. Under fixed solution conditions, the open circuit potentials of the chloride probe and potential probe were monitored for more than 10 hours and pH probes for up to 32 hours. As shown in Figure 3.5, the potential shift rate is 0.17 mV/h for the chloride ion probe, 0.28 mV/h for the potential probe and 0.22 mV/h for the pH probe. It may be concluded that these microelectrodes are sufficiently stable for most practical measurement situations.
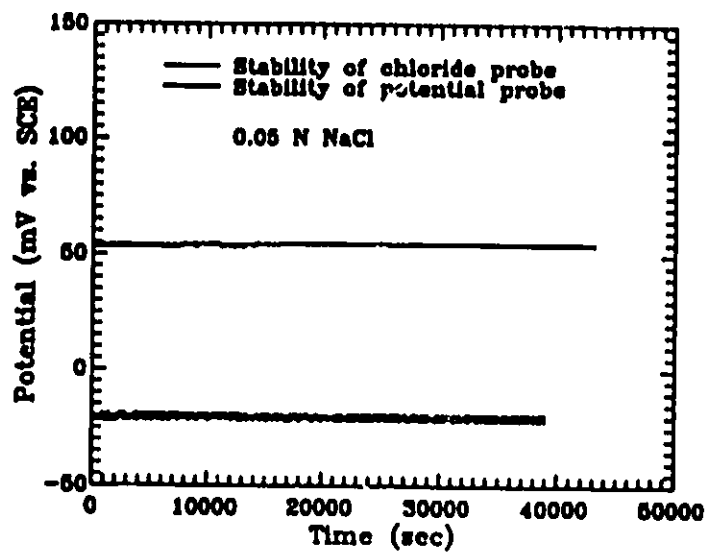
a
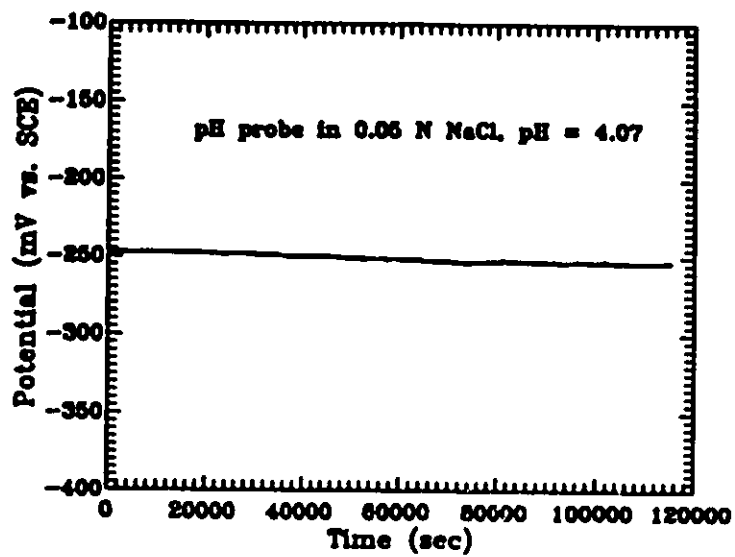
b

Figure 3.5 The results of the stability tests for (a). chloride probe and potential probe and (b). pH probe.

3.2.3. Spatial resolution

To examine the spatial resolution of the chloride ion probe, it was used to measure the distribution of chloride ion concentration in a well-defined concentration field. Compacted solid sodium chloride was placed at the bottom of a graduated cylinder which was then slowly filled with distilled water. A chloride ion concentration gradient developed gradually, and could be measured by scanning the probe in the y-direction, and repeating at various time intervals. The movement of the boundary was calibrated by optical method. The results are shown in Figure 3.6.
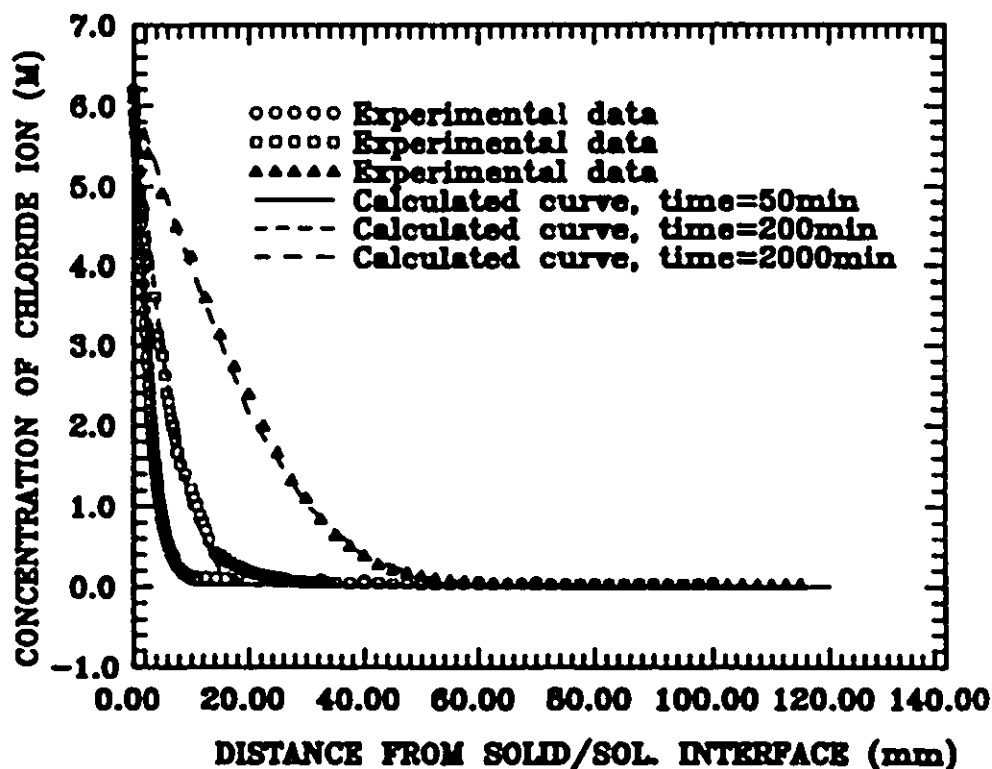
Figure 3.6 Comparison of the concentration distribution of chloride ions measured by a chloride ion probe and the calculated curves by the Error function.

The points are measured values and the solid lines are calculated using the standard solution of Fick's second law for the "semi-infinite medium" problem[144] represented by Equation [3.6].

$$c_{Cl^-}(y,t) = c_{Cl^-,s} \left[1 - erf\left(\frac{y}{2\sqrt{D_{Cl^-}t}} \right) \right]$$

[3.6]

where $c_{Cl^-,s}$ is equal to 6.1 molar[145]. From the data of Figure 3.6, D_{Cl^-} is determined as $(2.0\pm0.1)\times10^{-5}$ cm^2/s, which is a reasonable value comparing with 2.03×10^{-5} cm^2/s reported in the literature[146]. In the region where the chloride concentration gradient is high, the probe movement was kept at 10 µm as a step. Changes in the concentration of the chloride ions still could be detected by the probe, indicating the spatial resolution of the chloride probe is less than 10 µm.

The spatial resolution of the pH probe was determined by measuring the distribution of the pH across an interface between two layers of agar gel which had been prepared with pH values of 8.37 and 2.42, respectively. The measurements were performed at different times following the initial establishment of the interface. The results are shown in Figure 3.7. Again, the points represent data determined from the microelectrode, and the solid lines are calculated for the "diffusion couple" problem[147] at short times, employing the relationship:

$$c_{H^+}(y,t) = c_{H^+,2} + \frac{c_{H^+,1} - c_{H^+,2}}{2} \left[1 + erf\left(\frac{y}{\sqrt{D_{H^+}t}} \right) \right]$$

[3.7]
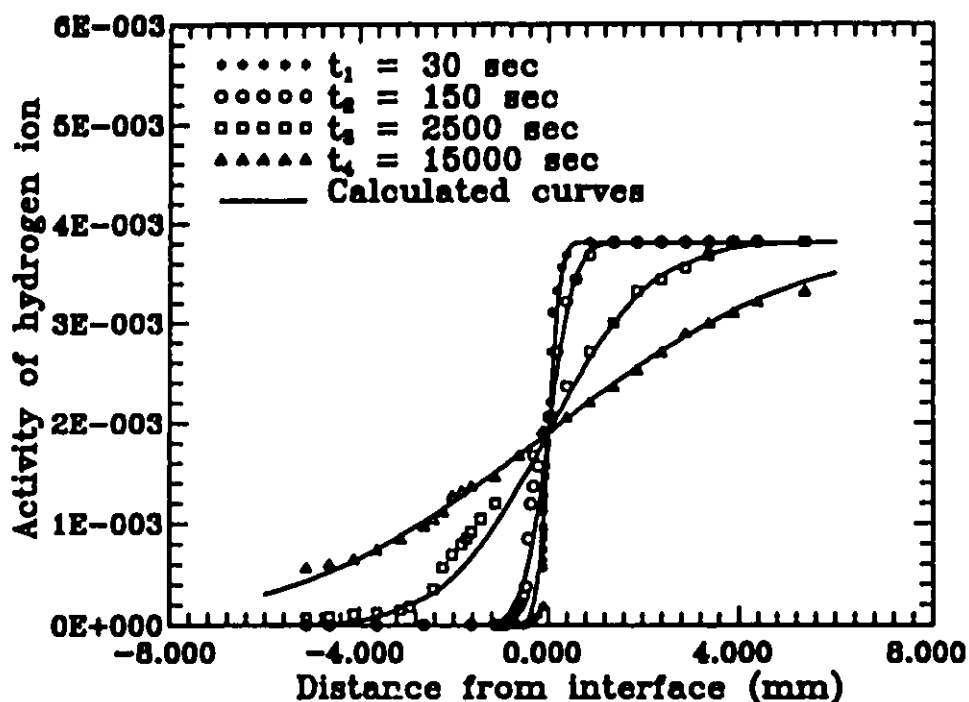
Figure 3.7 pH distribution across an interface of a pH 2.42 agar jelly and a pH 8.37 agar jelly measured by a pH probe.

D_H+ was found to be $(6\pm1)\times10^{-6}$ cm^2/s by direct curve fitting. The diffusivity of hydrogen ions in aqueous solution is 9.31×10^{-5} cm^2/s[69]. It is reasonable that the diffusivity of hydrogen ions in agar gel is smaller than that in aqueous solution. It can be concluded that the spatial resolution of the pH probe is less than 1 μm, being limited primarily by the sensitivity of the manipulator control.

3.2.4. Interference effects

No electrode is entirely selective towards the ion specified. The presence of the other ions can seriously impair electrode performance. In corrosion environments, more than one type of ion will usually exist in the solution. All ions

in the solution will influence the activity of the detected ions, while ions with the same sign as the detected ions will interfere with the electrode performance. Both effects will change the potential of the electrodes. It is therefore necessary to study the influence of the secondary ions on the electrode potential-activity characteristic and on the activity of the detected ions.

In a solution containing several ions and multiply charged species with the same sign, the electrode behaviour can be represented by a general equation[148]:

$$E = C + \frac{RT}{n_i F} \ln[a_i + k_{i,j}(a_j)^{n_i/n_j} + k_{i,k}(a_k)^{n_i/n_k} + ...]$$ [3.8]

Determination of the selectivity coefficients was carried out by a direct mixed-solution method[149,150]. Potential measurements were performed in solutions containing both the primary ion i and the interfering ion j. The selectivity coefficient $k_{i,j}$ is determined from the dependence of the electrode potential on the logarithm of the activity of ion j in the presence of a constant activity of ion i (a_i). The plot of cell emf versus log a_j gives two linear portions whose point of intersection gives the value of the activity of a_j at the "break point" of the curve. The ratio $a_i/a_j^{(n_i/n_j)}$ is equal to $k_{i,j}$. The selectivity coefficient value obtained holds only for the given experimental conditions and will be different for the different ion activities. For this reason, the electrode selectivity would be better described by a series of selectivity coefficient values in a certain ion activity range. In Figures 3.8, 3.9 and 3.10, only typical results at one activity of the primary ions are displayed.

In a solution containing ions i, j and k ..., the potential change due to presence of j and k ... ions can be estimated by Equation [3.8]. The activity of the

primary ion i can then be estimated from the potential after correction.

The activity coefficients of the detected ions in multi-component electrolytes are calculated by a model due to Pitzer[109]. The corresponding potentials of the probe were estimated based on the activity.

Reagents of analytical purity were used to make the 0.05 M NaCl solution with different concentrations of various kinds of ions. Deaeration was performed by purging with nitrogen for at least 2 hours before and throughout the duration of the experiments, with additional stirring provided by a magnetic stirrer.

3.2.4.1. Chloride ion probe

In a solution containing both Cl⁻ and, for example, SO_4^{2-}, the following exchange reaction would be established:

$$2AgCl + SO_4^{2-} \rightleftharpoons Ag_2SO_4 + 2Cl^-$$ [3.9]

The potential of the electrode would then be given by:

$$E = C - \frac{RT}{F} \ln[a_{Cl^-} + k_{Cl^- \cdot SO_4^{2-}} (a_{SO_4^{2-}})^{1/2}]$$ [3.10]

In a solution containing SO_4^{2-}, the potential change due to the presence of SO_4^{2-} is given by:

$$\Delta E = -\frac{RT}{F} \ln \left(\frac{a_{Cl^-} + k_{Cl^- \cdot SO_4^{2-}} (a_{SO_4^{2-}})^{1/2}}{a_{Cl^-}} \right)$$ [3.11]

The effects of the concentration of the sulphate ions on the potential variation of the chloride ion probe are tested. The experimental data are given in

Figure 3.8. The solid curve is the potential estimated from the activity of the chloride

ions calculated by the model[109] due to Pitzer. The corresponding potential of the

probe was established based on the activity. It shows that the measured potential

variation is due to the change of the activity of chloride ions. When the

concentration of sodium sulphate changes from 0.0001 to 1.5 M, the presence of

SO_4^{2-} does not interfere with the behaviour of the chloride ion probe. According to

the literature[113], the selectivity coefficient for Cl in the presence of SO_4^{2-}, $K_{Cl,SO_4^{2-}}$ is
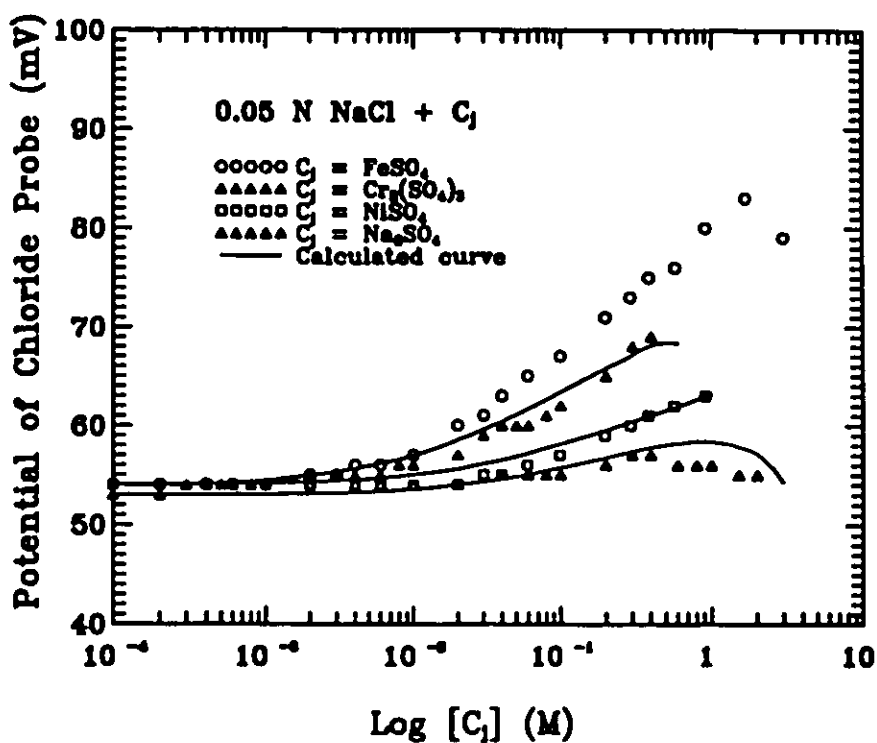
Figure 3.8 Potentiometric selectivity of the chloride ion probe to Cl in SO_4^{2-}/Cl
binary mixtures and the effect of the various ions on the potential of the
chloride ion probe.

equal to 10^{-6}. When the concentration of the primary ion, Cl^-, is larger than 0.05 M in the solution (as is likely in typical corrosion situations), the critical concentration for SO_4^{2-} to interfere with the chloride probe will be larger than its solubility, (viz. 1.95 molality in 0.05 M $NaCl^{131}$). When the concentration of SO_4^{2-} is less than 1.5 M, its interference is negligible. So there is no problem of interference by adding SO_4^{2-} to the system.

The influence of ferrous, chromium and nickel ions on activity of chloride ions, is also shown in Figure 3.8. The cation concentrations were adjusted by using $FeSO_4.7H_2O$, $Cr_2(SO_4)_3.15H_2O$ and $NiSO_4.6H_2O$. The potential variation of the chloride ion probe with the change of the concentration of these added salts is due to their influence on the activity of chloride ions in the solution. The experimental results indicated that when the concentrations of ferrous sulphate and nickel sulphate are higher than 0.01 M, they influence the activity of the chloride ions. Chromic sulphate starts to influence the activity of the chloride probe at about 0.02 M.

The influence of pH on the potential of the chloride ion probe was also checked. The result is shown in Figure 3.9. It was found that H_2SO_4 does not influence the activity of the chloride ions unless the pH is less than 1.The potentials of the chloride ion probe corresponding to the activity of the chloride ions calculated by the Pitzer model[109] are shown as solid curves in Figures 3.8 and 3.9. Comparing the measured data and the calculated curves, it is obvious that the potential of the chloride probe reflects the real chloride ion activity. The working curve of the potential vs. activity, rather than concentration, must therefore be used in order to avoid large errors when the concentration of secondary ions is high.
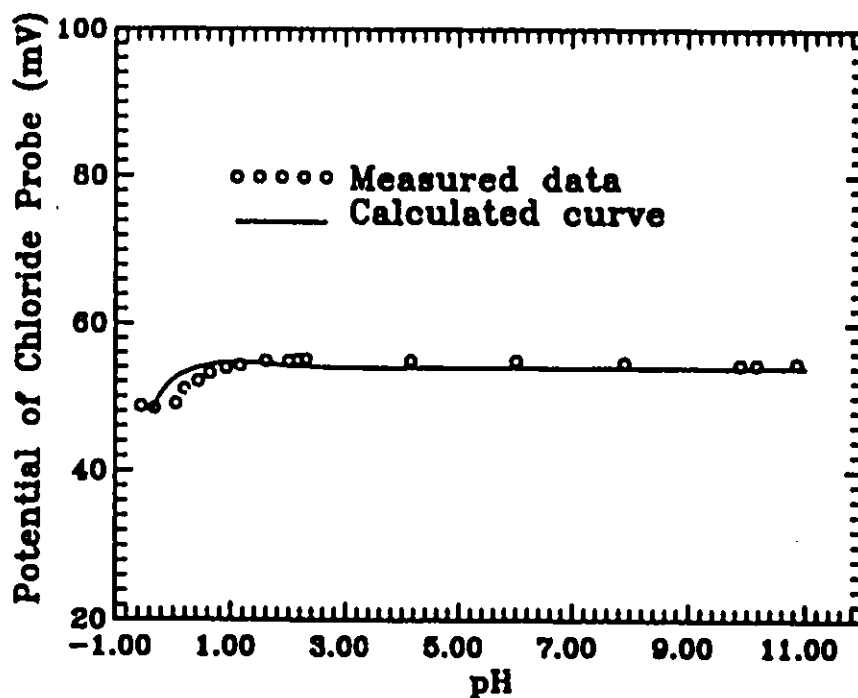
Figure 3.9 The effect of pH on the potential of the chloride ion probe in 0.05 M NaCl. The pH was adjusted by NaOH and H_2SO_4.

3.2.4.2. pH probe

The interference effects of nickel, chromium and ferrous ions on the pH probe are shown in Figure 3.10, where the concentrations were adjusted by using $NiSO_4.6H_2O$, $Cr_2(SO_4)_3.15H_2O$ and $FeSO_4.7H_2O$, respectively. The specific pH value chosen for each test solution was that at which the pH change resulting from the metal sulphate addition is negligible. As Figure 3.10 shows, when the concentration of nickel ions changes from 0.0001 to 2.38 M, (the saturated concentration), the

performance of the pH probe is not impaired. When the concentration of the chromic and ferrous ions is larger than 0.04 M and 0.006 M, respectively, the interference effect on the performance of the pH probe can not be neglected. The selectivity coefficients for pH in the presence of chromic ions and ferrous ions are estimated to be 0.41 and 0.76, respectively. Studies of pH distributions within growing pits on a nickel surface would need no correction. The situation on, for example, an Fe-Cr-Ni stainless steel, would need significant correction, because when
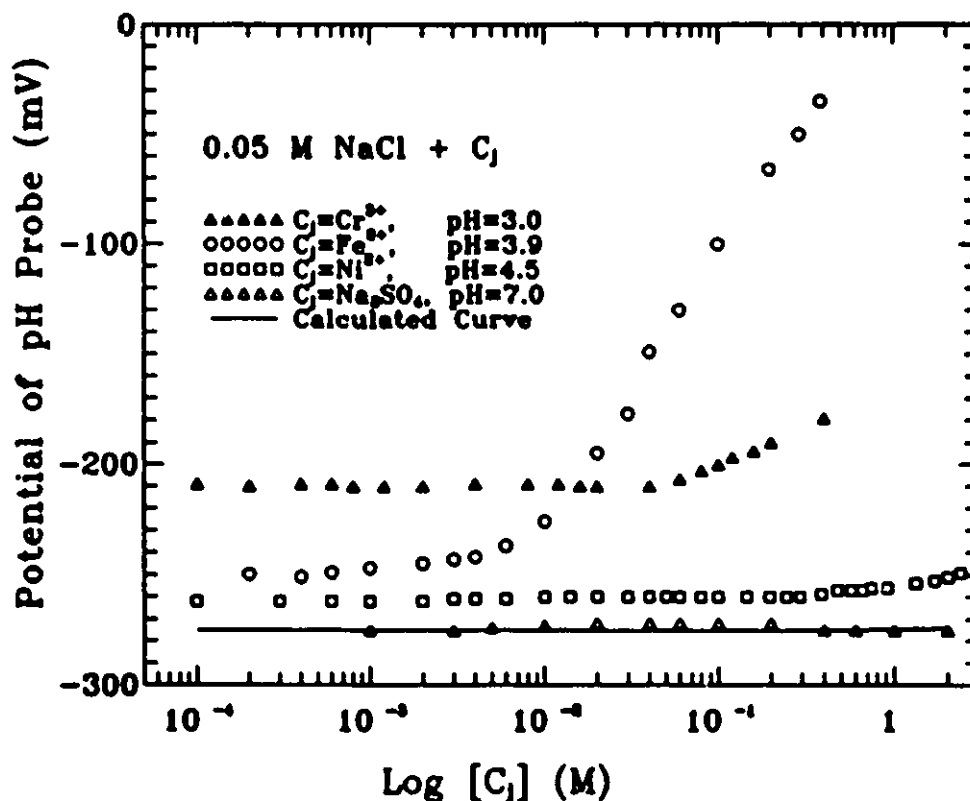
Figure 3.10 Potentiometric selectivity of the pH probe to pH in various binary mixtures as shown in the legend and the effect of Na_2SO_4 on the potential of the pH probe in 0.05 N NaCl.

localized corrosion occurs, the concentration of the chromic and ferrous ions will likely exceed 0.04 M and 0.006 M, respectively,

3.2.5. Compensation for local electric potential

Most of the measurements made on electrochemically controlled active pits are necessarily performed when the sample is subjected to an applied potential or current. Consequently, there is an IR drop between the microelectrode and the reference electrode. The total measured potential obtained by the microelectrodes is the sum of the IR drop and the net potential corresponding exclusively to the chloride ion activity, or pH, of the solution.

In order to determine the net potential, a potential probe could be employed to measure the IR drop. But the disadvantage is that the measurements of the potential probe and the pH probe or chloride ion probe cannot be done at the same time due to the small dimensions of the pits under investigation. Because the local conditions within a pit change with time, using a potential probe method to separate IR drop from the total potential would inevitably introduce errors into the measurement.

However, the IR drop interference may be eliminated by using a current-interrupt technique. Figure 3.11 shows the time dependence of both the current applied to a sample and the corresponding potential measured by a pH probe and a chloride ion probe, at an active pit bottom. In order to measure the proper steady-state potential, the "current-off" time must be longer than the "overshoot" time. As shown in Figure 3.11, the overshoot time for a pH probe is about 6 ms. The change in pH of the electrolyte during this time period, estimated as a diffusion problem,
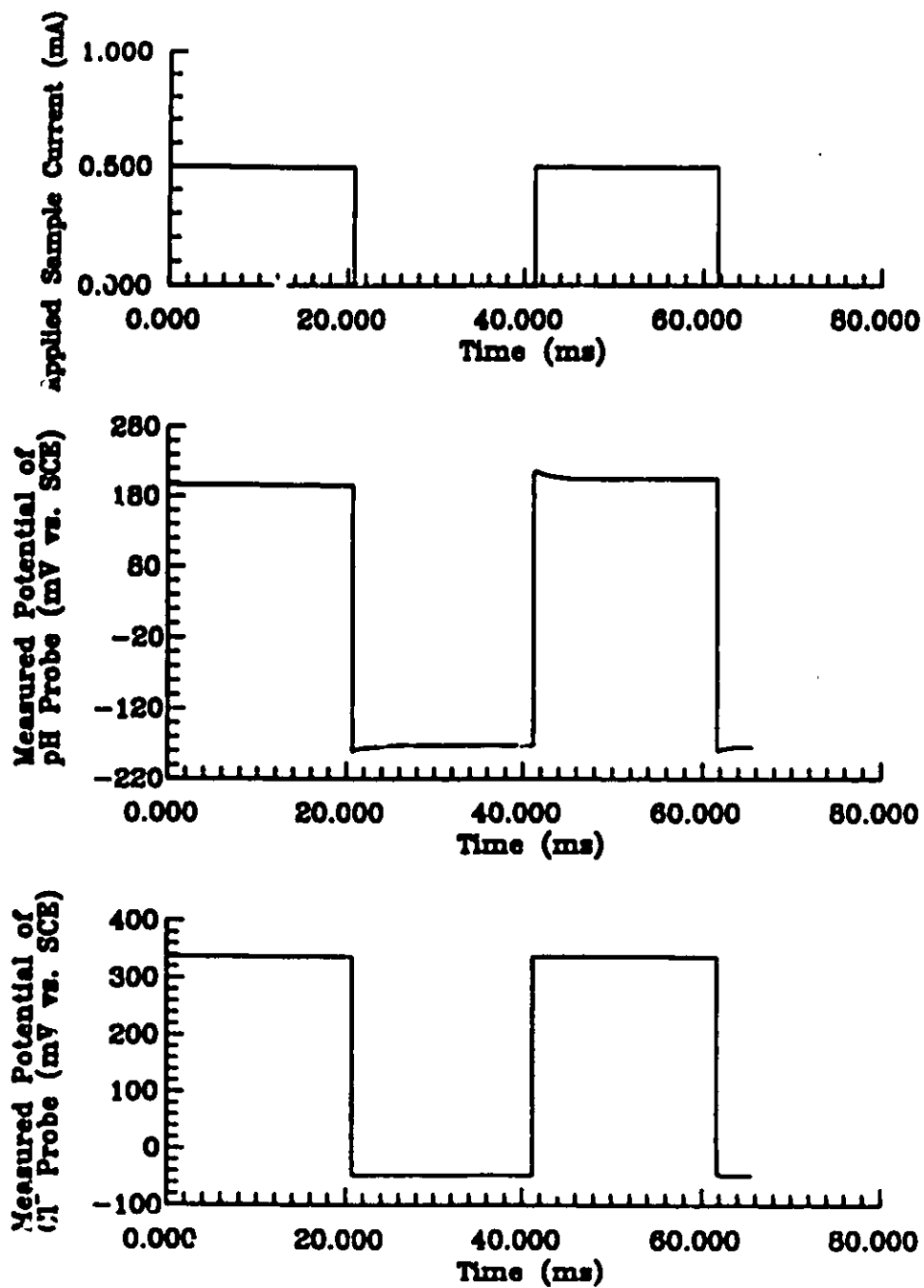
Figure 3.11 Potential response to a square current wave, as measured by the pH probe and chloride ion probe at a sampling interval of 2 μs per point.

would be less than 0.01, which is less than the detectable level and therefore is negligible. Figure 3.11 also shows that after the applied current changes, the potential of the chloride ion probe reaches a constant value so fast that no significant distortion of the potential square wave can be detected, even with a sampling time as short as $2\mu s$. The activity of the chloride ions inside a pit was also recorded over an extended current-off time (Figure 3.12). It was found that the local condition of
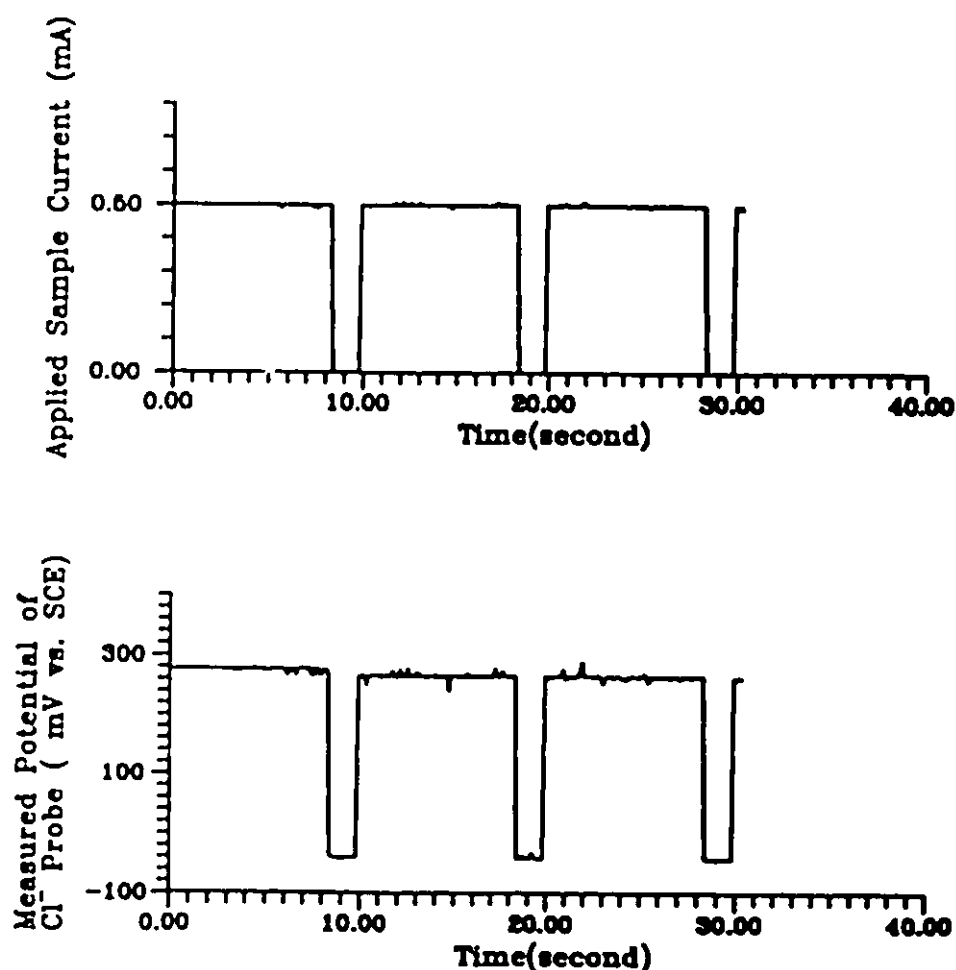
Figure 3.12   Potential response to a square current wave, as measured by the chloride ion probe at a current off time of 1.5 seconds.

the electrolyte will not have had sufficient time to change significantly from the steady state within 1.5 s. Consequently, this current interrupt time was selected for the pit analysis.

As an example of results obtained by a current-interrupt method, Figure 3.13 shows the time dependence of both the current applied to a simulated
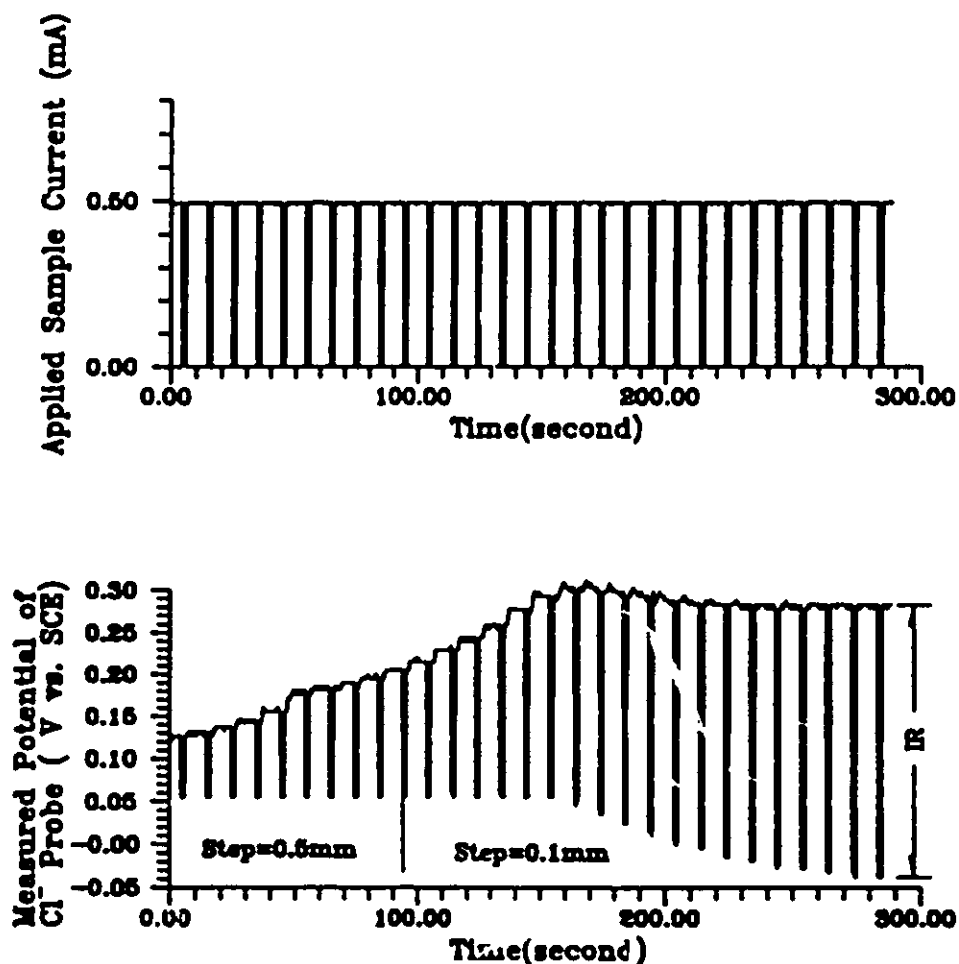
Figure 3.13   The current applied to the sample and the time dependence of the corresponding potential measured by a chloride ion probe. In each 10 s cycle the probe was moved into the pit by the noted step size.

pit and the corresponding potential measured by the chloride ion probe. The cycle of the square current wave was chosen to be 10 seconds. In each cycle, the probe was moved down into the pit by a predetermined step size. The last point of the potential of the chloride ion probe during the current-off period was taken to be that corresponding to the local chloride ion activity. These measurements also provide a built-in measurement of the IR drop. This is represented by the potential difference noted in Figure 3.13, and its variation with position can be followed by the height of the potential steps. The local pH profiles may be determined in the same manner.

3.2.6. Geometric interference

Difficulties may arise as the probe is brought into the restricted region of a corroding pit. The probe may disturb the pit solution[152] and change the local chemistry[153]. These experimental aspects must be considered when trying to improve the spatial resolution of the probe. Of particular interest is the influence of the rate at which the probe is moved down into the pit. Figure 3.14 shows the effect of probe speed on the measurements. This test has resulted in the adoption of an optimum speed to move the probes into the pits during the surveys. In order to eliminate the effect of change of the pit depth during the measurement, the activity of the chloride ions was plotted as a function of position, Z, normalized with respect to instantaneous pit depth. It may be seen that when the speed is less than 40 μm/s, the effect is negligible.

Figure 3.15 shows that for the current interrupt method, within the test range of the applied current period of cycle, the effect of the current interruption on the measurement of the distribution of chloride ions along the pit axis is very small.
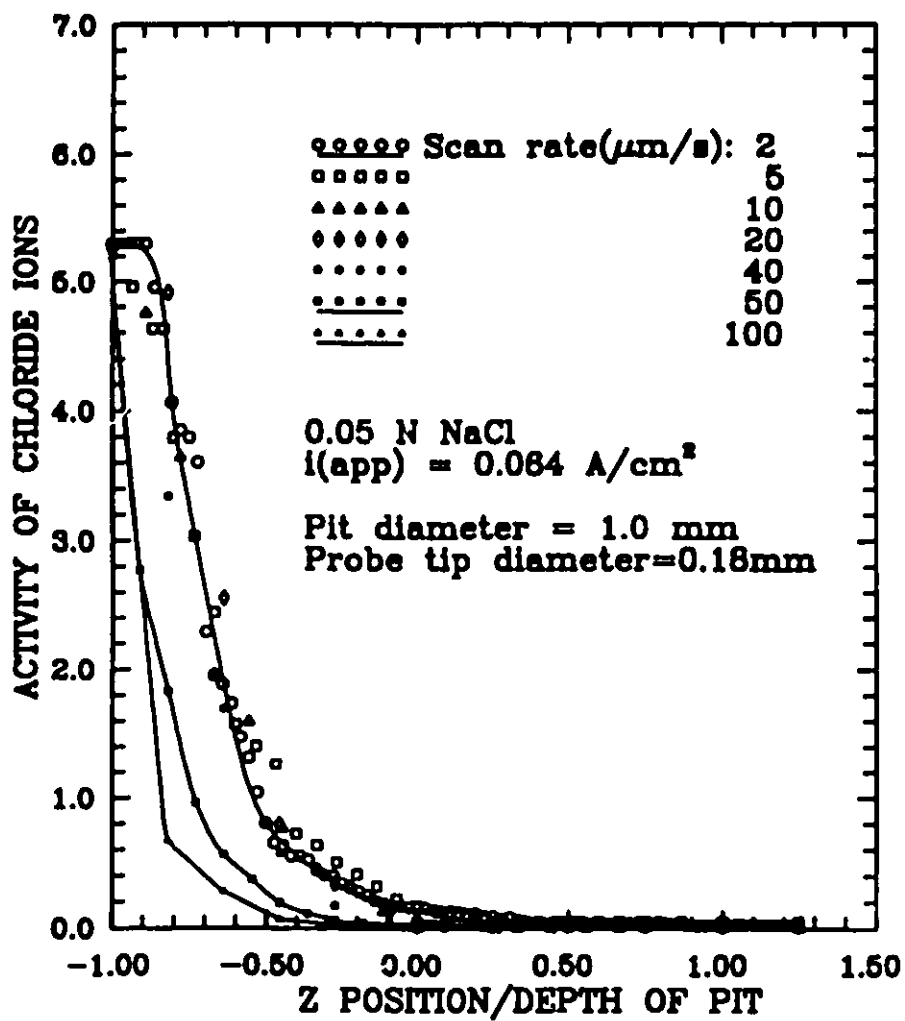
Figure 3.14 The effect of the chloride probe speed on the measured distribution of chloride ions along the pit axis.
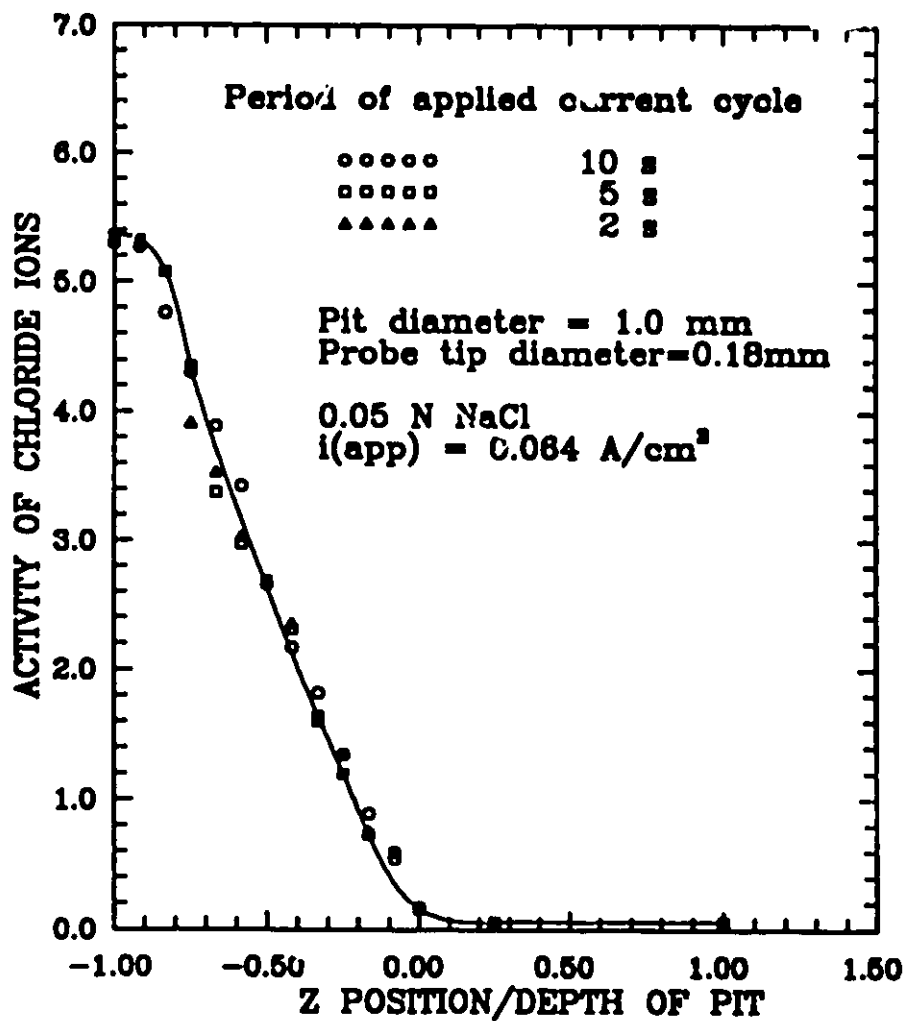
Figure 3.15 The effect of the applied current period of cycle on the measurements of the distribution of chloride ions along the pit axis.

3.3. Stepping motor

The movement of the probe in vertical direction Z, is controlled by an auto stepping motor driven by a specially designed controller and software, developed in McMaster University*, through an IBM PS/2 Model 30 computer. The position of the probe is recorded synchronously by the computer. The schematic diagram of apparatus is shown in Figure 4.1. The software is listed in Appendix C. The auto stepping motor was calibrated according to the scale on the manipulator. Therefore, under stepping motor control, the microelectrode measurements of the distribution of the local condition will be more accurate and reproducible than the results obtained manually.

So far the microelectrodes have been characterized and the stepping motor set up has been discussed. It is indicated that the microelectrodes are suitable to be used in identifying, under well-controlled motion, the distribution of ionic species within pits. However, a number of experimental details have to be arranged for real measurements and they are described in the next chapter.

---

* Designed and built up by Mr. V. Cers and Mr. J.D.R. Periard in the Science and Engineering Electronic Shop at McMaster University.

CHAPTER 4. EXPERIMENTAL DETAILS OF THE DISSOLUTION STUDIES

To test the theoretical model proposed in Chapter 2, the following experiments were designed in order to determine

(1). the local environmental conditions within pits, and

(2). the electrochemical response of the metal in the local environment.

4.1. Samples and preparation

The model pits were constructed from nickel wires with diameters of 1.00 mm, 0.76 mm, 0.50 mm and 0.25 mm embedded in epoxy resin. The geometry and co-ordinate system for a model pit was shown in Figure 2.2 and was used to simulate a pit in an otherwise passive surface.

Table 4.1 Dissolution of nickel wires under different conditions

i_{app} (A/cm^2)	Solution	dissolution form
<300	<0.5 N HCl	localized
200 - 300	1 - 2 N HCl	uniform
400	2.0 N HCl	uniform with gas evolution
>300	>2.5 N HCl	crevice

First, a constant current of 300 mA/cm^2, was applied to the sample in 0.5 N HCl for the time necessary to dissolve the nickel wire sufficiently to form a pit of required depth. This procedure was found to avoid both non-uniform attack of the nickel wire and crevice attack between the nickel and epoxy. The test details of the different applied current density and different solution concentrations are listed in Table 4.1. The pits were subsequently cleaned by distilled water in an ultrasonic bath for 2 minutes before commencing the microelectrode measurements.

Foil samples for the polarization test were wet ground with up to 600 grit emery paper, degreased with acetone in an ultrasonic cleaner and then mounted onto a plexiglass sample holder.

The wires were supplied by Johnson Matthey Limited. The 1 mm thick Ni foil was supplied by Aldrich Chemical Company, Inc. The compositions of nickel wires with diameters of 1.00 mm, 0.50 mm, 0.25 mm, and 1 mm thick Ni foil are listed in Table 4.2. The 0.76 mm diameter nickel wires is less pure and its composition is listed in Table 4.3.

Table 4.2 Composition of Nickel Samples

Materials		Elements							
		Cu	Fe	Ag	Si	Se	Mo	Zr	Na
Wire Dia. (mm)	1.00	7	7	1	<1	-	<3	<1	<1
	0.50	<	2	1	3	-	<3	<1	<1
	0.25	11	5	1	<1	-	<3	<1	<1
Foil		-	9	-	20	80	25	8	0.9

* All concentrations are quoted in parts per million by weight.

Table 4.3 Composition of 0.76mm diameter Nickel wire

Al	Si	S	Cl	K	Ca	Mn	Mo
0.70	1.50	0.62	0.30	0.17	0.16	0.19	0.14

* The concentration is quoted in parts percent by weight.
The composition was analyzed by X-ray fluorescence.

4.2. Solutions

Solutions were made from distilled water and analytical grade reagents. The base electrolyte was 0.05 N sodium chloride. Simulated pit electrolytes were chosen on the basis of the compositions determined by microelectrode measurements with the solutions being unstirred for microelectrode measurements. During the potentiodynamic polarization tests, the solution was stirred with a magnetic stirrer. No deaeration was attempted. The residual oxygen in the solutions was in the range of 5 to 7 ppm, measured by a YSI Model 5739 Oxygen Probe.

4.3. Experimental arrangement

A schematic diagram of apparatus and electrical circuitry for the microelectrode measurements is shown in Figure 4.1. The experiments were conducted under galvanostatic control to maintain a growing pit. One unit of a dual potentiostat/ galvanostat (Hokuto Denko Ltd. Model HR-101B) was used to control the current of the sample and the second unit was employed to measure the potential difference between microelectrodes and the reference electrode. For current interrupt method, a wave generator (E G & G PARC Model 175 Universal

programmer) was used to generate a square wave of appropriate frequency. An IBM PS/2 Model 30-286 personal computer recorded the signals through an A/D convertor and associated software ("Computerscope", EGAA, R.C. Electronics Inc.).

The variations of potential, chloride ion concentration and pH within a pit were determined in separate experiments. Step-wise motion of the appropriate probe was accomplished by employing the programmed micro-manipulator.

Potentiodynamic polarization tests were conducted in a conventional electrochemical cell with a Princeton Applied Research Model 273 Potentiostat/Galvanostat controlled by Model 342 SOFTCORR* CORROSION SOFTWARE run on an IBM PS/2 Model 30 Computer.
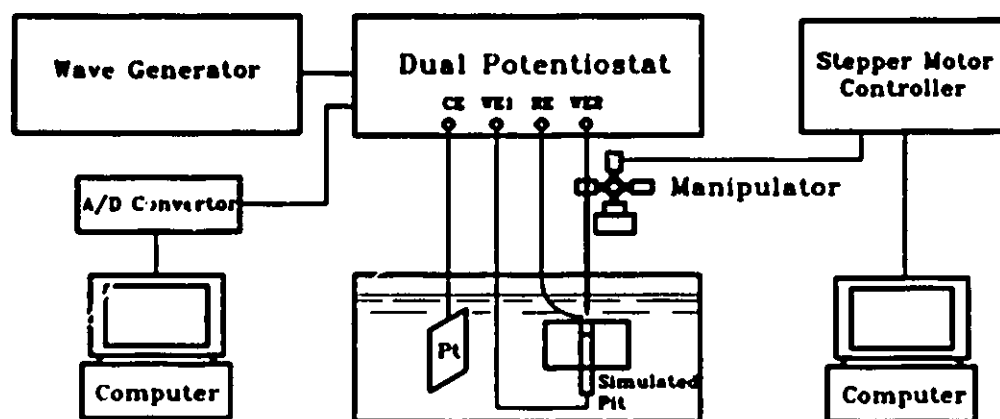
Figure 4.1 Schematic diagram of apparatus for micro-probe measurements.

---

* SOFTCORR is a trademark of EG & G Princeton Applied Research Corporation.

4.4. Procedures

4.4.1. Galvanostatic method

The applied current density was kept constant and the potential difference between the microelectrode and the reference electrode were recorded. At the same time, the potentials of the Ni samples vs. the reference electrode were recorded independently. A current interrupt method was used to eliminate the ohmic drop between the microelectrode and the reference electrode.

4.4.2. Potentiodynamic polarization

Potentiodynamic polarization tests were conducted in a conventional electrochemical cell to study the anodic behaviour of nickel in solutions simulating the local pH and chloride ion concentration within a pit. The scan rate was 0.17 mV/s.

The temperature was $22 \pm 1°$ C throughout. All potentials quoted refer to a saturated calomel electrode (SCE), which is equal to 0.2432 ± 0.0007 V vs. SHE obtained from Equation [4.1][154].

$$E(SCE) = 0.2412 - 6.61x10^{-4}(T-298)$$
$$-1.75x10^{-6}(T-298)^2 \quad\quad [4.1]$$
$$-9.0X10^{-10}(T-298)^3$$

The whole experimental work was implemented using the technique and experiment design introduced in Chapterr 3 and 4. The results obtained form the subject matter of the next section of this thesis.

CHAPTER 5. EXPERIMENTAL RESULTS AND DISCUSSION

As presented in Chapter 2, the modelling calculations have achieved the following results. (1) It determined the distributions of the species within a nickel pit in 0.05 N NaCl solution. (2). It is concluded that a steady state will not be achieved until a salt film is formed at the pit bottom. (3) A critical depth for a salt film formation is predicted and (4) it is independent of the initial pit depth. The purpose of the experimental work presented in this chapter is to verify the above theoretical results from the proposed model.

5.1. Distribution of ionic species and potential

In these experiments, 1 mm diameter model pits were galvanostatically controlled at $(63.7\pm0.1)\times10^{-3}$ A/cm^2. The potential of the microelectrode vs. time was recorded during the step-wise motion of the microelectrode in the Z direction. Knowing the moving rate of the probe, its position, Z, can be determined.

Figure 5.1 presents the distribution of the chloride ions in the Z direction measured by a chloride probe at increasing pit depths, using the data from plots like Figure 3.13. It is seen that the activity of chloride ions starts to increase at the pit mouth. At the bottom of the pit, the value reaches the maximum. It is clearly shown that the distribution of the chloride ions within a pit is a function of the pit depth. After a green coloration as shown in Figure 5.16, (due possibly to the formation of
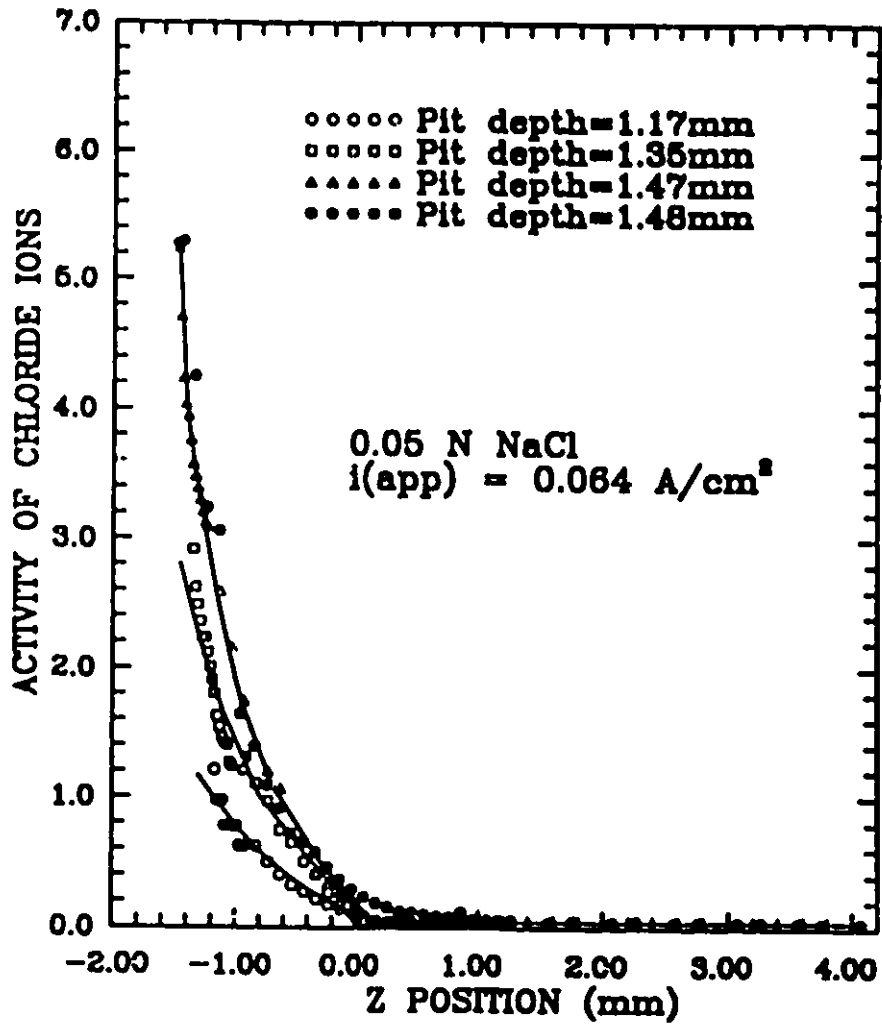
Figure 5.1 Measured distributions of chloride ions in the Z direction of the pit. The pit diameter is 1.0 mm.

nickel chloride layer), was observed at the bottom of the pit, the activity of the chloride ions reaches 5.3, near saturated value for nickel chloride film.

The decrease of pH was observed directly, as shown in Figure 5.2. It is a combined effect of the hydrolysis of the nickel ions plus the enrichment of chloride ions due to migration of the chloride ions under the applied field. The pH drop within a pit is also a function of the pit depth. When the pit depth changes from 0.5 mm to 0.8 mm, the pH at the pit bottom drops from 5.3 to 2.8.

Predicted distributions of the activity of the chloride ions and protons from the mathematical model(see Section 2.4) were compared with experimental results. Due to the end effect, which will be discussed in Section 5.3, the calculated
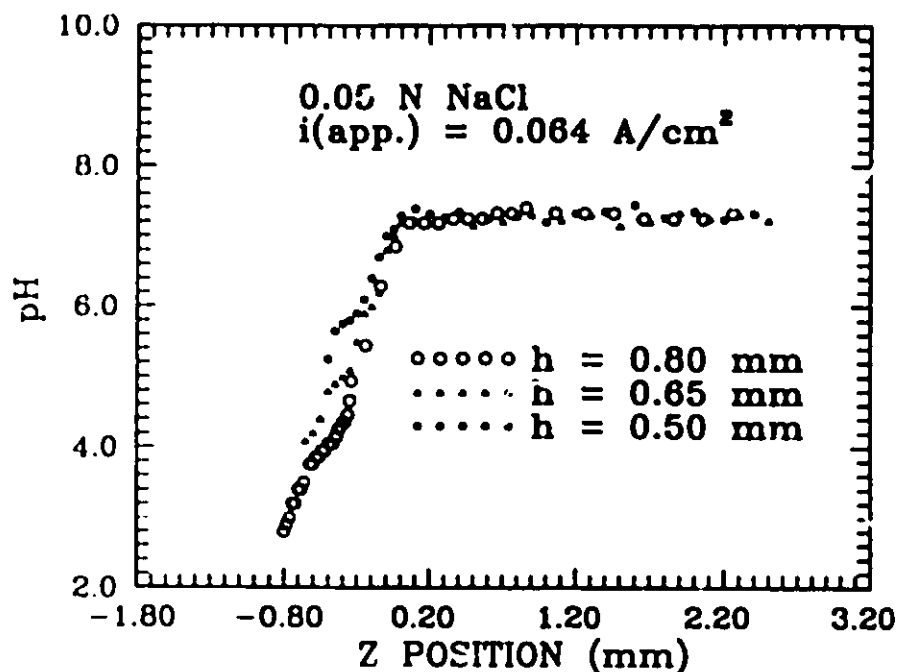
Figure 5.2 Variation of pH in the Z direction of the pit. The pit diameter is 1.0 mm.

distribution of the chloride ions should be corrected by a factor of 1.55 for Z position. This factor '1.55' signifies that the diffusion length is 1.55 times longer than the one used in the one dimensional model. As shown in Figure 5.3, the magnitude of the predicted distribution fits well with experimental values. There are some discrepancies in pH distribution as shown in Figure 5.4, which are believed to be due to the underestimation of the activity coefficients. It shows that the mass transport processes within a pit can be described by the model of Chapter 2.

Figure 5.5 depicts the distribution of potential as a function of the Z position for two pit depths measured by a chloride probe, as determined by the
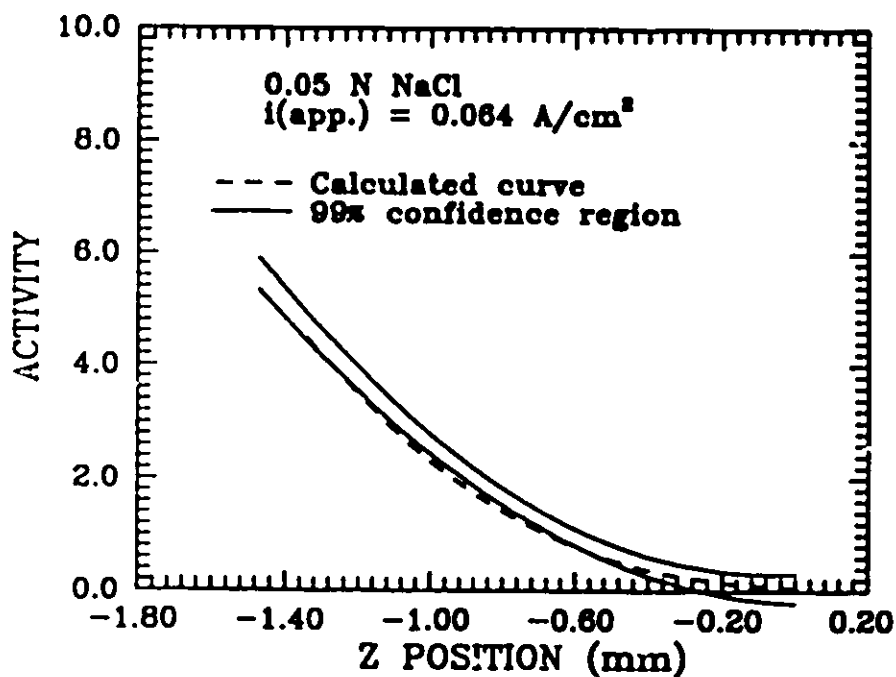
Figure 5.3 The theoretical prediction of the distribution of the chloride ions and experimental results. 99% of the measured data are in the region between the two solid lines.

current interrupt method (see Figure 3.13). It is seen that the potential gradient is larger at the pit mouth than within the pit. From Equation [2.18], one can see that the decrease in the potential gradient is due to the change in the composition of the electrolyte. It is proved by the measured distribution of the chloride ions and pH (Figures 5.1 and 5.2). Comparing the two curves in Figure 5.5, it is seen that as the pit grows, the potential gradient decreases, that is, the pit electrolyte becomes more concentrated, and since this involves activity of chloride ions and pH, the pit electrolyte becomes more aggressive.
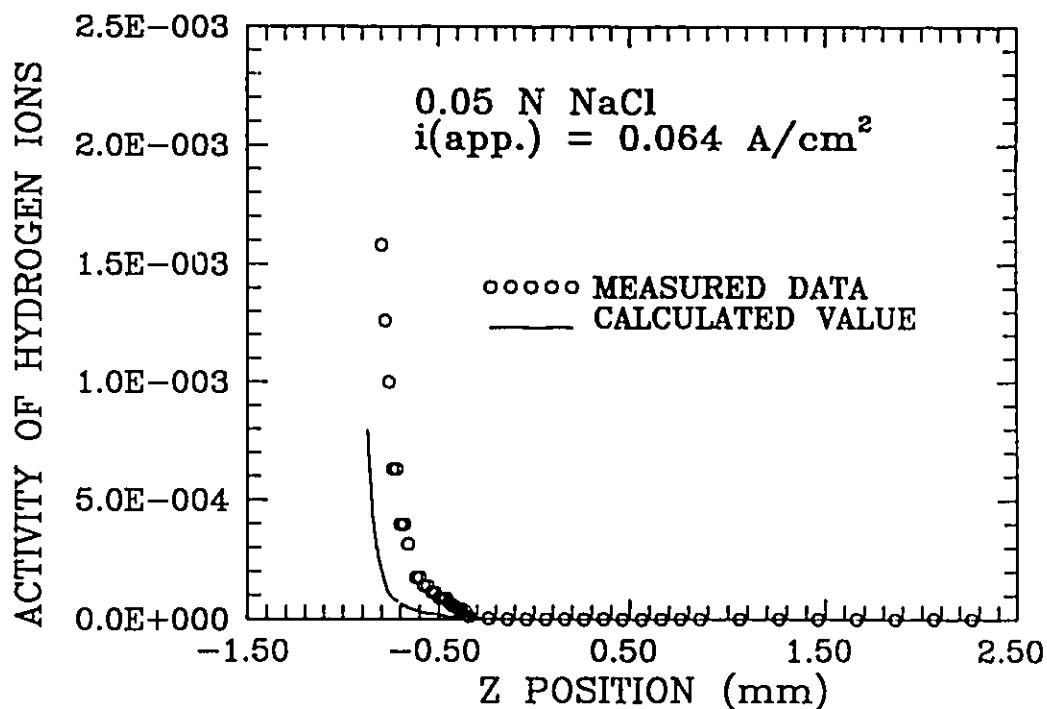
Figure 5.4 Comparison of the calculated and measured activity of the proton as a function of the Z position.
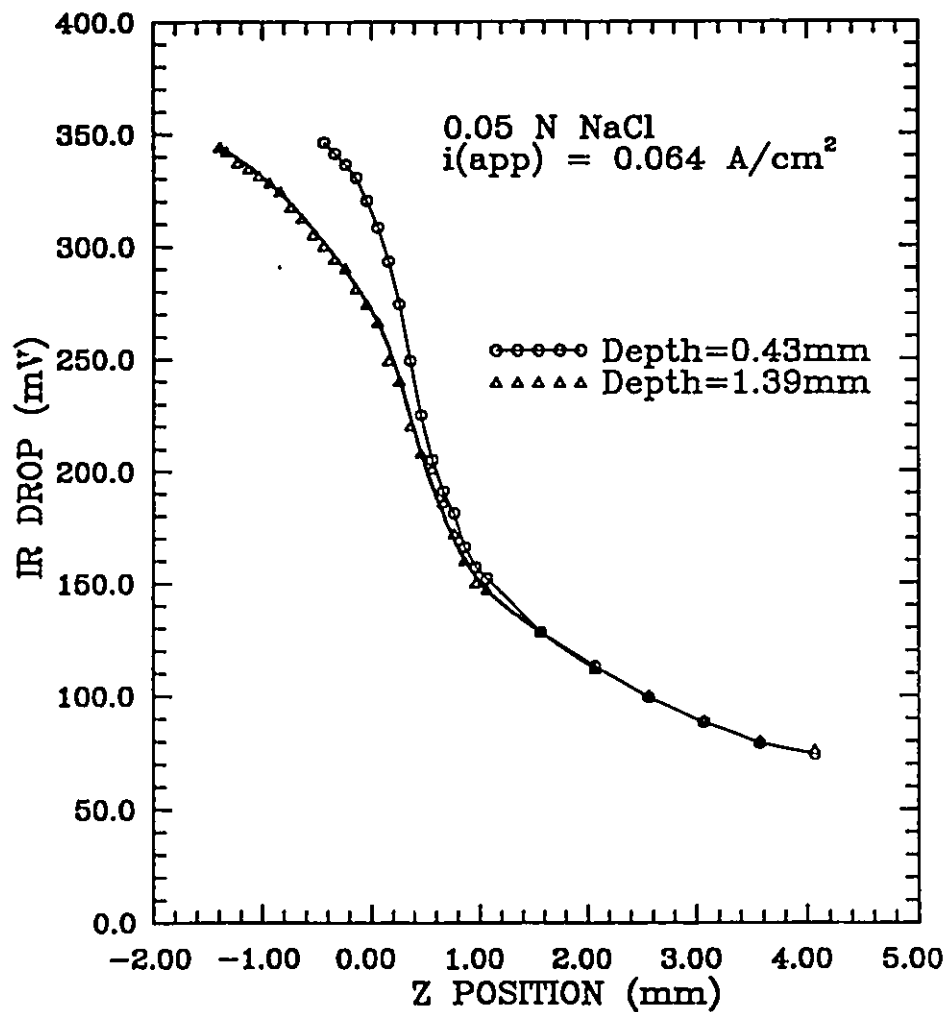
Figure 5.5 Distribution of potential in the Z direction of the pit measured by the chloride probe. The pit diameter is 1.0 mm.

5.2. The time dependence of the activity of the chloride ions within the pit

The time dependence of the activity of the chloride ions was measured by placing the chloride probe at the fixed position within the pit. The result is shown in Figure 5.6. After the current was applied to the sample, the activity of the chloride ions started to increase. The activity of the chloride ions kept changing until the salt film was observed at the pit bottom. It is confirmed that a steady state will not be achieved until a salt film is formed at the pit bottom as predicted by the modelling calculation.
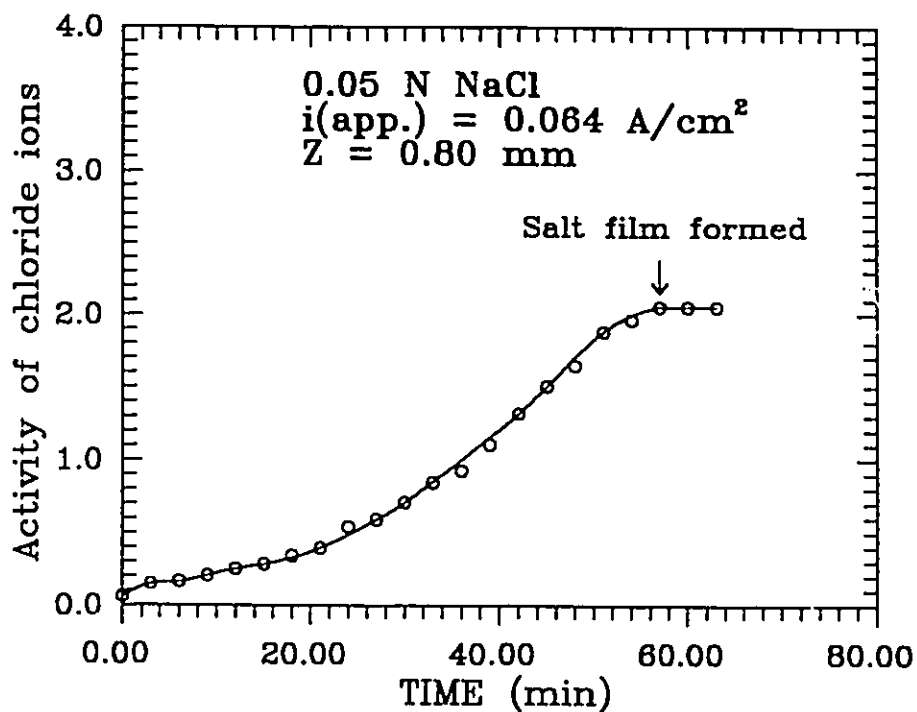
Figure 5.6 The time dependence of the activity of the chloride ions at position 1.100 mm from the pit mouth.

5.3. Salt film formation

To measure the build-up of the chloride ions at the pit bottom as a function of the pit depth, transition measurements were performed. The model pits in the nickel were forced to dissolve at a constant rate through galvanostatic control. The applied current density was kept at $(63.7\pm0.1)\times10^{-3}$ A/cm^2.

Because the current efficiency for nickel dissolution in the presence of chloride ions has been shown to be 100% in both neutral and acidic solutions[155,156], the receding rate of the metal surface under galvanostatic control can be estimated by Faraday's Law. Under an applied current density of $(63.7\pm0.1)\times10^{-3}$ A/cm^2, it is $(2.178\pm0.004)\times10^{-6}$ cm/s. If there is no accumulation of the surface layer, the rate of the pit deepening, v_{pit}, is equal to the receding rate of the metal surface. By controlling the chloride probe to move at the same rate as the pit bottom, the activity of the chloride ions at the pit bottom can be continuously monitored. The potential of the Ni sample vs. the reference electrode was recorded simultaneously.

Figure 5.7 is the measured activity of the chloride ions at the pit bottom and the potential of the nickel sample as a function of the depth of the pit with 1.00 mm diameter. It is showed that after the pit depth reaches a certain value, the activity of the chloride ions at the pit bottom increases significantly. At the same time, the potential of the nickel sample also increases, and a green coloration is observed at the pit bottom. Therefore, the large enrichment of the chloride ions and the green coloration at the pit bottom suggests the formation of a salt layer.
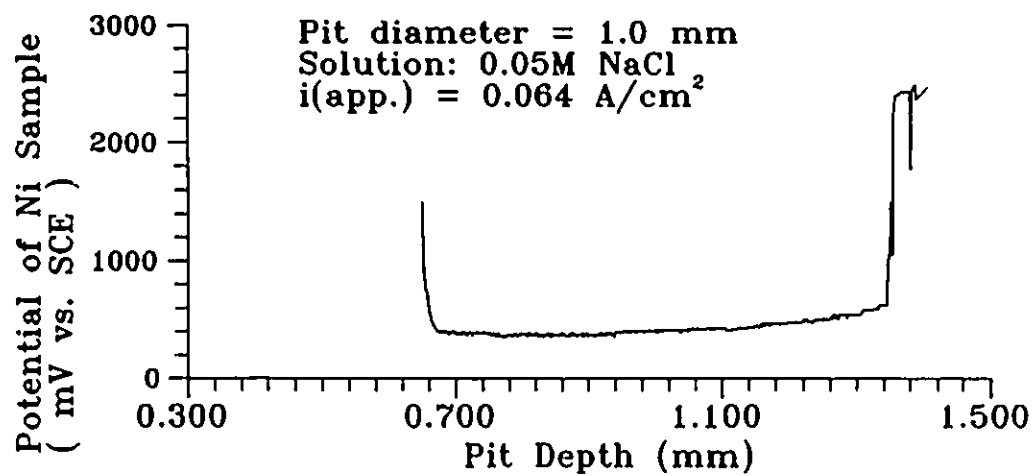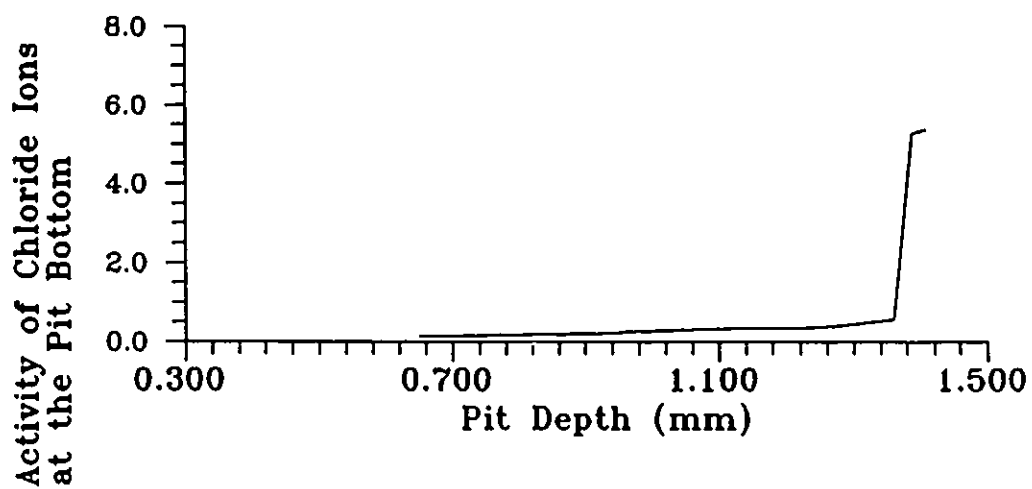
Figure 5.7 Chloride ion activity at the pit bottom and the potential of the Ni sample, as a function of the depth of pits with 1.00 mm pit diameter.
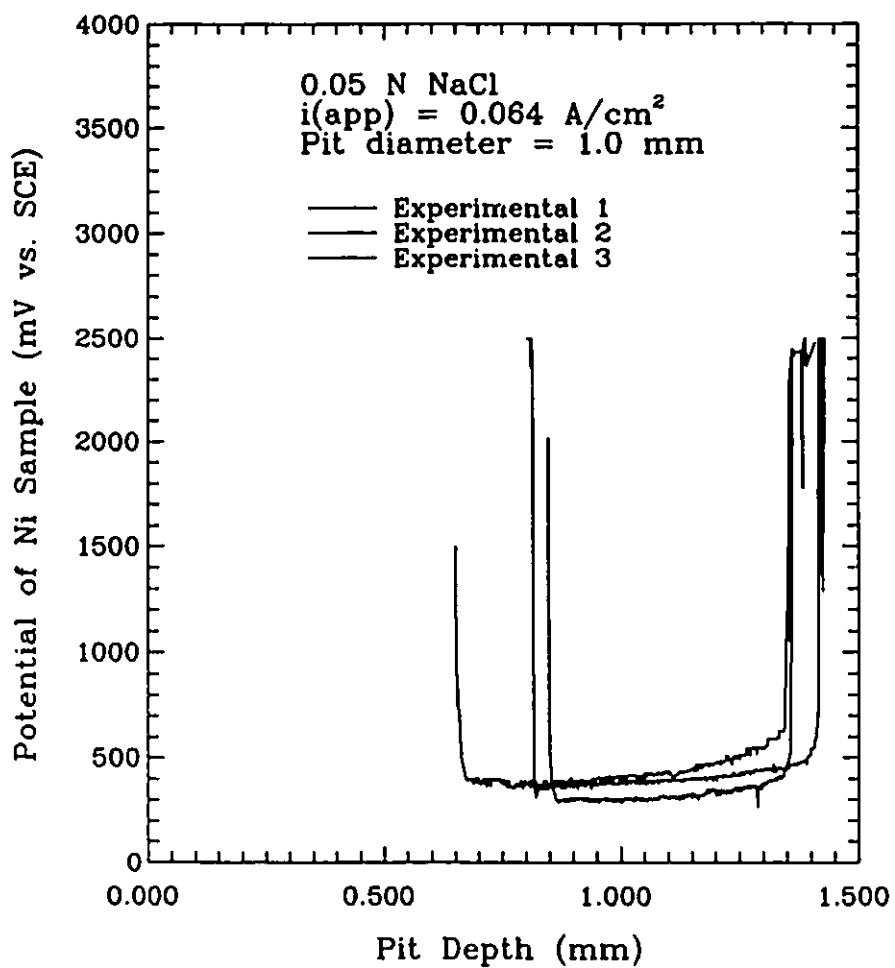
Figure 5.8 Measured potential of the Ni sample as a function of the depth of a 1.00 mm diameter pit.

From the model analysis (Chapter 2), the results also show that as a pit grows, the transport processes are slow with respect to the movement of the boundary, resulting in the accumulation of the nickel and chloride ions within a pit. The accumulation rate within a pit increases with the pit depth, especial at the bottom of a pit. It is predicted that there is a transition depth, at which the precipitation of a nickel chloride at the bottom of a pit occurs. Thus, it can be concluded that the considerable increase in the potential is a consequence of the formation of the salt film, resulted from the accumulation of the ionic species at a pit depth beyond the critical value.

Figure 5.8 shows the potential of the Ni sample vs. depth of the pit with 1.00 mm diameter with different initial pit depths. It was observed that the large potential increase occurs at a well-defined pit depth, regardless of the initial pit depth from which the experiment was started. The depth at which the potential increases is constant for a given pit diameter. This proved the theoretically predicted critical depth, h_t, at which a metal chloride layer is formed, and this critical depth is independent of the initial pit depth. But the measured value for h_t, 1.36 ± 0.05 mm, is larger than the predicted one, 0.88 mm. This discrepancy may be due to having not considered the supersaturation for the precipitation in the model. Because the accumulation of the ion species at the bottom of the pit is the result of mass transport, which depends on the shape of a pit, this discrepancy may be also due to the assumption of a unidirectional pit in the model. Therefore, this critical depth may depend on the pit diameter, d. In order to study the effect of the pit diameter on the critical depth, experiments were performed on pits with different diameters.
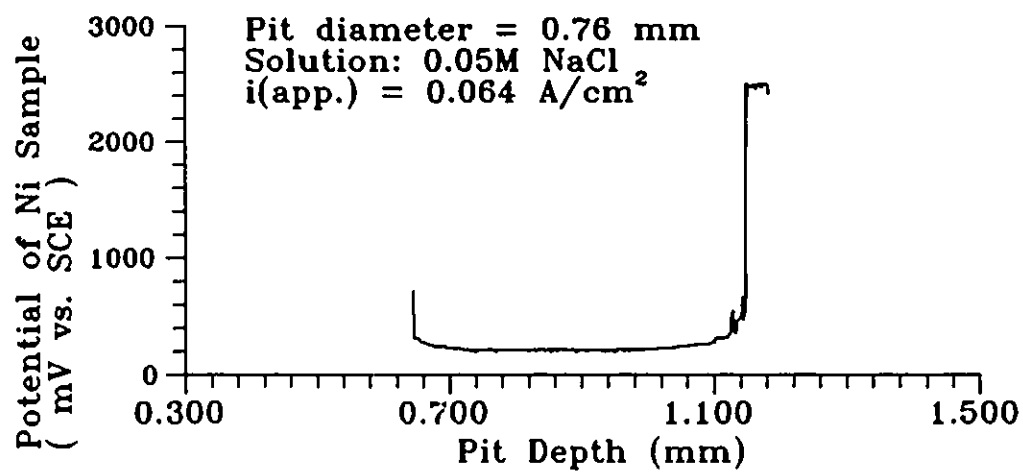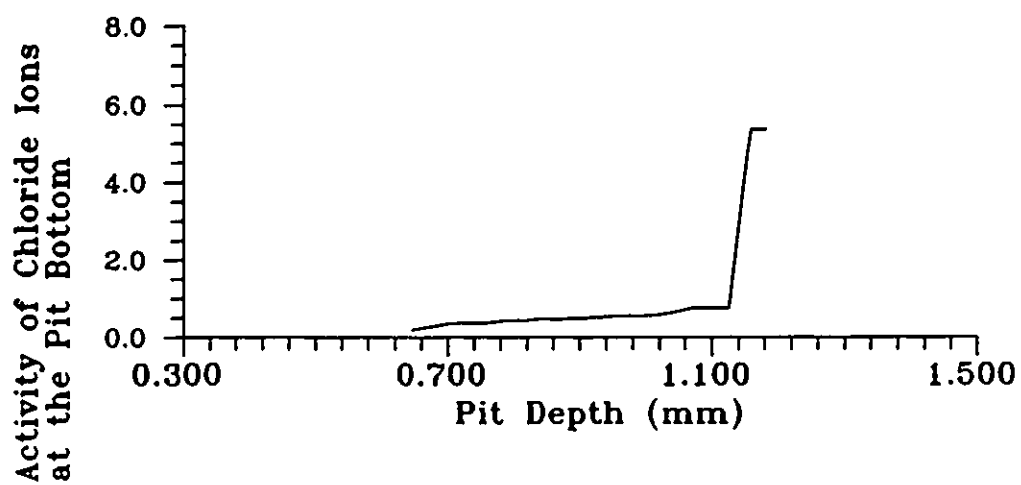
Figure 5.9 Chloride ion activity at the pit bottom and the potential of the Ni sample, as a function of the depth of pits with 0.76 mm pit diameter.
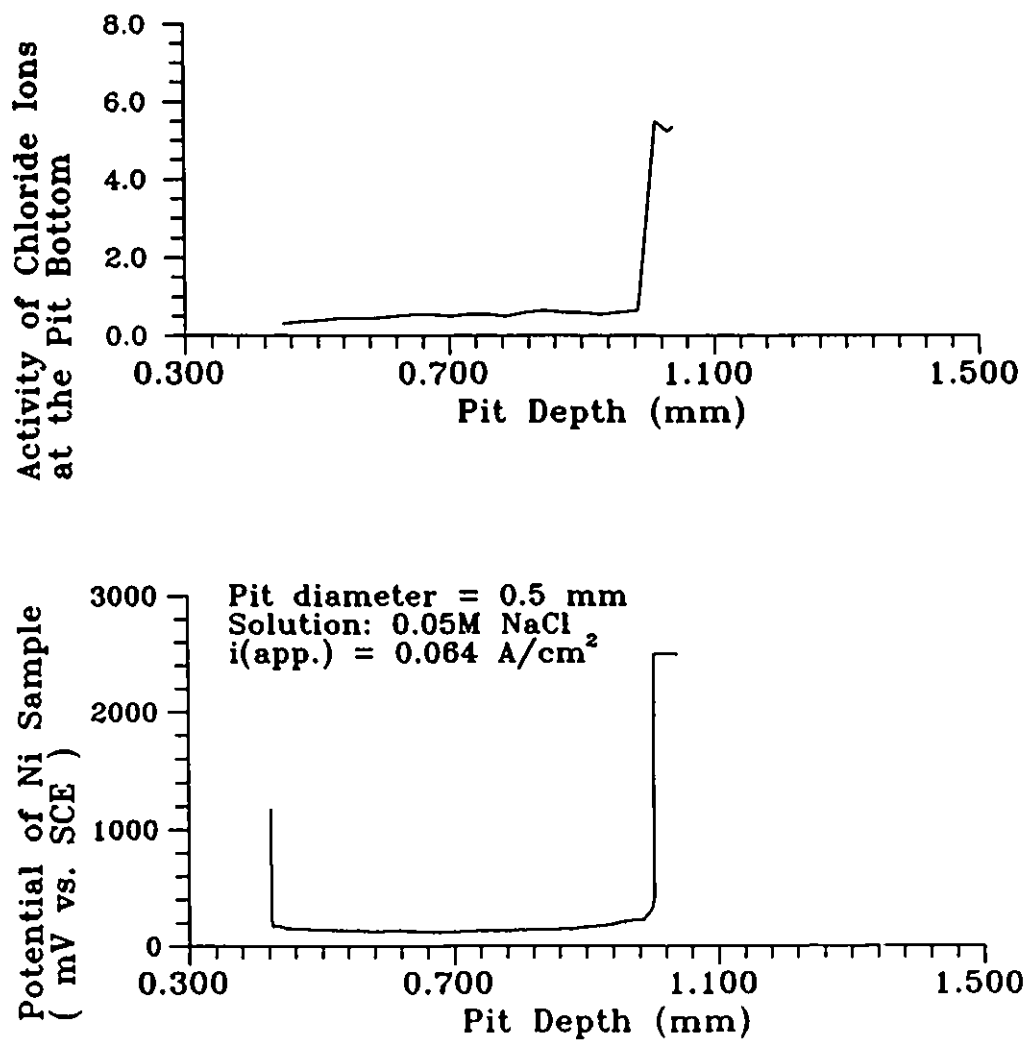
Figure 5.10   Chloride ion activity at the pit bottom and the potential of the Ni sample, as a function of the depth of pits with 0.50 mm pit diameter.
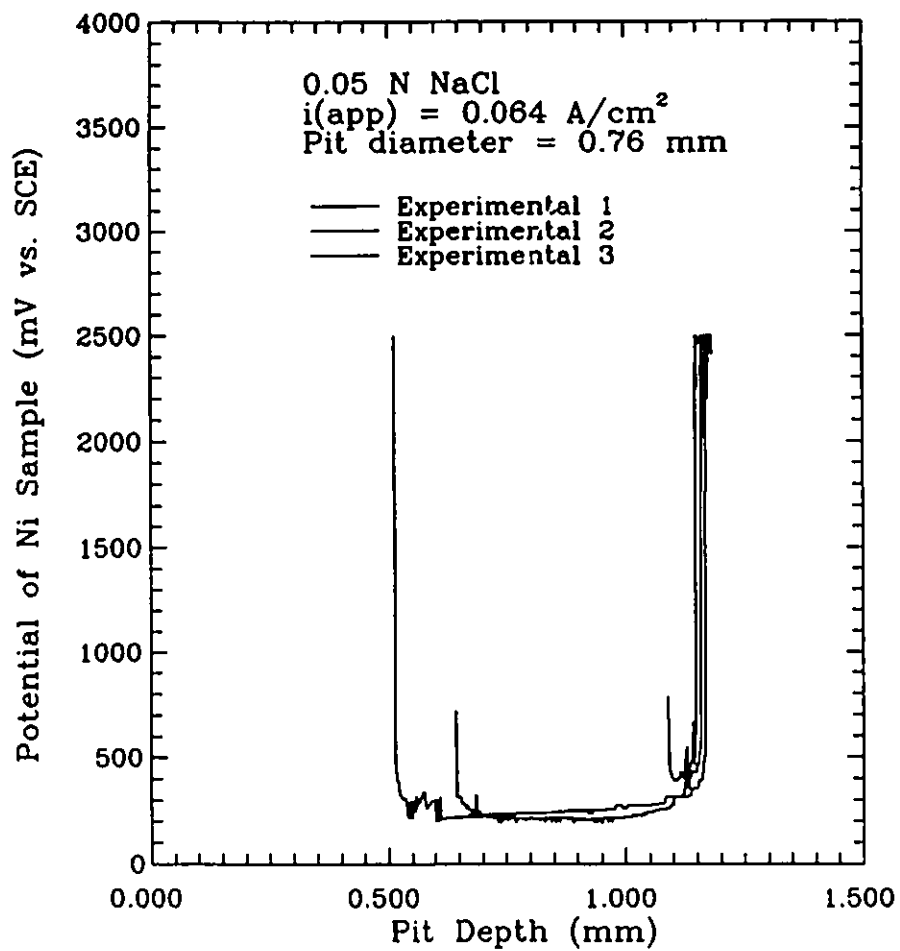
Figure 5.11   Measured potential of the Ni sample as a function of the depth of a 0.76 mm diameter pit.
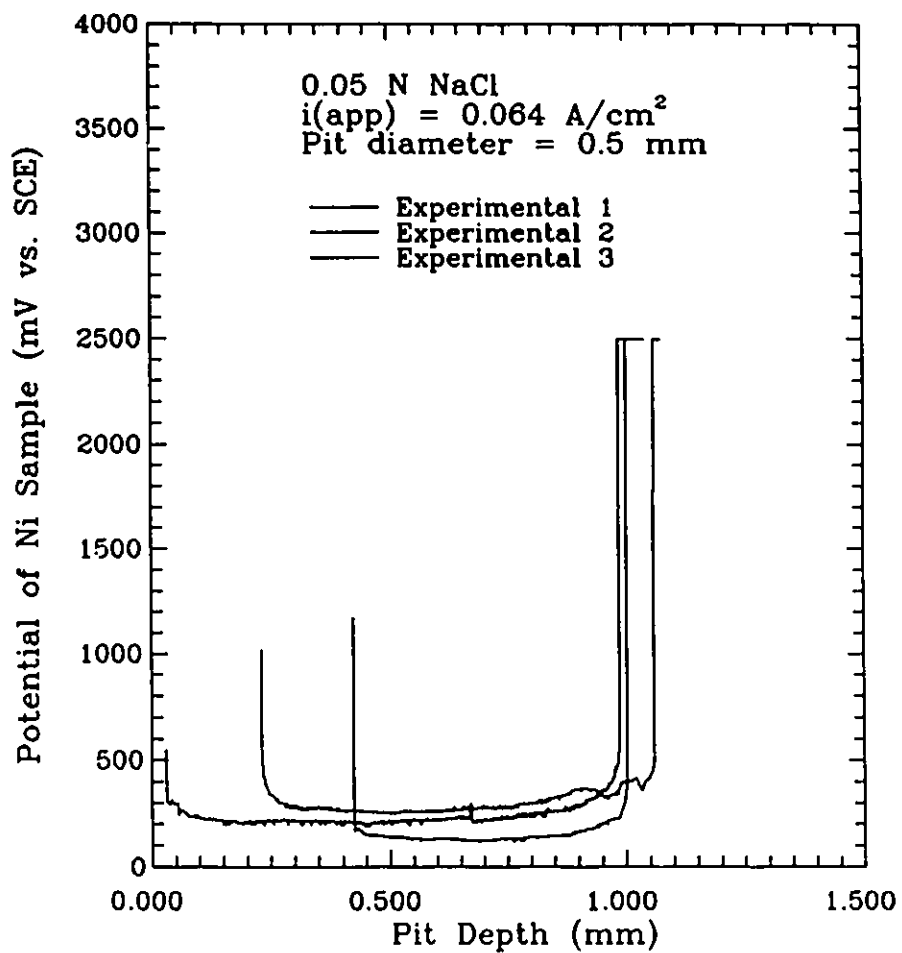
Figure 5.12   Measured potential of the Ni sample as a function of the depth of a 0.50 mm diameter pit.

0.05 N NaCl
i(app) = 0.064 A/cm^2
Pit diameter = 0.25 mm

——— Experimental 1
——— Experimental 2
——— Experimental 3
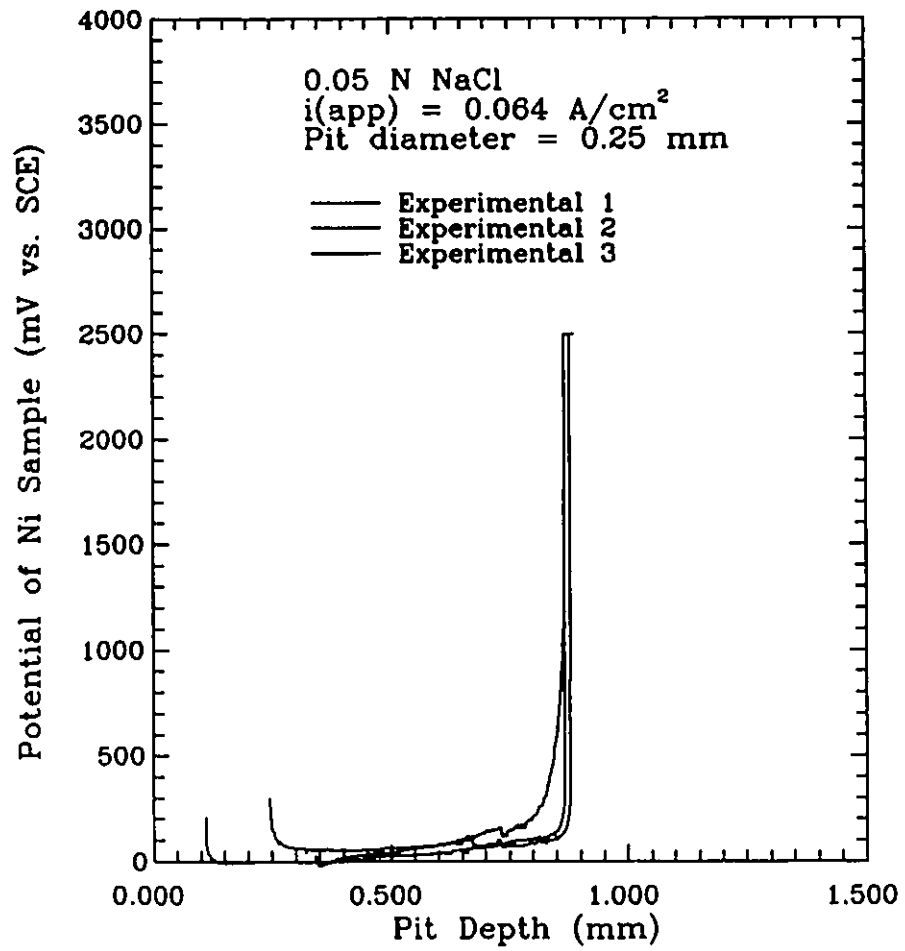
Figure 5.13   Measured potential of the Ni sample as a function of the depth of a 0.25 mm diameter pit.

Figures 5.9 and 5.10 display the measured activity of the chloride ions at the pit bottom and the potential of the nickel sample as a function of the depth of the pits with 0.76 mm and 0.50 mm diameters. The results in Figures 5.11, 5.12 and 5.13 present potential of the nickel samples as a function of the depth of the pits 0.76 mm, 0.50 mm and 0.25 mm in diameter with different initial pit depths. It is confirmed that for a fixed pit diameter, the critical depth is a constant and independent of the initial pit depth. But the critical depth is a function of the pit diameter.

Figure 5.14 is a plot of the measured transition depth vs. pit diameter. The best fit line to the points suggests the relationship

$$h_t = 0.8 + 0.55d^{3/2} \tag{5.1}$$

The first, constant, term could represent the depth over which one-dimensional diffusive flow exists and the second term, dependent on d, provides for the existence of an "end effect" where other than one-dimensional mass transport exists. It is this "end effect" that makes the actual critical pit depth h_t larger than the calculated value 0.88 mm. The end effect is presumably more complex for larger diameters, possibly due to additional convective effects. It will be interested to develop a model which includes the influence of the pit diameter. Lack of time did not permit this to be done. The empirical value, 1.55, was used in the current study to correct the diameter effect on the distribution of the chloride ions for comparing the theoretical calculated and experimentally measured values (Figure 5.3). Therefore, the geometry of the pit is an important factor which can be expected to influence pit growth.
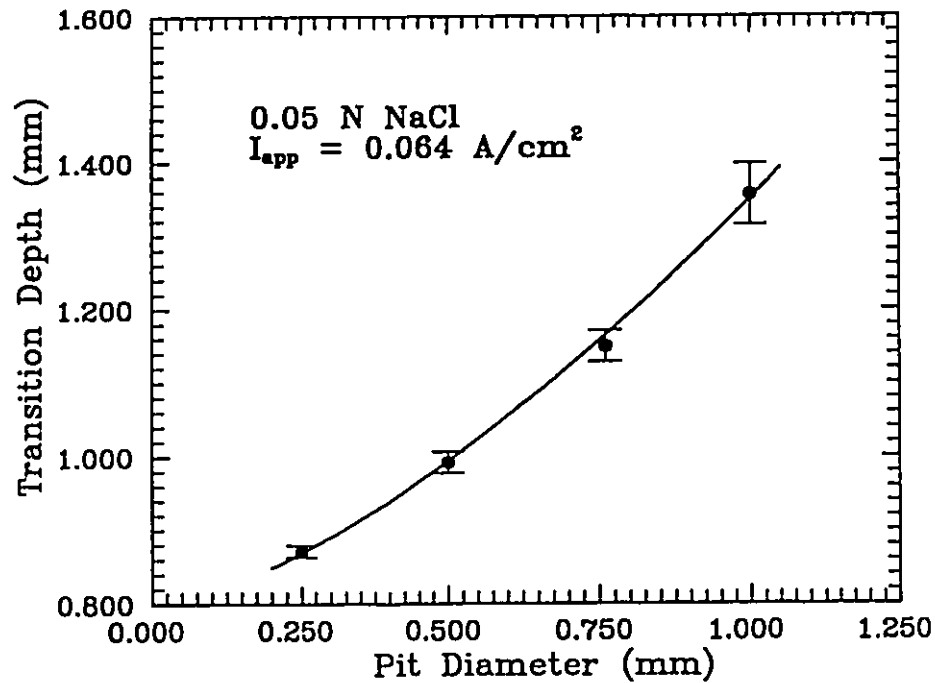
Figure 5.14   The transition depth as a function of the pit diameter for model pits in 0.05 N NaCl solution.

5.4. Properties of the salt film

5.4.1. Potential distribution across the salt film

After the salt film was formed at the pit bottom, the potential distribution within the film was studied by moving the potential or chloride probe at a rate slightly faster than the receding rate of the pit bottom. From the relative speed and time, the position of the probe within the salt film can be deduced.

Figure 5.15 is the potential distribution across the salt film after it is formed for 396±5 second measured by the potential probe. From Figure 5.15, it can

0.05 N NaCl
i(app) = 0.064 A/cm²
Pit diameter = 1.0 mm

Salt film

Solution

Measured Potential (mV vs. SCE)

Distance from Metal/Film Interface (μm)
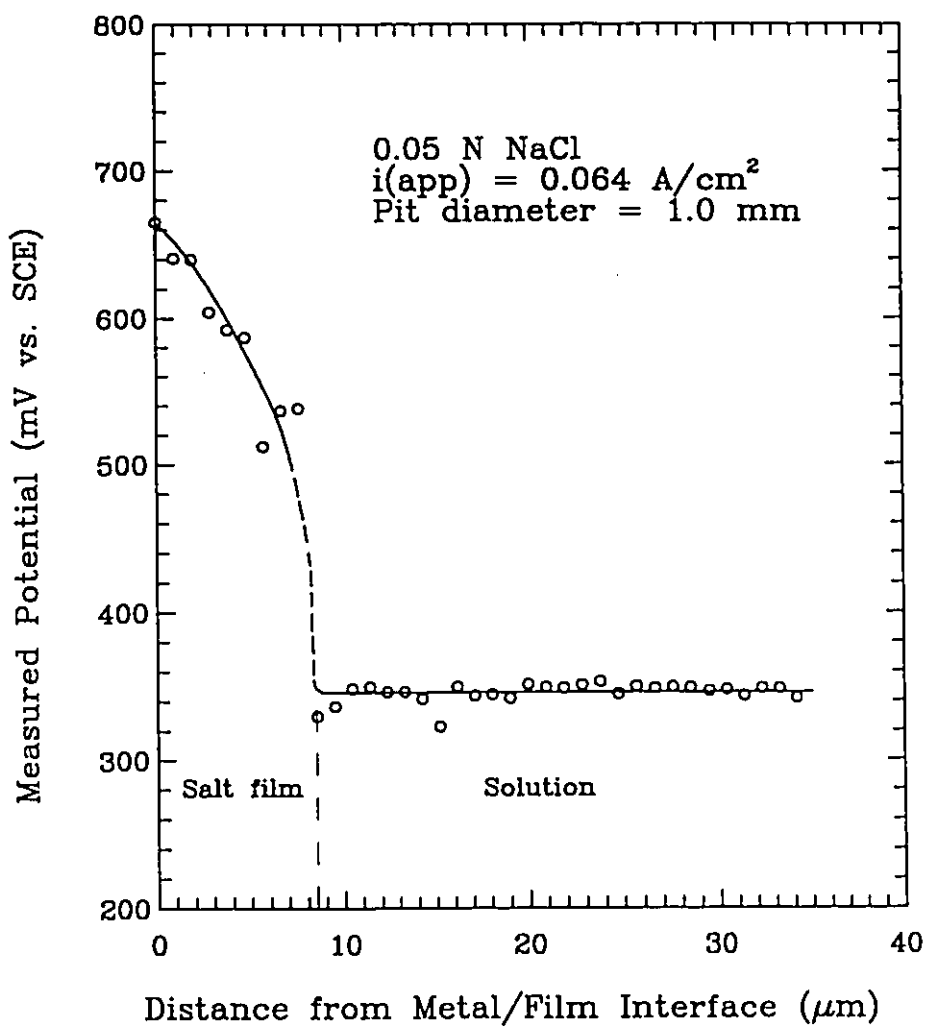
Figure 5.15   The potential distribution across the salt film measured by potential probe in a model pit 1.614 mm deep and 1.00 mm in diameter.

be estimated that after the salt film is formed for 396±5 seconds, the potential drop across the salt film and the thickness of the salt film are 330±10 mV and 8.5±1.4 μm respectively. The conductivity of the salt film, K_f, and the potential distribution has the following relation:

$$K_f = -\frac{i}{\dfrac{dE}{dZ_f}}$$ [5.2]

By Equation [5.2], the average conductivity of the salt film is calculated to be $(1.6 \pm 0.3) \times 10^{-4}\ \Omega^{-1} \cdot cm^{-1}$.

These values are similar to the observations of Hunkeler, Krolikowski and Bohni[29]. They studied the salt film on nickel by impedance and transient measurements and found that the electrical conductivity of the salt film is approximately $0.44 \times 10^{-4}\ \Omega^{-1} \cdot cm^{-1}$, the potential drop across the film ranges between 100 and 700 mV, and the thickness of the salt film that is formed at the bottom of a nickel model pit ranges between 3 and 8 μm. Vetter and Strehblow[21] suggested that the ordinary values of the layer thickness are 50 to 100 Å and consequently, not optically visible. The salt film formed under this experimental condition is thicker and also optically visible as shown in Figure 5.16.

5.4.2. Verification of the measured potential drop across the salt film

Theoretical analysis:

In order to justify the measured potential drop across the salt film, the theoretically determined charge transfer overvoltage can be compared with the one

estimated from the measured potential drop across the salt film. From Butler-Volmer equation,

$$i = i^\circ \exp\left\{\frac{(1-\alpha)nF\eta}{RT}\right\}$$

[5.3]

where $\eta = \eta_{CT} - E_0$. Rearranging Equation [5.3] gives:

$$\eta_{CT} = E_0 + \frac{RT}{(1-\alpha)nF}\ln\frac{i}{i^\circ}$$

[5.4]

Where $E_0 = E^\circ + \frac{RT}{nF}\ln\frac{a_{Ni^{2+}}}{a_{Ni}}$, which is known as Nernst Equation,

$E^\circ = -250$ mV (vs. SHE)[159],

$i^\circ = 1.1 \times 10^{-8}$ A/cm^2, $\alpha = 0.3$ [157],

$i = 0.0637$ A/cm^2, and

a_{Ni} and $a_{Ni^{2+}}$ are assumed to be 1 and 10^{-6}, respectively.

Substituting all values into Equation [5.4], one has

$\eta_{CT} = -143$ mV (SHE).

η_{CT} can also be expressed as

$\eta_{CT} = E_{Ni} - \eta_f - IR_{tot}$, and

$\eta_f + IR_{tot} = E_{pot,1}$(at metal/film interface) - $E_{pot,2}$(at reference electrode)

From the measurements:

$E_{Ni} = 270 \pm 10$ mV (vs. SCE)

$E_{pot,1} = 673 \pm 10$ mV (vs. SCE)

$E_{pot,2} = 6 \pm 1$ mV (vs. SCE)

therefore, η_{CT} is equal to - 397±14 mV vs. SCE, and -154±14 mV vs. SHE. This value for η_{CT} is reasonably close to the theoretical estimated value. Therefore, the measured η_t is reasonable.

5.4.3. Structure of the salt film

From the theoretical analysis, based on the last term in Equations [2.9] and [2.12], the flux of nickel and chloride consumed by the salt layer can be determined to be 1.4×10^{-9} mol/s/cm^2 and 2.7×10^{-9} mol/s/cm^2, respectively. The salt layer may be $NiCl_2 \cdot 6H_2O$, because it is more stable than $NiCl_2$[145]. The atomic weight is 237.69 g/mol [145]. The measured values of the thickness of the salt layer after it formed for 396 seconds is (8.5±1.4) μm. In this case, the density of the salt layer is estimated to be (1.5±0.2) g/cm^3. which is less than the density of a solid nickel chloride salt ($NiCl_2 \cdot 6H_2O$), 1.9 g/cm^3 [29]. This indicates that the salt layer formed in the experimental condition is a porous layer. Moreover, for the electric field strength of an ionic conductor, the typical order of magnitude is 10^6 V/cm [63]. From the measured potential distribution across the salt layer, average electric field is only 388 V/cm. Therefore, this is another evidence to show that the salt layer formed in this experimental condition is not a compact film.

5.5. The metallography of the pit bottom

Figure 5.16 shows the metallography of the pit bottom at the various stages. Figure 5.16. a. is the pit at the active dissolution stage. Under certain experimental conditions, e.g. when the depth of the pit reached the transition depth or the applied current is very high, it was observed that a green layer started to cover

90

the pit bottom and the shiny metal surface could be seen through it as shown in Figure 5.16. b. This layer gradually became opaque and the metal surface could no longer be seen as presented in Figure 5.16. c. The green layer was easily removed with a jet of water during the experiment.

The evolution of gas bubbles was frequently observed in a continuously developing pit as shown in Figure 5.16 b. and c. After a salt film is formed at the pit bottom, the small gas bubbles was observed at the pit bottom. Sometimes, the small bubbles agglomerated into a big one. The potential of the nickel sample increased during the growth of these bubbles and decreased on their release. At the high applied current, such a conglomerate bubble always formed. The deeper the pit, the faster the bubble forms. When the applied current was turned off, the bubble would shrink, but would not disappear. The shrinkage of the bubble may be the result of the termination of the Joule heat.

(a)   (b)   (c)
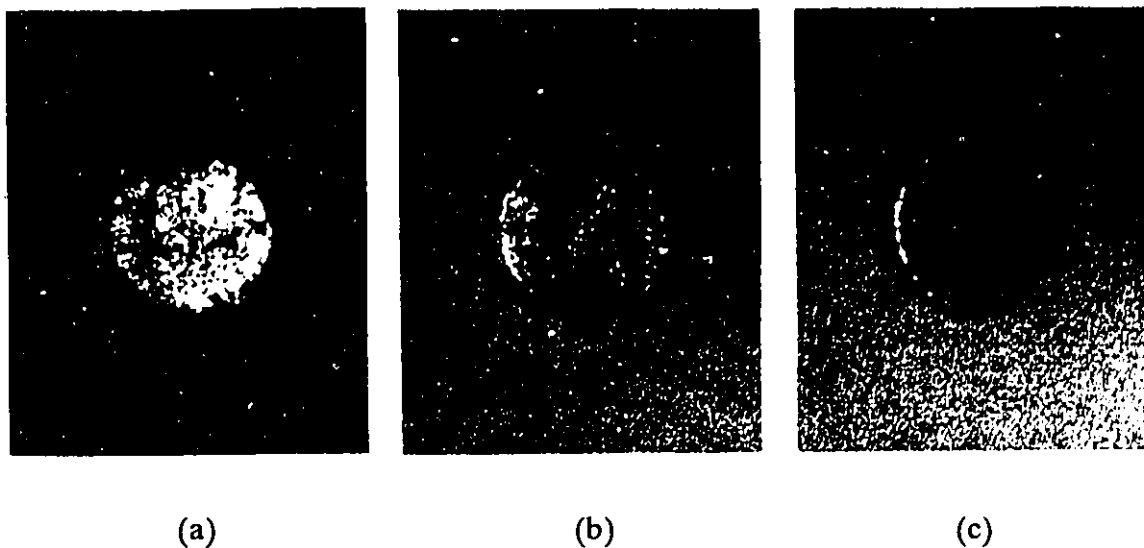
Figure 5.16   The metallography of (a). the pit before the salt film formation, (b). and (c). the salt film at the different stages. (x 23)

5.6. Hydrogen evolution

The IR drop in the solution and the potential drop across the salt layer at the pit bottom brings the potential of the metal surface to the state where hydrogen evolution may occur. Hence, it is possible that the gas bubbles observed during experiments are hydrogen as suggested by others[158].

To confirm this conclusion, the charge transfer overvoltage as estimated above is compared with the Pourbaix diagram[159] (Figure 5.17). It is shown that for Ni, η_{cr}, which is equal to -154 ± 14 mV, is located in the hydrogen evolution range when pH is less than 2.6 ± 0.2. The evolution of hydrogen inside pits in nickel is thermodynamically justified.

5.7. The conditions at the pit bottom at the various stages of pit development

To investigate the mechanism of pit development, one has to clarify the local chemistry and electric potential in three major forms of a pit: a) an active pit, i.e. a pit before a salt film is formed at the bottom, b) a pit with a salt film at the bottom, and c) a passivated pit. To study the pits in these three kinds of states, pits with diameter of 1.00 mm and a depth of 0.500 mm were tested under three applied current densities, viz. $(1.3\pm0.1)\times10^{-6}$ A/cm^2, $(63.7\pm0.1)\times10^{-3}$ A/cm^2 and (0.1273 ± 0.0002) A/cm^2. These three values were determined by the following observations: When the applied current density is 1.3×10^{-6} A/cm^2, the nickel surface remains in the passive state. The pit undergoes active dissolution at the current density of 63.7×10^{-3} A/cm^2 and with the pit depth less than 1.0 mm, i.e., under microscopic monitor, no salt film was observed. As the applied current density is
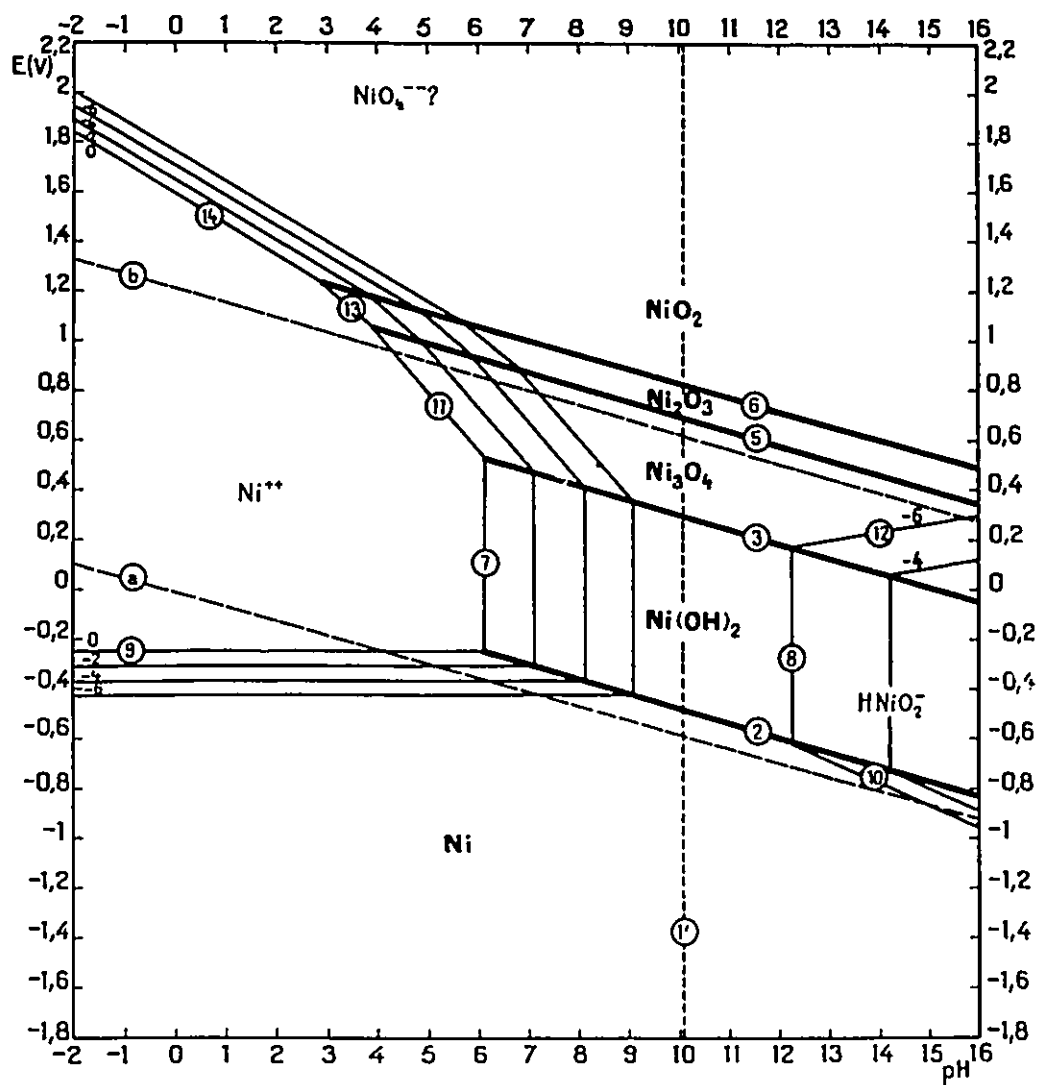
Figure 5.17 Pourbaix diagram for Ni[159].

changed from 63.7×10^{-3} A/cm^2 to 0.1273 A/cm^2, microscopic observation reveals that a green film starts to form at the pit bottom (as shown in Figure 5.16. b), as a result, the dissolution mechanism changes from mixed ohmic-charge transfer control to diffusion control. At these three different dissolution conditions, the distributions of the activity of the chloride ions, pH and the potential along the pit axis were measured by microelectrodes. The results are displayed in Figures 5.18, 5.19 and 5.21 for distribution of the chloride ions, pH, and potential, respectively.

Curves (a) in Figures 5.18, 5.19 and 5.21 show that the local conditions of the pit electrolyte at the passive state are not much different from those out in the bulk solution. When the pit undergoes active dissolution, the results from curves (b) in Figures 5.18, 5.19 and 5.21 display the obvious difference between the electrolyte inside the pit and the bulk solution. When a salt film is formed, the pH at the pit bottom changes from 2.2 to 1. The activity of the chloride ions there increases from 0.7 to 5.3. The salt film certainly will influence the pit growth.

The relationship between the measured potential of the nickel sample and the potential difference between the nickel substrate and pit surface is illustrated schematically in Figure 5.20. E_{Ni} is the potential difference between Ni sample and reference electrode; IR_{in} and IR_{out} are the IR drop inside and outside the pit, respectively; and E_{Re} is the reference electrode potential. From the potential of the sample and the measured IR drop in the solution, the potential difference between the metal and film/solution interface can be estimated. For convenience of discussion, this potential difference is defined as ϕ_s. When there is a surface film, ϕ_s is the sum of the charge transfer overvoltage and the potential drop across the film.
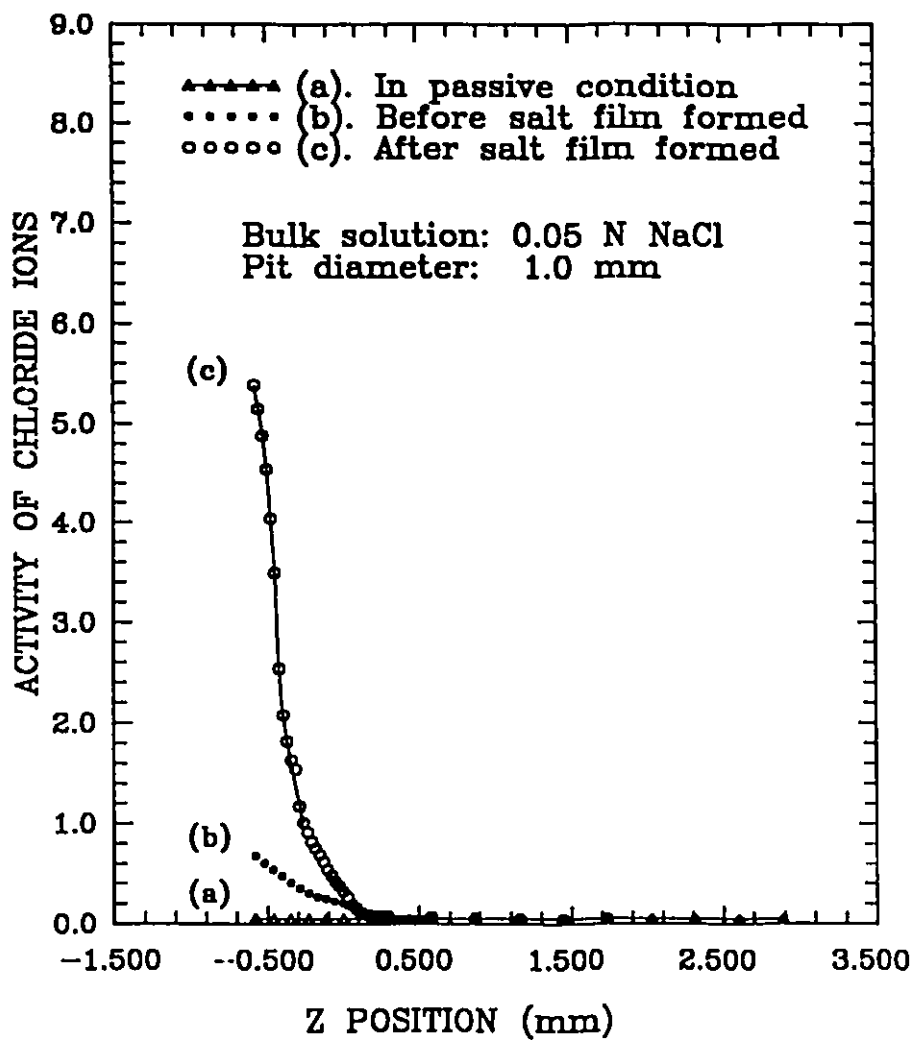
Figure 5.18   The distribution of activity of chloride ions in the Z direction of the pit when applied current density is (a) 1.27 μA/cm^2; (b) 64 mA/cm^2; and (c) 127 mA/cm^2.
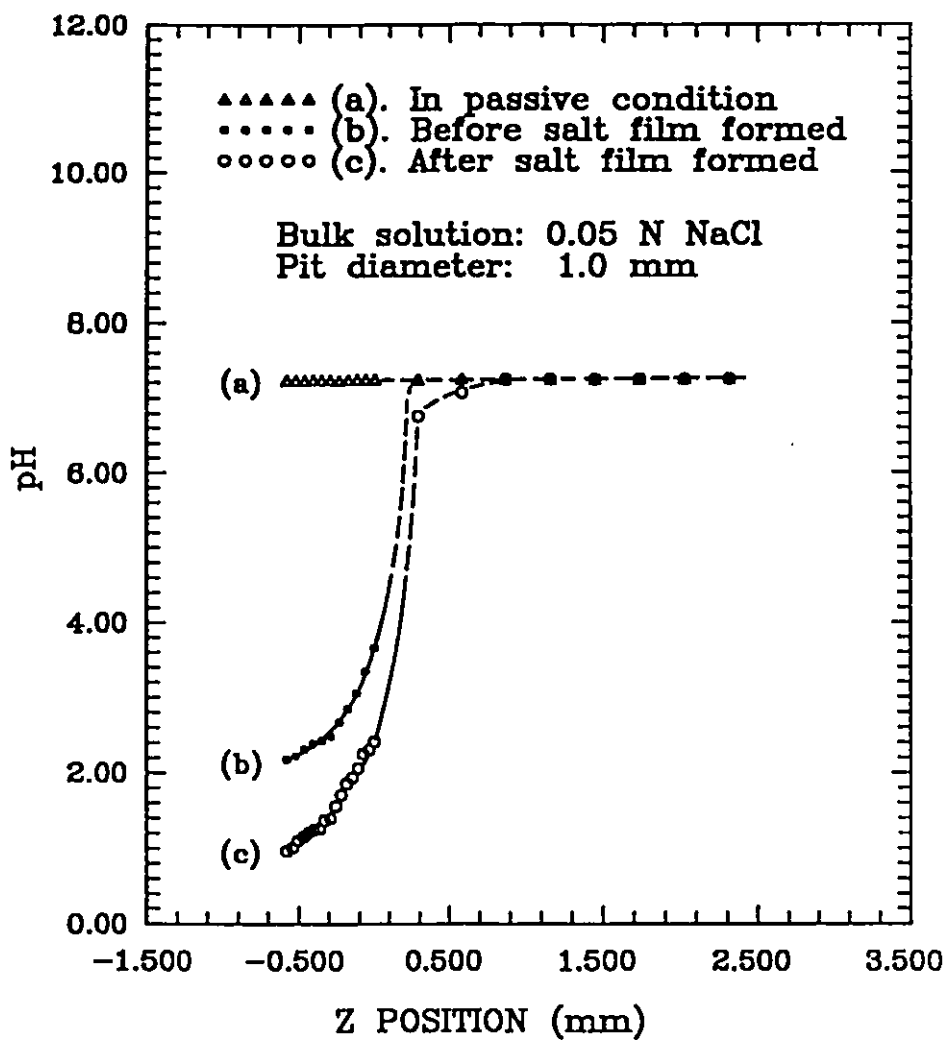
Figure 5.19 The pH distribution in the Z direction when applied current density is (a) 1.27 $\mu A/cm^2$; (b) 64 mA/cm^2; and (c) 127 mA/cm^2.

Figure 5.21 depicts the distribution of the IR drop in Z direction at different dissolution stages. The potential difference between the pit bottom and the pit mouth (z=0) is the IR drop within the pit. The potential difference between the pit mouth and point D is the IR drop outside the pit. The potential at point D indicated in Figure 5.21 is the potential where the reference electrode is located. The measured E_{Ni}, IR_{tot}, and ϕ_s are listed in Table 5.1.

Table 5.1 Measured E_{Ni}, IR_{tot}, and ϕ_s

Pit Stage	E_{Ni} (mV)	IR_{tot} (mV)	ϕ_s (mV)
Passivation	152±10	2±1	150±10
Before salt film formed	300±10	304±1	-4±10
After salt film formed	770±10	622±1	148±10
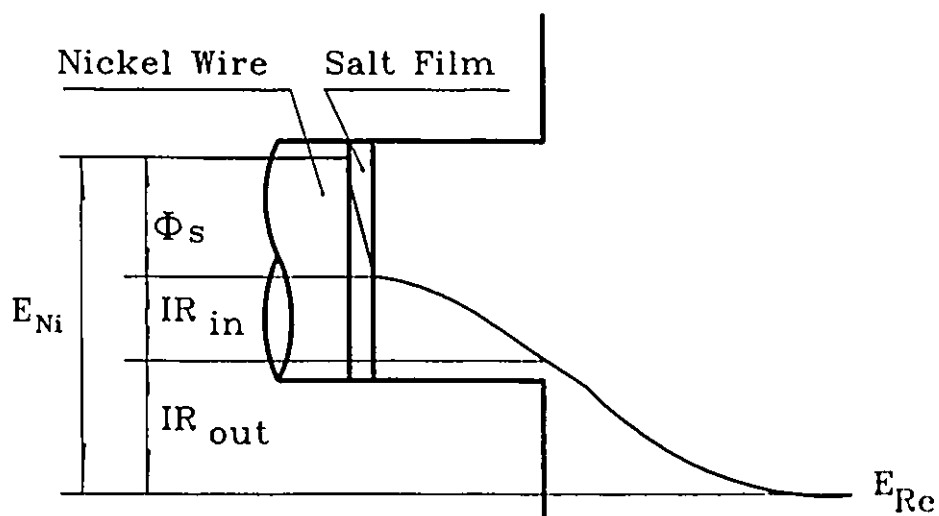
Figure 5.20   Schematic diagram of potential distribution between the nickel sample and reference electrode.
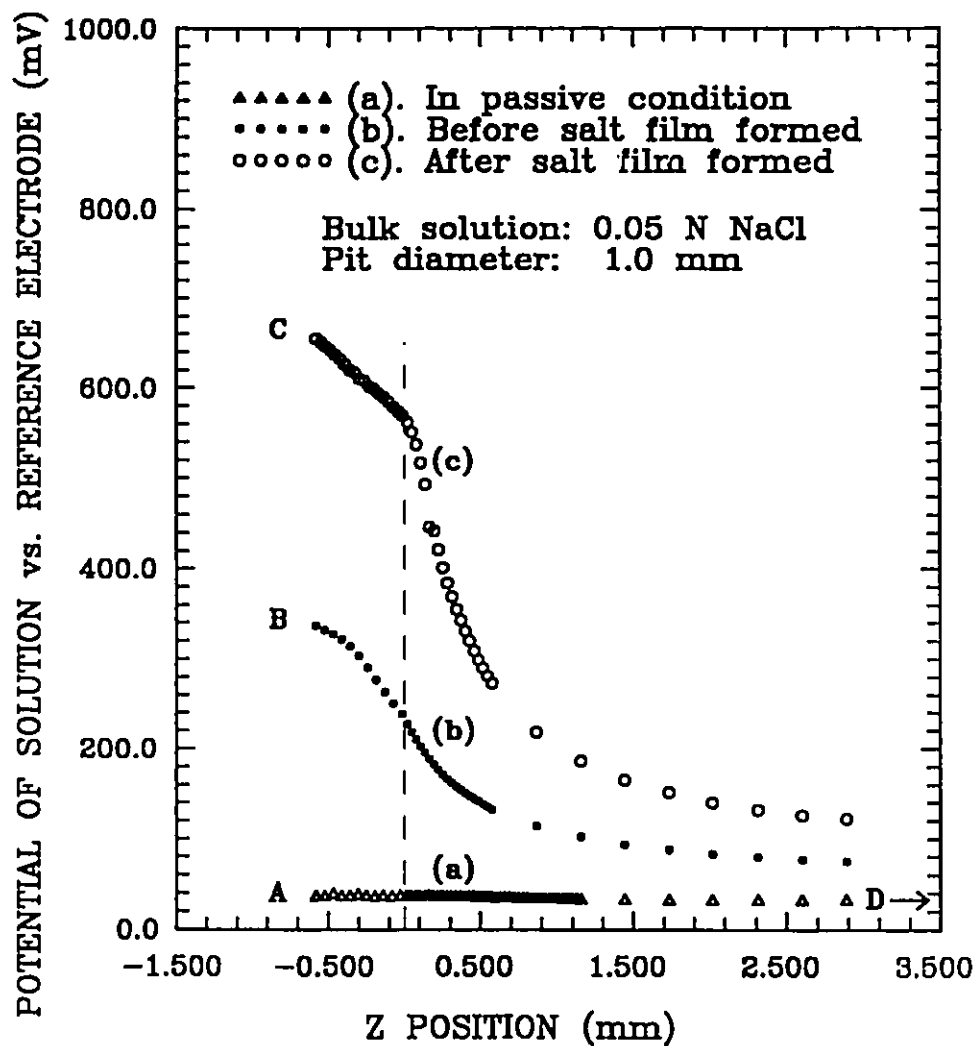
Figure 5.21   Potential distribution in the Z direction when applied current density is (a) 1.27 $\mu A/cm^2$; (b) 64 mA/cm^2; and (c) 127 mA/cm^2. "D" is the potential at the reference electrode.

5.8. The anodic behaviour of nickel in pit electrolytes corresponding to various stages of pit development

The anodic polarization behaviour of a pure nickel coupon has been determined in solutions which simulate the acidity and chloride ion concentration determined previously (Figures 5.18 and 5.19) within pits at different stages of development. Figure 5.22 shows the superimposed polarization curves of nickel in solutions corresponding to the local conditions:

(a) when the pit is passivated [0.05 M NaCl, pH 7.21];

(b) before salt film is formed [0.7 N $NiCl_2$, with pH adjusted to 2.2 by HCl]; and

(c) after salt film is formed [saturated $NiCl_2$ with pH adjusted to 1.0 by HCl].

Figure 5.22 can be used to explain the mechanism of pit development in nickel by locating the measured ϕ_s for each condition. Curve (a) in Figure 5.22 is the anodic behaviour of nickel in the bulk solution. The sample is passivated in the potential range between open circuit potential and 160 mV. As described above, ϕ_s of the repassivated pit is equal to 150 mV, i.e., at point E_a of curve (a) in Figure 5.22, which is located in the passive range.

Curve (b) in Figure 5.22 is the anodic behaviour of nickel in a solution simulating the electrolyte close to the pit bottom before salt film formation. In this condition, the polarization curve has a just-discernable active "nose" and a passive range. It is obvious that the potential of the pit bottom must be in the active region if the pit is to continue to develop. The IR drop is then a critical factor, as proposed by Pickering[89]. The minimum potential drop necessary has been called the critical IR
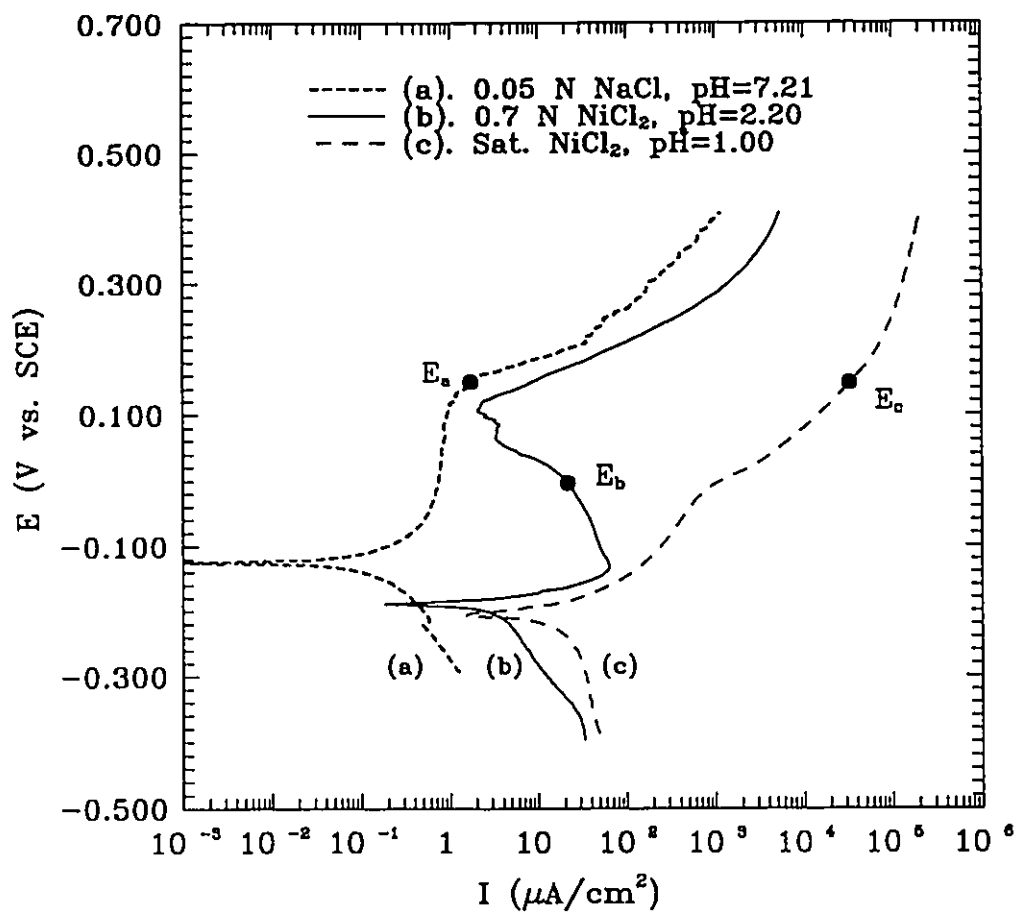
Figure 5.22 Superposition of the polarization curves for Ni coupons exposed to electrolytes which simulate the conditions close to the pit bottom (a) in passivation state, (b) before and (c) after salt film formation.

drop as defined in Figure 1.1. Only when the IR drop is larger than this value will the pit continue growing. Otherwise, the dissolution rate will drop dramatically. As a result, the local electrolyte will become less aggressive, and repassivation may occur. From Table 5.1, the ϕ_s before the salt film formed is -4 mV, corresponding to point E_b of the curve (b) in Figure 5.22. The potential of the continuously developing pit would then be located in the active region.

Curve (c) in Figure 5.22 is the polarization curve of nickel in a solution simulating the local chemistry close to the bottom after a salt film is formed. Because the pit electrolyte is so aggressive, the sample remains active throughout the whole applied anodic potential range. From Table 5.1, the ϕ_s after a salt film formed is 148 mV, noted as point E_c of curve (c) in Figure 5.22. Here, the IR drop is no longer important. There is always significant anodic dissolution due to the aggressiveness of the electrolyte. In this case, the local electrolyte composition controls pit development. The possibility of repassivation is low. Therefore, before any salt film forms, the pit is in a condition of unstable growth; after the salt film forms, the pit is stable and will develop steadily.

In broad outline, the experimental results support the conclusions from the modelling calculation. It shows that the mass transport processes within a pit fit the model proposed in Chapter 2. The conditions to achieve a steady state and the critical depth for a salt film formation are proved to be the same as predicted by the model. The conditions necessary for stabilization of pitting corrosion were characterized. The electrochemical response of the nickel in the local environments

permitted the deduction of the controlling factors which governed the pit growth. Before any salt film forms, the pit is in a condition of unstable growth and the solution ohmic drop is the controlling factor for pit development; after the salt film forms, the pit is stable because of the aggressiveness of the electrolyte.

CHAPTER 6. CONCLUSIONS AND FURTHER WORK

6.1. Contributions to knowledge

The objectives for this research were originally identified in Chapter 1. For convenience, they are briefly summarized below: A comprehensive model will be built to determine the local environmental conditions within pits. The conditions for the formation of the salt layer will be evaluated. And the conditions necessary for stabilization of pitting corrosion will be characterized. Then the model was tested experimentally through in situ measurements in a model nickel pit system.

Consideration of the content of the previous chapters shows that these objectives have all been achieved. Application of the microelectrodes to the study of the detailed local conditions within the corroding pits is proving to be very powerful. The results acquired with this technique have provided valuable insight into the pit development. From this research, the following conclusions are drawn:

1.   The in situ measurements obtained by microelectrodes provide the direct evidence of existence of a salt layer at the bottom of a developing pit under the conditions employed in these experiments. A critical depth is found to be necessary for the salt film formation in one dimensional pit.

2.   The mechanism of the salt film formation and its structure can be predicted by a theoretical model considering the mass transport processes, comprising diffusion and migration, reaction equilibria, multiple species in solution and interfacial reaction within a model pit.

The critical depth for salt-film formation ensures the maintenance of a local critical solution chemistry.

3.   The measurement of the potential distribution within the salt film has provided data for the potential drop across the salt film, its thickness and therefore its conductivity. Combining a theoretical model with experimental results, it is concluded that the salt film formed under the experimental condition is a porous layer.

4.   Salt film formation on the pit bottom is a sufficient condition for a steady developing pit. It assures the aggressiveness of the local chemistry, which enhances the local dissolution. Therefore the possibility of repassivation is rare. However, in the metastable pit, IR drop in solution at the site of localized attack is the controlling factor for pit development. If the IR drop is less than a critical value, repassivation may occur.

Last, it will be very important to study and compare the other factors, such as the pit shape, the form of the boundary conditions, different applied current or potential and bulk concentration, affecting the electrolyte composition, and therefore, the pitting stabilization.

6.2. Contributions to the literature

The microelectrode technique needed to perform in situ measurements within a pit was developed in our laboratory and formed the basis of a publication in Journal of Electroanalytical Chemistry and Interfacial Electrochemistry[160].

Three papers have been presented in conferences and published in proceedings based upon the content of the previous chapters[161,162,163].

Four papers have been produced and published as a result of the applications of the microelectrodes in localized corrosion of stainless steels[164,165,166] and iron in chloride containing solution[167].

6.3. Suggestions for further research

During the course of the researches described in this thesis, a number of other activities were attempted, or suggested themselves.

From this study, it is concluded that a salt film is an important factor for stabilizing pitting. The transition depth for the salt film formation is a function of the pit diameter because the transport processes are dependent on the geometry of the pit. Therefore, the geometrical effect on the stability of the pits should be studied. Theoretically, describing the transport processes in a two dimensional model will provide useful information and may give the explanation of the transition depth as a function of the pit diameter. Experimentally, it will be interesting to use pits having different geometries. For example, most natural pits are not open but covered. A covered pit has a condition to reduce the diffusion to its minimum. With a small hole to permit egress of corrosion product, the chloride ions would be more promptly enriched inside covered pits and therefore the salt films would form even more readily than in open pits. Some alloy elements have the effect of changing the shape of the pit. For instance, from our previous study[168], it was observed that the pits formed on NiMo alloy are shallower than those formed in pure nickel.

This study only characterized the salt film under a specific condition. Actually, the transition depth for the salt film formation depends on the current or potential and bulk concentration. So do the characteristics of the salt film. For example, the structure of the salt film may depend on the current passed through the metal interface. Therefore, studying how the transition depth and the characteristics of the salt film will be influenced by current and bulk concentration will be helpful to better understand the stabilization of pit development. This could readily be accomplished by using the microelectrode technique developed in this research.

Because the activity coefficients have significant influence on the distribution of the ionic species, therefore, the assumption that the activity coefficients of the complexes are equal to unity is not appropriate. The measurements of the activity coefficients of the complexes involved in the model and the parameters required in Pitzer's equation through defined experiments in the nickel chloride system are needed. Since the selectivity coefficient value may vary with different ion activities, it is necessary to determine experimentally a series of selectivity coefficient values for a range of activities. Therefore, correction for the interference effect by ions other than the detected ions on the potential of the pH probe will be more accurate.

The microelectrode technique required to perform in situ measurements can be improved in three ways: (1). The tungsten probe currently employed for pH measurement is not sensitive when pH > 4.7, therefore, it is necessary to develop a pH probe which is sensitive in all pH ranges. Iridium[169] and palladium[170] may be good candidates. (2). The distribution of the nickel ions within a pit predicted by the

model has not been experimentally tested. It is necessary to develop a micro nickel

ion probe. (3). The microelectrode facility developed in this research can be

combined with a mapping technique. For example, it can be used to map the

chloride ion concentration over a sample surface, which will show the aggregation

of the ions and its relationship with the pit nucleation.

REFERENCES

1.   F. Hunkeler and H. Boehni, Corrosion, 37, 645(1981)

2.   F. Hunkeler and H. Boehni, Corrosion, 40, 534(1984)

3.   H.W. Pickering, "Corrosion and Protection", R.F. Frankenthal and F. Mansfeld
      Eds., The Electrochemical Society, Pennington, 88(1981)

4.   H.W. Pickering, Conf. Proc. Advances in Localized Corrosion, NACE-9, H.
      Isaacs, U. Bertocci, J. Kruger and S. Smialowska, Eds., NACE, Houston, Texas,
      77(1990)

5.   H.S. Kim, Y.T. Kho, K. Osseo-Asare and W.H. Pickering, Metallurgical
      Transactions B, 22b, 323(1991)

6.   G. Herbsleb and H.J. Engell, Werkst. Korros., 17, 365(1966)

7.   C.M. Chen, F.H. Beck and M.G. Fontana, Corrosion, 27, 234(1971)

8.   H.W. Pickering, and R.P. Frankenthal, J. Electrochem. Soc., 119, 1297(1972)

9.   R.P. Frankenthal and H.W. Pickering, J. Electrochem. Soc., 119, 1304(1972)

10.   J.W. Pickering and R.P. Frankenthal, Proc. Conf. Localized Corrosion, NACE-3,
      R. Staehle, B. Brown, J. Kruger, A. Agrawal, Eds., NACE, Houston, Texas,
      261(1974)

11.   T.R. Beck, J. Electrochem. Soc., 120, 1317(1973)

12.   H. Boehni, Langmuir, 3, 924(1987)

13.   L. Stockert and H. Boehni, Proc. 8th European Corros. Cong. Centre Francais

de la Corrosion, Paris, France, 2, 22(1985)

14.   H. Kaesche, Z. Physik. Chem. NF, 34, 87(1962)

15.   W. Schwenk, Corrosion, 20, 129t(1964)

16.   H.J. Engell and N.D. Stolica, Z. Phys. Chem., NF, 20, 113(1959)

17.   H.-H. Strehblow and M.B. Ives, Corros. Sci. 16, 317(1976)

18.   T.R. Beck and R.C. Alkire, J. Electrochem. Soc., 126, 1662(1979)

19.   K.J. Vetter, Ber. Bunsenges. physik. Chem., 69, 683(1965)

20.   K.J. Vetter, and H.H. Strehblow, Ber. Bunsenges. physik. Chem., 74, 1024(1970)

21.   K.J. Vetter, and H.H. Strehblow, Proc. Conf. Localized Corrosion, NACE-3, R. Staehle, B. Brown, J. Kruger, A. Agrawal, Eds., NACE, Houston, Texas, 240(1974)

22.   T.R. Beck, Electrochim. Acta, 29, 485(1984)

23.   T.R. Beck, Conf. Proc. Advances in Localized Corrosion, NACE-9, H. Isaacs, U. Bertocci, J. Kruger and S. Smialowska, Eds., NACE, Houston, Texas, 85(1990)

24.   H. Boehni, "Corrosion in Power Generating Equipment", M.O. Speidel and A. Atrens Eds., Plenum Press, New York, NY, 29(1984)

25.   H.H. Strehblow, K.J. Vetter and A. Willgallis, Ber. Bunsenges. physik. Chem. 75, 822(1971)

26.   H.H. Strehblow, Werkstoffe und Korrosion, 35, 437(1984)

27.   H. Boehni and F. Hunkeler, Conf. Proc. Advances in Localized Corrosion, NACE-9, H. Isaacs, U. Bertocci, J. Kruger and S. Smialowska, Eds., NACE, Houston, Texas, 69(1990)

28.   G.S. Frankel, Conf. Proc. Advances in Localized Corrosion, NACE-9, H. Isaacs,
       U. Bertocci, J. Kruger and S. Smialowska, Eds., NACE, Houston, Texas,
       137(1990)

29.   F. Hunkeler, A. Krolikowski and H. Bohni, Electrochim. Acta, 32, 615(1987)

30.   H.S. Isaacs, J. Electrochem. Soc., 120, 1456(1973)

31.   A. Turnbull, Conf. Proc. Advances in Localized Corrosion, NACE-9, H. Isaacs,
       U. Bertocci, J. Kruger and S. Smialowska, Eds., NACE, Houston, Texas,
       359(1990)

32.   J.W. Tester and H.S. Isaacs, J. Electrochem. Soc., 122, 1438(1975)

33.   G.T. Gaudet, W.T. Mo, T.A. Hatton, J.W. Tester, J. Tilly, H.S. Isaacs, and R.C.
       Newman, AIChE Journal, 32, 949(1986)

34.   Y. Hisamatsu, Conf. Proc. Passivity and its Breakdown on Iron and Iron Based
       Alloys, R. Staehle and H. Okada Eds., NACE, Houston, Texas, 99(1976)

35.   S.M. Gravano and J.R. Galvele, Corros. Sci., 24, 517(1984)

36.   J.R. Galvele, Corros. Sci., 21, 551(1981)

37.   J. R. Galvele, J Electrochem. Soc., 123, 464(1976)

38.   N. Sato, "Corrosion and Protection", R.F. Frankenthal and F. Mansfeld Eds.,
       The Electrochemical Society, Pennington, 101(1981)

39.   N. Sato, J. Electrochem. Soc., 129, 260(1982)

40.   N. Sato, T. Nakagawa, K. Kudo and M. Sakashita, Proc. Conf. Localized
       Corrosion, NACE-3, R. Staehle, B. Brown, J. Kruger, A Agrawal, Eds., NACE,
       Houston, Texas, 447(1974)

41. H. Boehni, "Corrosion in Power Generating Equipment", M.O. Speidel, A. Atrens, Eds., Plenum Press, New York, NY, 29(1984)

42. H.J. Engell, Electrochim. Acta, 22, 987(1977)

43. Z. Szklarska-Smialowska, "Pitting Corrosion of Metals", NACE, Houston, Texas, 362(1986)

44. I.L. Rosenfeld, I.S. Danilov, R.N. Oranskays, J. Electrochem. Soc., 125, 1729(1978)

45. R. Alkire, D. Ernsberger, T.R. Beck, J. Electrochem. Soc., 125, 1382(1978)

46. M. Datta and D. Landolt, Electrochim. Acta, 25, 1255(1980)

47. T.R. Beck and S.G. Chan, J. Electrochem. Soc., 130, 1289(1983)

48. R. Alkire and A. Cangellari, J. Electrochem. Soc., 130, 1252(1983)

49. T.R. Beck and D.E. Rice, J. Electrochem. Soc., 131, 89(1984)

50. T.R. Beck, Electrochim. Acta, 30, 725(1985)

51. V.M. Novakovski, A.N. Sorokina, Corros. Sci., 6, 227(1966)

52. H.H. Strehblow, J.Wenners, Z. Phys. Chem., 98, 199(1975)

53. J.Wenners, Dissertation, Freie University, Berlin, (1977)

54. R. Kirchheim, K. Maier, G. Tolg, J. Electrochem. Soc., 128, 1027(1981)

55. T.R. Beck, J. Electrochem. Soc., 129, 2412(1982)

56. H.H. Strehblow and J. Wenners, Electrochim. Acta, 22, 421(1977)

57. F. Hunkeler and H. Bohni, Conf. Proc. Corrosion Chemistry within Pits, Crevices and Cracks, A. Turnbull Ed., HMSO, London, 27(1987)

58. F. Hunkeler, G.S. Frankel and H. Boehni, Corrosion, 43, 189(1987)

59.   H.S. Isaacs and R.C. Newman, "Corrosion and Protection", R.F. Frankenthal and F. Mansfeld Eds., The Electrochemical Society, Pennington, 120(1981)

60.   G.S. Frankel, L. Stockert, F. Hunkeler and H. Boehni, Corrosion, 43, 429(1987)

61.   L. Stockert and H. Boehni, Proc. Conf. Electrochemical Methods in Corrosion Research, B. Elsener Edt. Trans. Tech. Publications, Switzerland-Germany-UK-USA, 313(1989).

62.   Y. M. Kolotyrkin, J. Electrochem. Soc., 108, 209(1961)

63.   R.D. Grimm, Ph.D Thesis, Ecole Polytechnique Federale de Lausanne (1991).

64.   A.C. West, R.D. Grimm, C. Deslouis, B. Tribollet and D. Landolt, Extended Abstracts, 180th Electrochemical Society Meeting, Phoenix, Arizona, October 13-17, 245(1991).

65.   T.R. Beck, Electrochim. Acta, 30, 725(1985)

66.   N.D. Greene and M.G. Fontana, Corrosion, 15, 49 and 55(1959)

67.   R. Alkire, D. Ernsberger, and D. Damon, J. Electrochem. Soc., 123, 458(1976)

68.   J. Galvele, "Passivity of Metals", R. Frankenthal, J. Kruger, Eds., The Electrochemical Society, Princeton, NJ, 285(1978)

69.   M. Watson and J. Postlethwaite, Corrosion, 46, 522(1990)

70.   T.T. Tokuda and M.B. Ives, J. Electrochem. Soc., 118, 1404(1971)

71.   M.B. Ives and T.T. Tokuda, Corros. Sci., 11, 297(1971)

72.   M.B. Ives and M. Zamin, J. Electrochem. Soc., 121, 1141(1974)

73.   M.B. Ives and M. Zamin, Corrosion, 29, 319(1973)

74.   Guo Ruijin and M.B. Ives, Corrosion, 45, 572(1989)

75.   J.A. Smith, M.H. Peterson and B.F. Brown, Corrosion, 26, 539(1970)

76.   D.A. Meyn, Met. Trans., 2, 853(1971)

77.   R.A.H. Edwards and P. Schuitemaker, Conf. Proc. Corrosion Chemistry within Pits, Crevices and Cracks, A. Turnbull Ed., HMSO, London, 413(1987)

78.   F.D. Bogar, Report of NRL Progress, 26, Nov.(1975)

79.   F.D. Bogar and C.T. Fujii, NRL Rept., 7690, AD 778 002, March(1974)

80.   N. J. H. Holroyd, G. M. Scamans and R. Hermann, Conf. Proc. Corrosion Chemistry within Pits, Crevices and Cracks, A. Turnbull Ed., HMSO, London, 495(1987)

81.   J.C. Greiss, Corrosion, 24, 96(168)

82.   T. Suzuki, M. Yamabe and Y. Kitamura, Corrosion, 29, 18(1973)

83.   J. Mankowski and Z. Szklarska-Smialowska, Corros. Sci., 15, 493(1975)

84.   D.F. Taylor and M. Silverman, Corrosion, 36, 447(1980)

85.   T. Mizuno, Corros. Sci., 31, 497(1990)

86.   R.C. Thomas, "Ion-sensitive Intracellular Microelectrodes", Academic Press(1978)

87.   R.A. Durst, Proc. Conf. Localized Corrosion, NACE-3, R. Staehle, B. Brown, J. Kruger, A. Agrawal, Eds., NACE, Houston, Texas, 151(1974)

88.   J.A. Davis, Proc. Conf. Localized Corrosion, NACE-3, R. Staehle, B. Brown, J. Kruger, A. Agrawal, Eds., NACE, Houston, Texas, 168(1974)

89.   H.W. Pickering, Corros. Sci., 29, 325(1989)

90.   K. Cho and H.W. Pickering, J. Electrochem. Soc., 137, 3313(1990)

91.   A. Valdes and H.W. Pickering, Conf. Proc. Advances in Localized Corrosion, NACE-9, H. Isaacs, U. Bertocci, J. Kruger and S. Smialowska, Eds., NACE, Houston, Texas, 393(1990)

92.   H.S. Isaacs, Corrosion, 46, 677(1990)

93.   H.S. Isaacs and G. Kissel, J. Electrochem. Soc., 119, 1628(1972)

94.   H. S. Isaacs, Corros. Sci., 29, 313(1989)

95.   I.L. Rosenfeld and I.S. Danilov, Corros. Sci., 7, 129(1967)

96.   C.D.S. Tuck, Corros. Sci., 23, 379(1983)

97.   G. Butler, H.C.K. Ison and A.D. Mercer, Br. Corros. J., 6, 31(1971)

98.   Y. Hisamatsu, T. Yoshii and Y. Matsumura, Proc. Conf. Localized Corrosion, NACE-3, R. Staehle, B. Brown, J. Kruger, A. Agrawal, Eds., NACE, Houston, Texas, 427(1974)

99.   T. Tsuru, K. Hashimoto and S. Haruyama, "Critical Issues in Reducing the Corrosion of Steels", H. Leidheiser,Jr. and S. Haruyama Eds., NACE, Texas, 110(1986)

100.   P.C. Caldwell, J. Physiol., 126, 169(1954)

101.   D.A. Robinson, Proc. Inst. Elect. Electron. Engrs., 56, 1065(1968)

102.   T. Ogawa, P.O. Bishop and W.R. Levick, J. Neurophysiol., 29, 1(1966)

103.   W.R. Levick, Med. & Biol. Eng., 10, 510(1972)

104.   E.G. Merrill and A. Ainsworth, Med. & Biol. Eng., 10, 662(1972)

105.   R. Nie, R. Zhu, W. Zhang, J. Guo and H. Li, Proc. 9th International Congress on Metallic Corrosion, NRC, Ottawa, 491(1984)

106.   J.N. Harb and R.C. Alkire, J. Electrochem. Soc., 138, 2594(1991)

107.   P. Zaya and M.B. Ives, Proc. 9th International Congress on Metallic Corrosion, NRC, Ottawa, 2, 135(1984)

108.   R.C. Alkire, Conf. Proc. Corrosion Chemistry within Pits, Crevices and Cracks, A. Turnbull Ed., HMSO, London, 129(1987)

109.   K.S. Pitzer, "Reviews in Mineralogy", Vol. 17: "Thermodynamic Modelling of Geological Materials: Minerals, Fluids and Melts", I.S.E. Carmichael & H.P. Eugster, Eds., Mineralogical Society of America, BookCrafters, Inc., Chelsea, Michigan, 97(1987)

110.   M. Magini, G. Paschina, and G. Piccaluga, J. Chem. Phys., 76, 1116(1982).

111.   D. A. Netzel and H. A. Droll, Inorg. Chem., 2, 412(1963).

112.   D. F. C. Morris, G. L. Reed, E. L. Short, D. N. Slater, and D. N. Waters, J. Inorg. Nucl. Chem., 27, 377(1965).

113.   T. M. Florence, Aust. J. Chem., 19, 1343(1966).

114.   R. H. Herber and J. W. Irvine, Jr., I. Am. Chem. Soc., 78, 905(1956).

115.   M. Magini, M. De Moraes, G. Licheri, and G. Piccaluga, J. Chem. Phys., 83, 5797(1985).

116.   G. W. Neilson and J. E. Enderby, Proc. R. Soc. London, Ser. A, 390, 353(1983).

117.   Z. Libus and H. Tialowska, J. Solution Chem., 4, 1011(1975).

118.   R.H. Stokes, S. Phang and R. Mills, J. Solution Chem., 8, 489(1979)

119.   J.S. Newman, "Electrochemical Systems", Prentice-Hall, Inc., Englewood Cliffs, NJ(1973)

120. J. Newman, Proc. Conf. Localized Corrosion, NACE-3, R. Staehle, B.F. Brown, J. Kruger, A.K. Agrawal, Eds., NACE, Houston, Texas, 45(1975)

121. J.S. Kirkaldy and D.J. Young, "Diffusion in the Condensed State", The Institute of Metals, London, 216(1987)

122. P.C. Harris and T.E. Moore, Inorg. Chem., 7, 656(1968)

123. L.G. Sillen and A.E. Martell, "Stability Constants of Metal-Ion Complexes", Special Publication 17, The Chemical Society, Burlington House, London, (1964)

124. Personal communication with Dr. O.E. Hileman and Dr. A. Corsini, Dept. of Chemistry, McMaster University

125. H. Ch. Kuo and D. Landolt, Electrochim. Acta., 20, 393, (1975)

126. J.S. Newman, "Electrochemical Systems", Prentice-Hall, Englewood Cliffs, NJ, 229(1973)

127. P. Heimgartner and H. Boehni, Corrosion, 41, 715(1985)

128. C.F. Beas and R.E. Mesmer, "The hydrolysis of Cations", John Wiley, New York, (1976)

129. H. Wendt, Chimia, 27, 575(1973)

130. R. L. Burden and J. D. Faires, "Numerical Analysis", 4th Ed., PWS-KENT Publishing Co., Boston, 285(1989)

131. N.K. Madsen and R.F. Sincovec, ACM Transactions on Mathematical Software, 5, 326(1979)

132. G.J. Janz, "Reference Electrodes", J.G. Ives and G.J. Janz Eds., Academic Press, 179(1961)

133.   E. Pungor and K. Toth, Analyst, 95, 625(1970)

134.   M. Pourbaix, "Atlas of Electrochemical Equilibria in Aqueous Solutions", English translation by J.A. Franklin, NACE, Houston, Texas, 281(1974)

135.   W.M. Latimer, "The Oxidation States of the Elements and Their Potentials in Aqueous Solutions", Second Edition, New York, Prentice-Hall Inc. (1952)

136.   K.S. Pitzer and L.F. Silvester, J. Soln. Chem., 5, 269(1976)

137.   K.S. Pitzer, J. Soln. Chem., 4, 249(1975)

138.   C.E. Harvie, N. Moller and J.H. Weare, Geochim. Cosmochim. Acta, 48, 723(1984)

139.   C. R. Paige, Ph.D. Thesis, Department of Chemistry, McMaster University (1989)

140.   V.K. Filippov, N.A. Charykov and N.D. Solechnic, J. Applied Chemistry of the USSR, 58, 1811(1985)

141.   J.F. Zemaitis, Jr., D.M. Clark, M. Rafal, and N.C. Scrivner, "Handbook of Aqueous Electrolyte Thermodynamics", AICHE, New York, 390(1986)

142.   K.H. Khoo, J. Chem. Soc., Faraday Trans. 1, 82, 1(1986)

143.   T.P. Gilbert, "Electrode Processes", Faraday Society, London, (320)1974

144.   J.D. Verhoeven, "Fundamentals of Physical Metallurgy", John Wiley & Sons, New York, 144(1975)

145.   "Handbook of Chemistry and Physics", 70th Ed., R.C. Weast et. al. Eds., CRC Press, Inc., Florida, (1978)

146.   L.I. Antropov, "Theoretical Electrochemistry", Second ed., Mir Publishers,

Translated by A. Beknazarov, Table 6.1(1977)

147.   R.M. Barrer, "Diffusion In And Through Solids", University Press, Cambridge, 9(1951)

148.   D.A. Skoog, "Principles of Instrumental Analysis", Saunders College Publishing, 612(1985)

149.   E. Pungor and K. Toth, Anal. Chim. Acta, 47, 291(1969)

150.   N. Lakshminarayanaiah, "Membrane Electrodes", Academic Press, 126(1976)

151.   J.F. Zemaitis, Jr., D. M. Clark, M. Rafal, N.C. Scrivner, "Handbook of Aqueous Electrolyte Thermodynamics", American Institute of Chemical Engineers, New York, (1986)

152.   L.F. Jaffe and R. Nuccitelli, J. Cell Biology, 63, 269(1974)

153.   K. Tokuda, T. Gueshi, K. Aoki, and H. Matsuda, J. Electrochem. Soc., 132, 2390(1985)

154.   L.I. Antropov, "Theoretical Electrochemistry", Second ed., Mir Publishers, Translated by A. Beknazarov, 142(1977)

155.   M. L. Kronenberg, J.C. Banter, E. Yeager and F.Hovorka, J. Electrochem. Soc., 110, 1007(1963)

156.   C. Clerc, M. Datta and D. Landolt, Electrochim. Acta, 29, 1477(1984)

157.   A.J. Bard ed. "Encyclopedia of Electrochemistry of the Elements", Marcel Dekker, Inc., New York, Volume III, 282(1975)

158.   A.A. Seys, M.J. Brabers and A.A. van Haute, Corrosion, 30, 47(1974)

159.   M. Pourbaix, "Atlas of Electrochemical Equilibria in Aqueous Solutions", English

translation by J.A. Franklin, NACE, Houston, Texas, 334(1974)

160.   J.L. Luo, Y.C. Lu and M.B. Ives, accepted by J. Electroanal. Chem.(1992)

161.   J.L. Luo and M.B. Ives, Conf. Proc. Critical Factors in Localized Corrosion, G.S. Frankel, R.C. Newman Eds., The Electrochemical Society, Inc., Pennington, NJ, 134(1992)

162.   J.L. Luo, Y.C. Lu and M.B. Ives, Conf. Proc. Electrochemical Methods in Corrosion Research, Helsinki, July(1991)

163.   M. B. Ives, and J. L. Luo, Conf. Proc of 11th International Corrosion Congress, Associazione Italiana Di Metallurgia, Florence, Italy, April, 3, 451(1990)

164.   J.L. Luo, Y.C. Lu and M.B. Ives, The NACE Annual Conference, NACE, Houston, Texas, Paper No. 233, (1992)

165.   Y. C. Lu, J. L. Luo and M. B. Ives, Invited Paper to J. of Iron and Steel Institute of Japan Special Issue for Corrosion, 31, 210(1991)

166.   M. B. Ives, Y. C. Lu and J. L. Luo, Corros. Sci., 32, 91(1991)

167.   Y.C. Lu, J.L. Luo and M.B. Ives, Corrosion, 47, 835(1991)

168.   J.L. Luo, A transfer Report from M. Eng. to Ph.D, Dept. of Materials Science & Engineering, McMaster University (1988)

169.   K. Fink, Poster paper #12, The NACE Annual Conference, Cincinnati, Ohio, March(1991)

170.   Personal communication with J. Rodda, Institute for Material Research, McMaster University

APPENDIX A. LOCAL CONDITIONS WITHIN NATURAL PITS FORMED ON A COMMERCIAL STEEL

In this section, another application is presented to show the ability of the microelectrodes for in situ measurements of the local conditions within a natural pit.

The conditions for growing pits formed in UNS S30100 stainless steel in 0.05 M NaCl solutions have been clarified by microelectrode measurements. Figure A.1 is the pH distribution within and above a growing pit, as determined with the tungsten microelectrode. Special consideration of the interference effects of Fe^{2+} and Cr^{3+} on the measurements of the activity of the chloride ions and pH is discussed in Section 3.2.4. Here is an example of the need for a correction for the interference effect on the measurement of the pH.

The true pH distribution due to presence of the cations can be calculated from the following equation:

$$E_{measured}=C+\frac{RT}{F}\ln[a_{H^+}+k_{H^+,Fe^{2+}}(a_{Fe^{2+}})^{1/2}+k_{H,Cr^{3+}}(a_{Cr^{3+}})^{1/3}]$$ [a.1]

Values of a_{Fe2+} and a_{Cr3+} may be derived as follows: First, the concentration distribution is estimated by Fick's second Law and Faraday's Law. Ignoring the migration of the ions, the distribution of the concentration of the ferrous ions or chromic ions c_i in the direction of the pit axis is presented by Equation [a.2]:

$$c_j = c_{0,j} \left[1 - erf \left(\frac{Z}{2\sqrt{D_j t}} \right) \right]$$ [a.2]

The boundary condition was determined by Fick's first law,

$$\frac{i}{n_j F} = D_j \frac{dc}{dZ}$$

$$\frac{dc}{dZ} = - \frac{c_{0,j}}{\sqrt{\pi D_j t}} \exp\left(- \frac{Z^2}{4 D_j t} \right)$$ [a.3]

At time t_h, when the pit depth is equal to h,

$$c_{0,j} = i \frac{\sqrt{\pi t_h}}{n_j F \sqrt{D_j}} \exp\left(\frac{h^2}{4 D_j t_h} \right)$$ [a.4]

t_h can be estimated by Faraday's Law:

$$t_h = \frac{n_j F h}{i V_j}$$ [a.5]

Where V_j is the molar volume of metal j. After substituting Equations [a.4] and [a.5] to Equation [a.2], the concentration c_j takes the form

$$c_j = \sqrt{\frac{i \pi h}{n_j F D_j V_j}} \exp\left(\frac{i h V_j}{4 D_j n_j F} \right) \left[1 - erf\left(\frac{Z}{\sqrt{D_j t}} \right) \right]$$ [a.6]

The concentration is then converted to activity by using the Pitzer model[109]. Figure A.1 shows the effect of making such a correction for the pH measured in an active pit in a UNS 30100 stainless steel.

Figure A.2 shows the activity distribution of chloride ions adjacent to and inside of a pit. The potential distribution of a pit is given in Figure A.3.

From the anodic behaviour of UNS S30100 stainless steel in simulated pit electrolytes, chosen on the basis of the compositions determined by microelectrode measurements, the dissolution mechanisms at the various stages of the dissolution can be discussed.

Comparing the measured distribution of the chloride ions, pH and potential from the pits formed on 'lead-in pencil' pits and natural pits, one can see that they have the same tendency. It means that it is appropriate to use a 'lead-in pencil' pit to understand the pit development in real pitting situation. As Heimgartner and Bohni concluded that the rate law for a model pit and a naturally growing pit can be very similar[127].
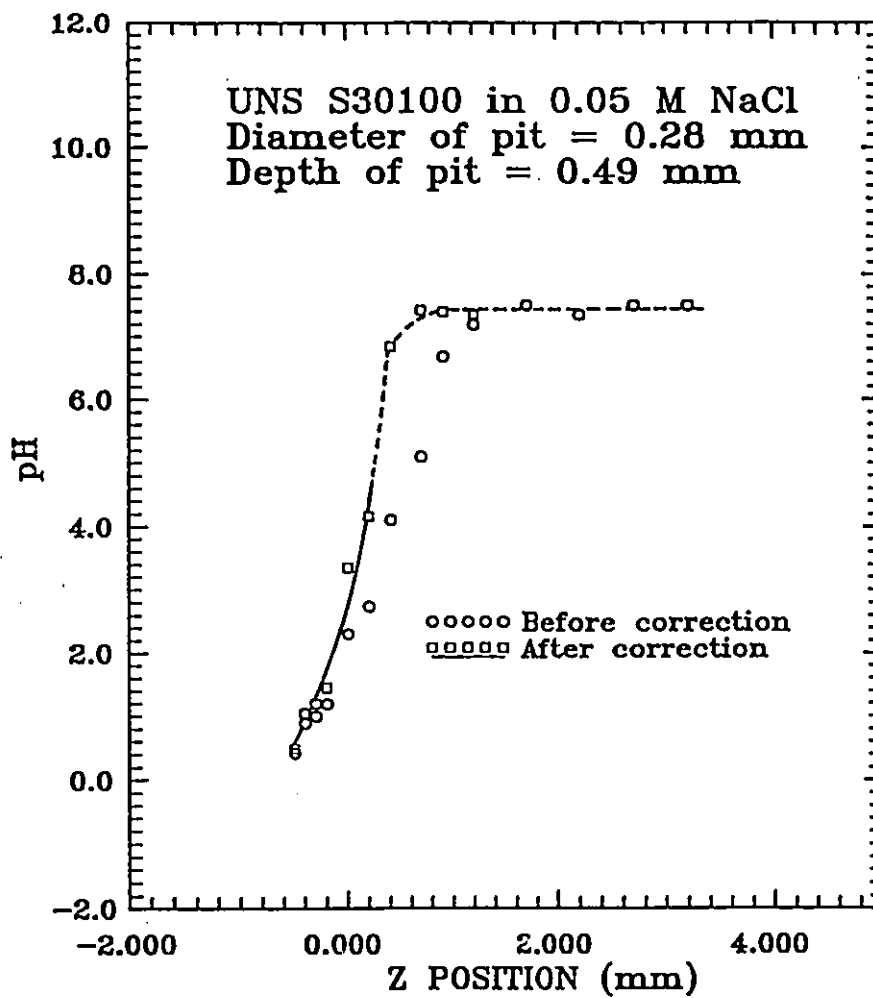
Figure A.1   The pH distribution along the depth direction of a natural growing pit
in UNS S30100 obtained by a pH probe before and after correcting for
the interference due to the presence of cations.
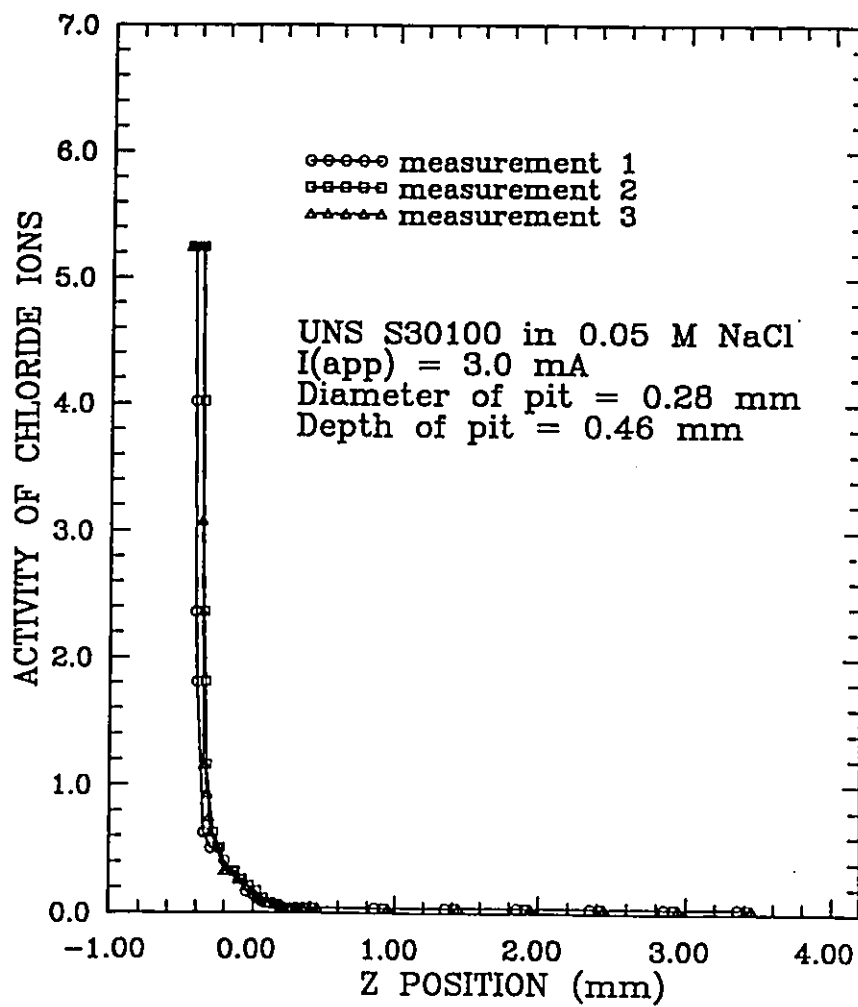
Figure A.2   The chloride ion activity variation in the growth direction of a natural growing pit on UNS S30100.
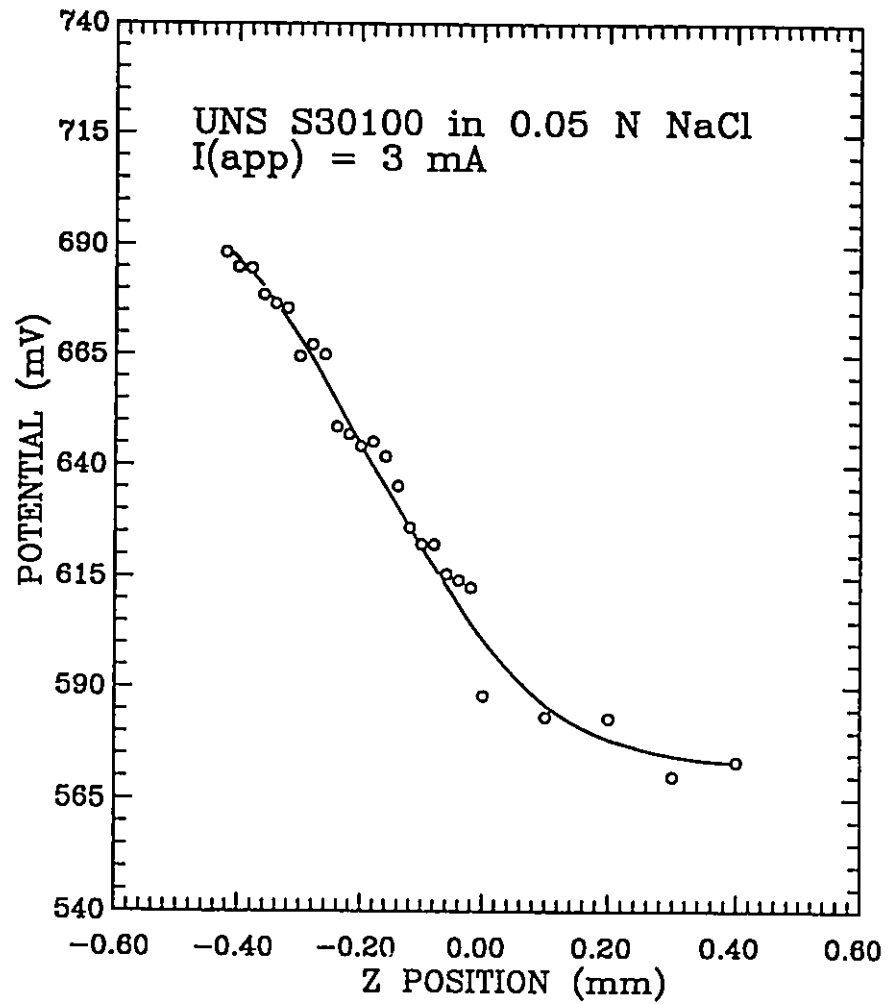
Figure A.3   The potential distribution in growth direction of a natural pit in UNS
S30100 stainless steel.

APPENDIX B. PITZER MODEL

The Pitzer expressions for osmotic and activity coefficients, as formulated by Harvie et al.[138], are given by:

$$\sum_i m_i(\phi-1)=2(\frac{-0.392I^{3/2}}{1+1.2\sqrt{I}})+\sum_{c=1}^{N_c}\sum_{a=1}^{N_a}m_c m_a(B_{ca}^\phi+ZC_{ca})$$

$$+\sum_{c=1}^{N_c-1}\sum_{c'=c+1}^{N_c}m_c m_{c'}(\Phi_{cc'}^\phi+\sum_{a=1}^{N_a}m_a\psi_{cc'a})$$

$$+\sum_{a=1}^{N_a-1}\sum_{a'=a+1}^{N_a}m_a m_{a'}(\Phi_{aa'}^\phi+\sum_{c=1}^{N_c}m_c\psi_{aa'c})$$

$$+\sum_{N=1}^{N_N}\sum_{a=1}^{N_a}m_N m_a\lambda_{Na}+\sum_{N=1}^{N_N}\sum_{c=1}^{N_c}m_N m_c\lambda_{Nc}$$

[b.1]

$$\ln\gamma_M=n_M^2F+\sum_{a=1}^{N_a}m_a(2B_{Ma}+ZC_{Ma})+\sum_{c=1}^{N_c}m_c(2\Phi_{Mc}+\sum_{a=1}^{N_a}m_a\psi_{Mca})$$

$$+\sum_{a=1}^{N_a-1}\sum_{a'=a+1}^{N_a}m_a m_{a'}\psi_{aa'M}+|n_M|\sum_{c=1}^{N_c}\sum_{a=1}^{N_a}m_c m_a C_{ca}+\sum_{N=1}^{N_N}m_N(2\lambda_{NM})$$

[b.2]

$$\ln\gamma_x=n_x^2F+\sum_{c=1}^{N_c}m_c(2B_{cx}+ZC_{cx})+\sum_{a=1}^{N_a}m_a(2\Phi_{xa}+\sum_{c=1}^{N_c}m_c\psi_{xac})$$

$$+\sum_{c=1}^{N_c-1}\sum_{c'=c+1}^{N_c}m_c m_{c'}\psi_{cc'x}+|n_x|\sum_{c=1}^{N_c}\sum_{a=1}^{N_a}m_c m_a C_{ca}+\sum_{N=1}^{N_N}m_N(2\lambda_{Nx})$$

[b.3]

$$\ln\gamma_N = \sum_{c=1}^{N_c} m_c(2\lambda_{Nc}) + \sum_{a=1}^{N_a} m_a(2\lambda_{Na})$$

[b.4]

$$\ln a_{H_2O} = -\frac{18.0153}{1000}(\sum_i m_i)\phi$$

[b.5]

Where I is ionic strength:

$$I = \frac{1}{2}\sum_i m_i n_i^2$$

[b.6]

In the expression for individual ion activity coefficients, m_c and n_c are the molality and charge of cation c, respectively. N_c is the total number of cation species. Similar symbolism is used for anions, a, and neutrals, N. The parameter, λ, accounts for the interactions between neutral species and ionic species in the solution[136]. The subscripts M, X, and N refer to cations, anions, and neutral species, respectively. The sum over i in equations [b.1] and [b.5] represents the sum over all solutes: cations, anions and neutrals. The remaining terms are defined as follows:

$$F = -0.392(\frac{\sqrt{I}}{1+1.2\sqrt{I}} + \frac{2}{1.2}\ln(1+1.2\sqrt{I}))$$

[b.7]

$$+\sum_{c=1}^{N_c}\sum_{a=1}^{N_a} m_c m_a B'_{ca} + \sum_{c=1}^{N_c-1}\sum_{c'=c+1}^{N_c} m_c m_{c'}\Phi'_{cc'} + \sum_{a=1}^{N_a-1}\sum_{a'=a+1}^{N_a} m_a m_{a'}\Phi'_{aa'}$$

$$C_{Mx} = \frac{C_{Mx}^\phi}{2}\sqrt{|n_M n_x|}$$

[b.8]

$$Z = \sum_i |n_i| m_i$$

[b.9]

The Φ_{ij}, which depend on ionic strength, are given the following form[137]:

$$\Phi_{ij}^{\phi} = \theta_{ij} + E_{\theta_{ij}}(I) + IE_{\theta_{ij}'}(I)$$

$$\Phi_{ij} = \theta_{ij} + E_{\theta_{ij}}(I)$$

[b.10]

$$\Phi_{ij}' = E_{\theta_{ij}'}(I)$$

The functions, $E_{\theta ij}(I)$ and $E_{\theta ij}'(I)$ are functions only of ionic strength and the electrolyte pair type. Integral defining these terms are given by Pitzer[137].

The second term, B, in Equations [b.1], [b.2], [b.3] and [b.7] is given the following ionic strength dependence:

$$B_{Mx}^{\phi} = \beta_{Mx}^{(0)} + \beta_{Mx}^{(1)} \exp(-\alpha_{Mx}\sqrt{I}) + \beta_{Mx}^{(2)} \exp(-12\sqrt{I})$$

[b.11]

$$B_{Mx} = \beta_{Mx}^{(0)} + \beta_{Mx}^{(1)} g(\alpha_{Mx}\sqrt{I}) + \beta_{Mx}^{(2)} g(12\sqrt{I})$$

[b.12]

$$B_{Mx}' = \frac{\beta_{Mx}^{(1)} g'(\alpha_{Mx}\sqrt{I})}{I} + \frac{\beta_{Mx}^{(2)} g'(12\sqrt{I})}{I}$$

[b.13]

The functions g and g' are defined by the equations:

$$g(x) = 2(1 - (1+x)e^{-x})/x^2$$

[b.14]

$$g'(x) = -2(1 - (1+x+x^2/2)e^{-x})/x^2$$

[b.15]

with $x = \alpha_{Mx}\sqrt{I}$ or $12\sqrt{I}$. When either cation M or anion x is univalent $\alpha_{Mx} = 2.0$. For 2-2 or higher valence pairs $\alpha_{Mx} = 1.4$. The constants, θ_{ij}, Ψ_{ijk}, C_{Mx}, $\beta_{Mx}^{(0)}$, $\beta_{Mx}^{(1)}$ and $\beta_{Mx}^{(2)}$ are parameters specific to each solute. In most cases, $\beta_{Mx}^{(2)}$ equals zero for univalent pairs. For 2-2 valence electrolytes a non-zero $\beta_{Mx}^{(2)}$ is more common.

Table B.1 Single electrolyte solution parameter values

Cation	Anion	$\beta^{(0)}$	$\beta^{(1)}$	$\beta^{(2)}$	C^ϕ	Ref
Na	Cl	0.0765	0.2664	-	0.00127	138
Ni	Cl	0.44104	2.34470	-0.53354	-0.02156	140
H	Cl	0.1775	0.2945	-	0.0008	138

Table B.2 Common-ion two electrolyte parameter values

i	j	k	θ_{ij}	Ψ_{ijk}	ref.
Na	Ni	Cl	0.0	-0.003	141*
Na	H	Cl	0.036	-0.004	138
Ni	H	Cl	0.082	0.005	142

* Because the parameters for this system are not available to date, the data for Na-Mn-Cl from reference[141] substitute for missing data.

APPENDIX C. PROGRAM FOR CONTROLLING THE STEPPING MOTOR

```c
/*-------------------------------------------------------------------------------

Title        : mcman2.c
Function     : controlling a micromanipulator in the Z-axis
Written by   : R. Periard
Date         : 11-OCT-1990
Revision     : 2.00


---------------------------------------------------------------------------*/

#include <stdio.h>
#include <fcntl.h>
#include <string.h>
#include <conio.h>
#include <dos.h>
#include <graphics.h>
#include <alloc.h>
#include <stdlib.h>

#define DisPerCnt 0.48828 /* Micrometers */

char*box_bit[ ] = {"                                                    ",
                   "                                                    ",
                   "                                                    "};

char*prompts[]={ "Please Enter a File name...............................",
                 "Saving Profile Information ...........................",
                 "Can not open profile file                             ",
                 "Do You Want to Save This Profile(y/n)?                ",
                 "Please enter the direction (U/D)                      ",
                 "Displacement (μmeters)                                ",
                 "\nAdjust Initial position.......strike any key to continue ",
                 "Duration (seconds)                                    ",
                 "Do you Have More data to Enter (y/n)?                 ",
                 "                                                      ",
                 "Are All These Parameters correct (y/n)?               ",
```

```
                     "Number of times                         "};

char*err_msg[]={     "Please Enter (Y/N) only                 ",
                     "Input is Out Of Range                   ",
                     "Maximum is 4 Times .....                ",
                     "\n    Error(2): PHYSICAL LIMIT EXCEEDED  ",
                     "\n    Error(1): ADJUSTING PROFILE        ",
                 .   "     Get Serious .........!!!            "};

struct link_type {
        int    disp;
        int    durat;
        int    dir;
        struct link_type *next;
        struct link_type *previous;
};

struct link_type *head = NULL;
struct link_type *tail = NULL;

/* define the prototypes used in this program */

void SET_UP(void);
struct link_type *init_list(int temp[]);
void delete_link(struct link_type *link);
void insert_link(int temp_arry[], struct link_type *place);
struct link_type *create_link(int temp[]);
void push(int temp[]);
void pull(int temp[]);
void input_err(int err_num);
int build_prof(void),dir,dur;
void save_prof(FILE *fpw,struct link_type *list);
void move(int disp);
FILE *fpprof;
int  cnt_err;

void main(int argc,char *argv[])
{       int i,temp[3],save_p,dis;
        int numChang,ind;
        char ans2,ans,fname[12];
        FILE *fpw,*fp;

        if(argc>1){
```

```
                if((fp=fopen(argv[1],"rb"))==NULL){
                        puts(prompts[2]);
                        exit(1);
                }
        }
        else{
                if((fpprof=fopen("data.dat","w+"))==NULL){
                        puts(prompts[2]);
                        exit(1);
                }
                printf("\nno command line");sleep(1);
                numChang=build_prof();
                gotoxy(1,25); /* initially clear the screen */
                for (i=0;i<=25;i++){
                        printf("\n");}
                while(1){
                   gotoxy(20,20);
                   puts(prompts[3]);gotoxy(60,20);/*Does user wish to save profile */
                   ans=getch();
                   if(ans == 'n' || ans == 'N'){
                                save_p = 0;
                                break;}
                   if(ans == 'y' || ans == 'Y') {
                                save_p = 1;
                                break;}
                   else input_err(0);
                }
                if(save_p){            /* if Profile is to be saved */
                        gotoxy(20,20); /* get filename and open file */
                        puts(prompts[0]);
                        gotoxy(60,20);
                        scanf("%s",&fname);
                        if((fpw=fopen(fname,"wb+"))==NULL)
                        {       puts(prompts[2]);
                                exit(1);}
                        gotoxy(20,20);
                        puts(prompts[1]);
                        save_prof(fpw,head);
                }
        }
        outportb(555,00);
        puts(prompts[6]);
        ans2=getch();
```

```
/*        printf("numChang=%d\n",numChang);*/
          SET_UP();
          for(ind=0;ind<=(numChang-1);ind++){
                  pull(temp);
                  dir=temp[2];
                  dis=temp[0];
                  dur=temp[1];
/*                printf("\nDirection:%d Disp:%d Duration:%d\n",dir,dis,dur); */
                  move(dis);
                  delay(dur-(int)(dis/1.25));
          }
          fclose(fpprof);
}
void SET_UP(void)
{
          outportb(552,4); /* sets ports a,b+d as input, c as output */
          outportb(555,16);delay(1);outportb(555,dir); /*reset counters*/
          cnt_err=0;
}
```

/*_____

Title   : init_list()
Function: initializes a linked lists with the first data set.
Returns : a pointer of the link type.

_____ */

```
struct link_type *init_list(int temp[])
{
          struct link_type *create_link();
          head=tail=create_link(temp);
          return(head);
}
```

/*_____

Title   : delete_link()
Function   : used to delete a link from the list and free the space
Returns   : nothing

_____ */

```
void delete_link(struct link_type *link)
{         struct link_type *previous_link, *next_link;
```

```
        previous_link = link->previous;
        next_link = link->next;
        if(link == head)
        {
                head=next_link;
        }
        if(link == tail)
        {
                tail=previous_link;
        }
        if(previous_link != NULL)
        {
                previous_link->next=next_link;
        }
        if(next_link != NULL)
        {
                next_link->previous=previous_link;
        }
        free(link);
}
```

```
/*_____

Title         : insert_link()
Function      : used to insert a link into a list
Returns       : nothing
_____*/
```

```
void insert_link(int temp_arry[], struct link_type *place)
{
        struct link_type *next_link, *newlink;
        newlink = create_link(temp_arry);/* create a link with this data    */
        next_link = place->next;         /* This is the old tail            */
        place->next = newlink;           /* relationship to new link        */
        newlink->previous= place;        /* and original link               */
        if(next_link != NULL)            /* if there was a tail             */
        {
                newlink->next=next_link;
                next_link->previous=newlink;
        }
        else
        {
                tail=newlink;                    /* reset tail pointer       */
```

```
        }
}

/*_____

Title       : create_link()
Function    : allocated  memory for a link, set up pointers, and copies data into
              the link. Used internally by insert_link and init_list.
Returns     : pointer to the link.
            _____*/

struct link_type *create_link(int temp[])
{
        struct link_type *newlink;
        newlink = (struct link_type *) malloc(sizeof(*newlink));
        newlink->next=NULL;
        newlink->previous=NULL;
        newlink->disp=temp[0];
        newlink->durat=temp[1];
        newlink->dir=temp[2];
        return(newlink);
}


/*_____

Title       : push()
Function    : pushes a velocity profile onto the queue
Returns     : nothing.
            _____*/

void push(int temp[])
{
        if(head==NULL)
        {
                init_list(temp);
        }
        else
        {
                insert_link(temp, tail);
        }
}
```

```
/*_____

Title   : pull()
Function: pulls a velocity profile out of the queue
Returns : nothing.
                                                    */

void pull(int temp[])
{
        temp[0]=head->disp;
        temp[1]=head->durat;
        temp[2]=head->dir;
        delete_link(head);
}


/*_____

Title        : input_err()
Function     : This function is used to write error messages to the screen,
               for approximately 2 seconds.
Requires     : a pointer to the appropriate error message.
Returns      : Nothing.
                                                    */

void input_err(int err_num)
{
        gotoxy(20,20);
        puts(err_msg[err_num]);
        sleep(2);
        gotoxy(20,20);
        puts(prompts[10]);
}


/*_____

Title        : build_prof()
Function     : This function is used to build a velocity profile from user input
Requires     : user input
Returns      : a velocity profile which can be written to disk, for future
               experiments.
                                                    */

int build_prof(void)
```

```c
{
int elements=0, i=1, i2, temp[4], repeat;
float tempf;
char ans;
        while(i){
                gotoxy(1,25);           /*  initially clear the screen */
                for (i=0;i<=25;i++){
                        printf("\n");
                }
                gotoxy(10,10);          /* Get the displacement information */
                puts(prompts[4]); gotoxy(65,10);        /* Direction */
                ans=getch();

                if(ans=='u'||ans=='U')
                {
                        temp[2]=2;
                        ans='U';
                }
                else
                {
                        ans='D';
                        temp[2]=0;
                }
        putch(ans);
                gotoxy(10,12); puts(prompts[5]); gotoxy(65,12); /* Displacement */
                scanf("%*[a-zA-Z]%d%*[a-zA-z]", &temp[0]);
                /*temp[0]=atoi(ascii_input);*/
                gotoxy(10,14);puts(prompts[7]); gotoxy(65,14);  /* Duration */
                scanf("%*[a-zA-Z]%f%*[a-zA-Z]", &tempf);
                temp[1]=(int)(tempf*1000);
        while(1){
                        gotoxy(20,20);
                        puts(prompts[10]); gotoxy(65,20);   /* is every thing OK */
                        ans=getch();
                        if(ans == 'n' || ans == 'N'){
                                i2 = 0;
                                break;
                        }
                        if(ans == 'y' || ans == 'Y') {
                                i2 = 1;
                                break;
                        }
                        else input_err(0);
```

```
        }
        if(i2){
                gotoxy(20,20);
                puts(prompts[11]); gotoxy(65,20);  /* How many repeats */
                scanf("%*[a-zA-Z]%d%*[a-zA-z]", &repeat);
                gotoxy(65,20);printf("    ");
                for(i=1;i<=repeat;i++){
                        push(temp);}
        elements+=repeat;
        }
        while(1){
                gotoxy(20,20);
                puts(prompts[8]);gotoxy(65,20);  /* Do you have more data */
                ans=getch();
                if(ans == 'n' || ans == 'N'){
                        i = 0;
                        break;
                }
                if(ans == 'y' || ans == 'Y') {
                        i = 1;
                        break;
                }
                else input_err(0);
        }
        }
        return(elements);
}


/*_____

Title   : save_prof
_____*/

void save_prof(FILE *fpw,struct link_type *list)
{
        while(list != NULL){
                /*fprintf(fpw,"%d %d %d %d", list->rate, list->accel, list->durat,
                   list->dir); */
                fwrite(&list,sizeof(struct link_type),1,fpw);
                list=list->next;
        }
}
```

```
/*_____

Title    : get_prof
                                    */
_____

/*
void get_prof(FILE *fp,struct link_type *list)
{
        struct link_type *templ;
        int    temp_prev,temp_next,temp[6];
        while(
}   */

void box(void)
{
        char i;
        gotoxy(5,5);
        puts(box_bit[0]);
        for(i=0;i<=15;i++){
          gotoxy(5,6+i);
          puts(box_bit[1]);
        }
        gotoxy(5,6+i);
        puts(box_bit[2]);
}

void move(int disp){
        int count,stepped,stat,x,x2,x3;
        int start,curr;
        count=(int)disp/DisPerCnt;
        /* get initial position */
        start =inportb(553); /* read low byte of position counter */
        start+=(256*(inportb(554)));  /* read high byte of position counter */
        dir|=13;
        stepped=0;
        count=count-cnt_err;
        for(x=1;x<=count;x++){
          stat=inportb(556);
          stat=stat&3;
          if(stat==2){
                puts(err_msg[3]);
                exit(1);}
          if(stat==1){
```

```
        puts(err_msg[4]);
        exit(1);}        /* continue */
    outportb(555,dir);  /* toggle the pulse input on the 203TH */
    delay(1);           /*for(x2=0;x2<=100;x2++);*/
    dir&=14;
    outportb(555,dir);
    delay(1);
}
printf("%5.3f ",start*DisPerCnt);
while(!stepped){
    curr =inportb(553); /* read low byte of position counter */
    curr+=(256*(inportb(554))); /* read high byte of position counter */

    if(dir==12){
        cnt_err=count-(curr-start);        /* down direction */
        if(cnt_err>=4){
            outportb(555,dir+1);
            for(x3=0;x3<=100;x3++);
            outportb(555,dir);
        }
        else{
            stepped=1;
            break;}
    }
    if(dir==14){
        cnt_err=count-(start-curr);
        if(cnt_err>=4){
            outportb(555,dir+1);
            for(x3=0;x3<=100;x3++);
            outportb(555,dir);
        }
        else{
            stepped=1;
            break;}
    }
}
printf("%5.3f \n",curr*DisPerCnt);
}
```